Optical aberrations and cone photoreceptor sampling during normal emmetropization and emmetropization to imposed defocus

by

Mengyuan Ke

A thesis
presented to the University of Waterloo
in fulfillment of the
thesis requirement for the degree of
Master of Science
in
Physics (Nanotechnology)

Waterloo, Ontario, Canada, 2018

AUTHOR'S DECLARATION

This thesis consists of material all of which I authored or co-authored: see Statement of Contributions included in the thesis. This is a true copy of the thesis, including any required final revisions, as accepted by my examiners.

I understand that my thesis may be made electronically available to the public.

Statement of Contributions

The thesis author is the sole author of all written chapters. Coauthors for earlier materials presented at conferences:
Coauthors for International Myopic conference 2017 (*Following emmetropization, the residual retinal optical blur matches cone photoreceptor resolution in chicks*) are Dr. Elizabeth Irving; Marsha Kisilak; Laura Emptage; Ian Andrews; Dr. Melanie Campbell.

Coauthors for Canadian Association of Physicists 2017 (*During growth, defocus reduces until optical blur is similar to the resolution of the cone photoreceptors*) are Marsha Kisilak; Laura Emptage; Ian Andrews; Dr. Melanie Campbell.

Coauthors for Association of Vision and Ophthalmology Annual Meeting (ARVO 2018) (*Cone photoreceptors and optical signals to defocus following emmetropization to lenses in chicks*) are Dr. Elizabeth Irving; Marsha, Kisilak; Dr. Melanie Campbell.

Data on aberrations and defocus for 3 groups of birds goggled with -15D lenses measured from day 0 to day 14 was taken from Marsha Kisilak's Hartman-Shack measurements, cone densities for the same groups of birds were measured by Marsha Kisilak. The thesis author was the principle experimenter for another two groups of birds (see below). Aberrations and defocus for 1 group of birds goggled with +10D lenses measured on day 0 and day 14 was taken from Marsha Kisilak and Dr. Elizabeth Irving's raw Hartman-Shack measurements, cone densities for same group of birds were measured by Marsha Kisilak and Dr. Elizabeth Irving.

The thesis author performed the experiments for one group of bird goggled with -15D lenses from day 9 to day 21 and the cone density measurements for this group of birds. She was assisted by Ian Andrews, Laura Emptage. The thesis author analyzed the Harman Shack images for this group of birds with -15D lenses and the group of birds with +10D lenses, cone densities measured for these birds were also calculated by the thesis author.

The thesis author then combined the 5 groups of birds, performed the calculation of optical blur for all birds and compared this with cone resolution calculated from cone density. Dr. Campbell made helpful comments on the analysis and discussion presented within the thesis, made editorial changes to the text and assisted in writing the abstracts presented at conferences prior to the writing of the thesis.

This research is supported by Natural Sciences and Engineering Research Council (NSERC), the University of Waterloo and Soochow University.

Abstract

The eye grows in a coordinated fashion during normal emmetropization which results in an image close to being in focus on the retina for distance vision. Myopia results from the failure of normal emmetropization. Myopia increases the risk factors of a range of ocular diseases, such as retinal detachment, and is a leading cause of blindness. In addition, a rapidly increasing myopia rate has been reported in the last decade which requires more research into its mechanisms. Furthermore, understanding the mechanisms underlying normal emmetropization may lead to interventions that limit or prevent myopia. Instead of emmetropia, which equates with zero refractive error, a small nonzero refractive error following emmetropization has been reported in children, chicks and monkeys.

Chicks are a popular animal model in which to study refractive development. When defocusing lenses are placed in front of the eye, the rate of eye growth changes to compensate the amount of defocus similar to normal emmetropization. Optical aberrations, which degrade the image quality of the eye, and cone photoreceptor sampling are important in studying the control of emmetropization. The right eyes of chicks were raised with positive (+10D) or negative (-15D) lenses while left eyes grew normally. Image quality degraded by optical aberrations and defocus was studied and compared to cone photoreceptor sampling in goggled eyes with the different lenses, and in control eyes.

An image quality metric, equivalent blur, used here is a simpler calculation than other metrics calculated from point spread functions but still gives a good approximation of the radial extent of point spread function.

Adaptive optics (AO) allows the longitudinal measurement of cone densities *in vivo*. The change of angular photoreceptor spacing with age in chick, measured and calculated from AO, was not affected by inducing either positive or negative defocus blurs. Thus, age changes in cone angular photoreceptor spacing do not appear to be influenced by optical blur. This spacing is compared for the first time to the extent of the optical blur on the retina. The minimum optically resolvable separation of two points (given by the Rayleigh criterion) achieved near the endpoint of refractive development matches the Shannon sampling resolution, given by the cone photoreceptor matrix. In turn, the minimum resolvable separation of two points is equal to the radius of the optical blur. The optical blur plateaus at the value which matches the limit of cone sampling. This may mean that the blur is no

longer “visible” to the cones. This in turn may explain the nonzero refractive error found in chicks and possibly in monkeys and human.

As previously found, astigmatism, particular oblique astigmatism increases in the eyes goggled with -15D lenses. At the time of and following the plateauing of optical blur, the presence of astigmatism generates a difference in the orientation of the PSF as the refraction varies in the goggled eyes goggled with positive or negative lenses over a short time period (with measured accommodation) and in control eyes with modeled accommodation. This orientation change can be resolved by the cone photoreceptors indicating that oblique astigmatism may provide a cue to the sign of defocus in goggled eyes and possibly in control eyes as well.

Acknowledgements

I would like to thank all people who have assisted me over the last two years I have spent at the University of Waterloo.

First, I would like to extend my appreciation for my supervisor Dr. Melanie Campbell whose patience and intelligence has guided me through my graduate studies. My committee members Dr. Irving for all the insightful questions in the committee meeting. Dr. Kostadinka Bizhewa, thank you for being on my regular committee. I also thank Dr. Joe Sanderson for agreeing to be on the examining committee.

My amazing colleagues from Campbell lab, Marsha, Kisilak, thank you for your initial help for the starting of this project. Laura Emptage, thank you for your companionship as a friend. David DeVries, Tao Jin, Ian Andrews, Rachel Redekop, Heqing Huang, Kaitlin Bunghardt, Riley Delaney, Maryam Mozaffari, Michael Hamel, Eric Mason, Monika Kitor, Yunyi Qiu, Ji Ren, Rui Fan.

This two-year journey has been a rewarding experience for me. I am glad to have a superb supervisor and meet all the talented people.

Dedication

Dedicated to my mom and dad.

Appreciate the presence, enjoy the present.

Table of Contents

CONTENTS

List of Figures

List of Tables

Chapter 1 Introduction

1.1 Introduction

In most species studied, the eyes at birth have a hyperopic defocus (Wallman & Winawer, 2004a). Emmetropization is a process of eye growth that coordinates the mismatch between eye size and shape and optics of the eye (power of the eye) during the postnatal period, which is expected to produce a refractive error-free state, known as the emmetropic state (Figure 1.1 a). However, research in animals and humans report a non-zero refraction as the endpoint of normal emmetropization. Mild hyperopia has been reported in children (Morgan, Rose, Ellwein, & Refractive Error Study in Children Survey Group, 2010), chicks (Shao, 2015) and monkeys (Qiao-Grider, Hung, Kee, Ramamirtham, & Smith, 2007).

Myopia occurs as a failure of normal emmetropization. The elongated eyeball fails to focus the image at the photoreceptor layer, thereby causing a defocus error with the focus in front of the photoreceptors. Increasing prevalence of myopia has called much attention to this public health issue because of its links to other ocular pathologies such as glaucoma (Mitchell, Hourihan, Sandbach, & Wang, 1999), retinal detachment (Baba et al., 2003; Stirpe & Michels, 1990), cataract (Lim, Mitchell, & Cumming, 1999) and age-related macular degeneration (Wong, Klein, Klein, & Tomany, 2002) (AMD). In 2050, it is estimated that half the population worldwide will be myopic (Hopf & Pfeiffer, 2017).

When placing defocus lenses in front of the eye, the eye growth can be accelerated (with negative lenses in figure 1.1 e) or retarded (with positive lenses in figure 1.1 g) respectively. This is a compensatory eye growth, a process defined as emmetropization to lenses. Compensatory eye growth in response to imposed defocus has been studied in animals ranging from chick (Irving, Callender, & Sivak, 1991; Schaeffel, Glasser, & Howland, 1988), tree shrew (Amedo & Norton, 2012), through monkey (Hung, Crawford, & Smith, 1995; Zhu, McBrien, Smith, Troilo, & Wallman, 2013) and supports the concept of active emmetropization via feedback loops in response to optical blur.
Of all the animal models listed, chicks show most impressive refractive plasticity, being able to fully compensate to lens powers from -30D to 20D (Irving, Sivak, & Callender, 2015). Interventions that shift the image plane either behind the retina (Figure 1.1 b) or in front of the retina (Figure 1.1 d) using optical lenses are commonly used to manipulate the development of refractive errors in animal models. Negative lenses induce hyperopic defocus which cause myopia due to excessive enlargement

of the eye (Figure 1.1 a b e). Positive lenses induce myopic defocus, causing hyperopia (Figure 1.1 a d g). The response to the opposite lens sign is not symmetric, hyperopia develops at a faster rate and over a larger range than myopia. Young chicks showed better compensation to induced defocus than older ones (Irving et al., 2015). Incomplete compensation to imposing defocus was reported by early studies for chicks wearing spectacle lenses for 5 days, which is attributed to the short lens wear time and the starting point of chick age (C. Wildsoet & Wallman, 1995).

The exact signals responsible for the emmetropization mechanism are not fully understood. Accommodation (Buehren & Collins, 2006), monochromatic aberrations (Wilson, Decker, & Roorda, 2002) (astigmatism and higher order aberrations) and diurnal variation of refraction (M. C. Campbell, Bunghardt, Kisilak, & Irving, 2012) are possible candidates as optical signals to regulate eye growth. All of them affect the image perceived by the retina and directly affect the blur on the retina.

It was suggested that the retina itself might be able to detect the sign of retinal blur. Chick eyes with optic nerve section showed compensatory growth to imposed myopic defocus but a shift towards hyperopia was observed for the set point during refractive development (C. Wildsoet & Wallman, 1995). Chicks with optic nerve section wearing occluders exhibited similar compensation to form-deprivation myopia while eyes with optic nerve section but without occulders were more hyperopia than normal growth eyes (Troilo, Gottlieb, & Wallman, 1987). Despite the detection of blur by the retina, a connection to the brain may help the eyes to have a finer mechanism to regulate growth. The retina itself can independently perform image processing, and even detect defocus sign (Schaeffel & Wildsoet, 2013). Regardless, cone photoreceptors in the retina play important roles as they act as photon detectors to sample the light. Thus, changes in cone photoreceptor densities during growth are one important focus of this project. Adaptive optics imaging is a robust technique to visualize cone photoreceptors in the living eye (Roorda et al., 2002).

I wish to determine the changes of optical aberration and cone photoreceptor density in chick models with positive or negative defocus lenses and without lenses. I will also study whether astigmatism provides a signal to the direction of defocus towards the end of emmetropization in order to have a better understanding of emmetropization.

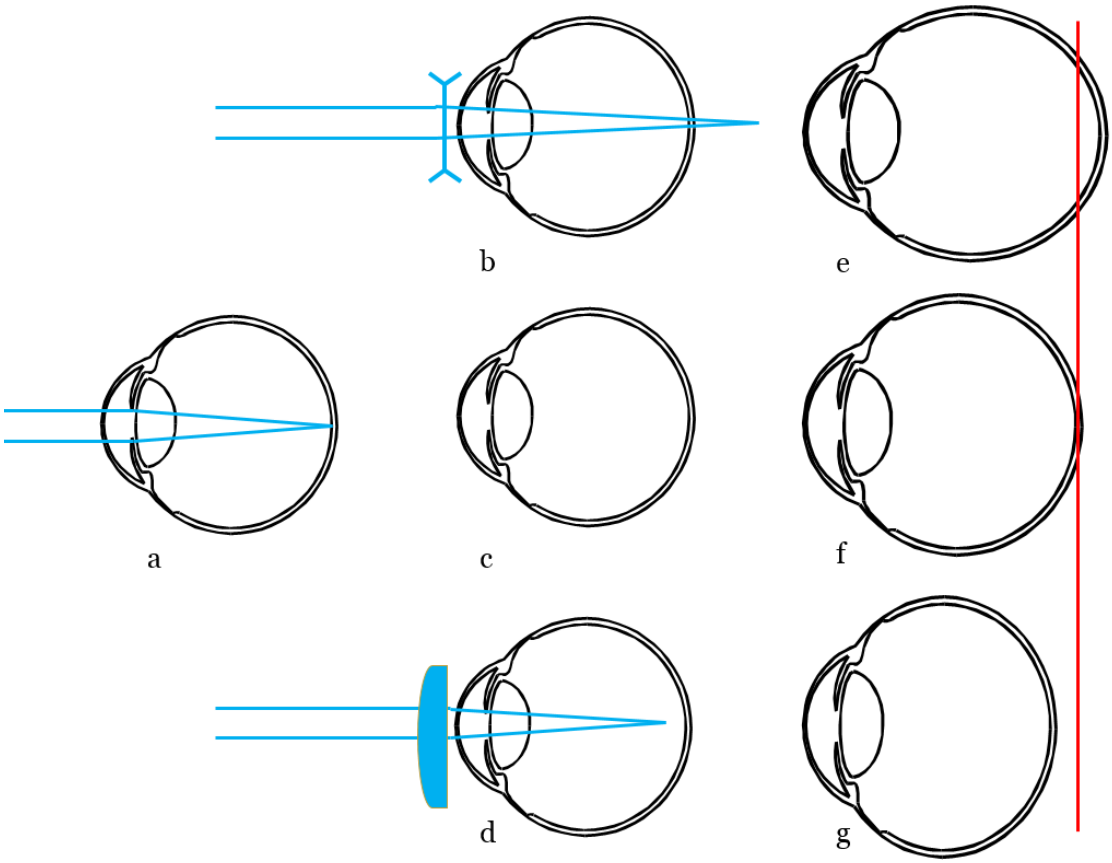

Figure 1. 1 Eye growth with and without defocusing lenses: a) initial state b) Negative lens treated eye, c) Eye with no lens treatment, d) Eye treated with a positive lens, e) after negative lens treatment, f) Normal growth, g) after positive lens treatment.

In the rest of the introduction, general concepts such as aberrations, image metrics, possible optical signals to direction of defocus and the imaging modality for cone photoreceptor imaging will be introduced.

1.2 Aberrations in the eye and image quality

The optical system of the eye is comprised of the cornea, pupil, and crystalline lens to project an image onto the retina. During growth, the ocular components change rapidly in early life in a way more complex than proportional scaling. As optics of eye ages, the image quality is affected by aberrations which change with age (Hunter, Campbell, Kisilak, & Irving, 2009; Kisilak, Campbell, Hunter, Irving, & Huang, 2006). Image quality of the eye is affected by the types and amount of aberration present. It has been shown that the eye grows in a finely tuned mechanism regulated by retinal images (or retinal blur) during emmetropization (Wallman & Winawer, 2004b).

To better understand how this growth mechanism works and why it breaks down in non-emmetropic (ametropic) eyes, it is important to compare the image quality (retinal blur) in normal developing eyes and eyes with lenses which impose defocus.
This section introduces the aberration types and image metrics used in this thesis to assess retinal image quality (retinal blur) in order to study its longitudinal changes as eye grows.

1.2.1 Sources of aberrations in the eye

There are limited studies on the relative contribution to total aberrations from ocular components due to the lack of techniques to accurately measure the internal surfaces and an accurate model of the gradient of refractive index in the chick crystalline lens. This means that we cannot accurately model the relative contributions of separate components to the aberrations in chicks. However, the anterior surface of the cornea contributes to the optical aberrations of the eye while the rear surface contributes little. The lens contributes aberrations, both from its surface refractions and the internal gradient of refractive index. The aberrations associated with the gradient of refractive index are, in most animals, opposite in sign and partially balance those of the cornea. The retinal contributes little to optical aberrations. It is the overall effects of aberrations on retinal images that are of interest here, total aberrations of the complete eye were studied in this thesis.

1.2.2 Wavefront Aberration and image quality

The wavefront is the surface perpendicular to the direction of light ray propagations which links all wave segments with the same phase. Wavefront error is defined as the difference of the wavefront from its reference spherical wavefront (Figure 1.2). This difference can be represented mathematically using a series expansion. In chapter 2, Methods of the thesis, the ways to measure the aberrations of a complete eye and Zernike polynomials to fit aberrations are introduced. The second-

order polynomial terms represent the sphero-cylindrical refractive errors, terms higher than second order are collectively known as higher order aberrations.

Despite the complexity of the optical system of the eye, wavefront error measurements (Fig 1.2) provide a way to study the image formation of the eye as a whole and metrics derived from the wavefront or image give estimates of the image quality of the optics. Some metrics such as root mean square wavefront aberrations (W_{RMS} Equation 1.1) do not have a good assessment of the image quality unless it is small (Thibos, Hong, Bradley, & Applegate, 2004a).

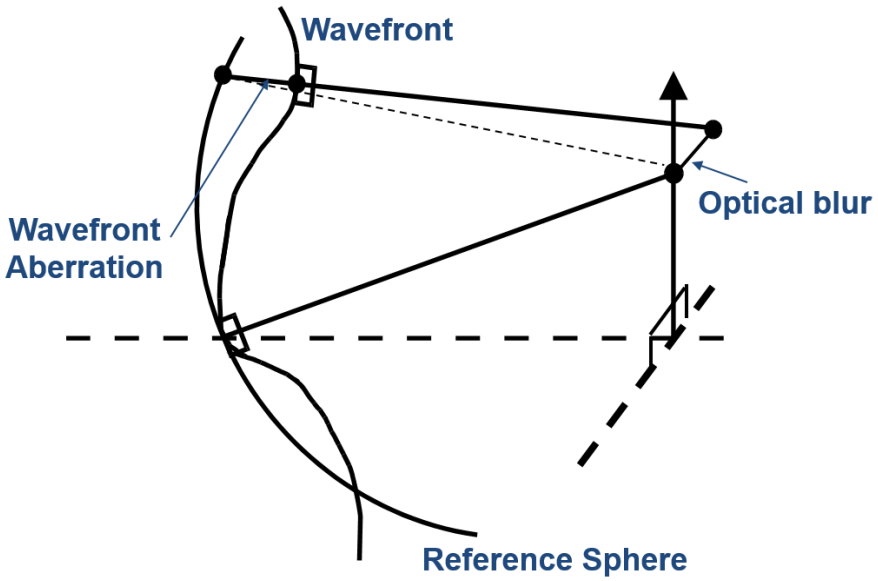

Figure 1. 2 Wavefront aberration (Used from Campbell labs with permission of Prof. Campbell)

$$W_{RMS} = \sqrt{\overline{W^2} - \overline{W}^2}$$

Equation 1. 1

This section focuses on the subtype of monochromatic aberrations in depth and its influence on image quality. In addition to monochromatic aberrations, the image can also be degraded by chromatic aberrations due to the dispersion of light in media, which is briefly introduced here.

Chromatic aberrations

Chromatic aberrations arise because of the differences in refractive index for different wavelengths. Short wavelengths is refracted more than the longer wavelength. Longitudinal chromatic aberration (LCA) is termed as the focusing power difference on axis (Figure 1.3). Transverse chromatic aberration (TCA) is the focuses difference off axis, altering the location of retinal image (Figure 1.4). TCA depends on the refractive index difference and the alignments between the cornea, lens, and retina.

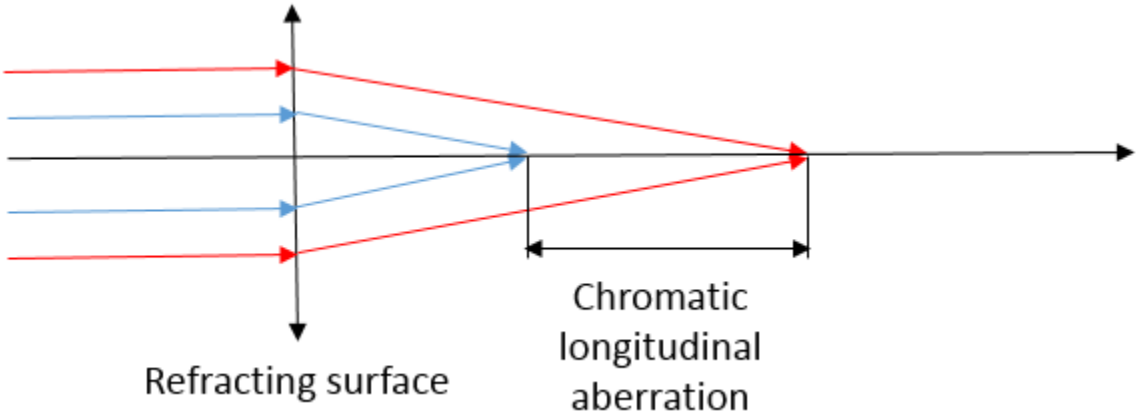

Figure 1. 3 Schematic of longitudinal chromatic aberration

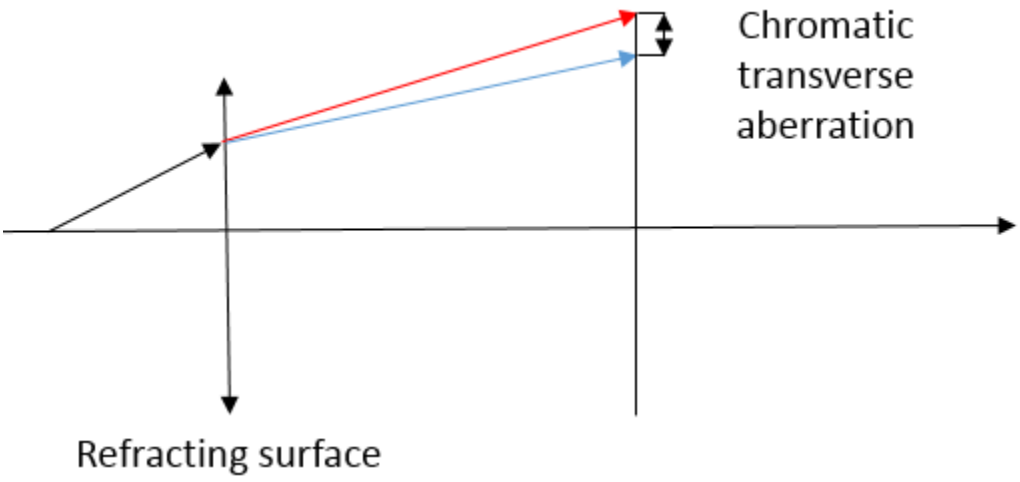

Figure 1. 4 Schematic of transverse chromatic aberration

1.2.3 Monochromatic aberrations

The components of the total wavefront error are called monochromatic aberrations (spherical defocus, astigmatism, and higher order aberrations) and have different effects on image blur.

Spherical defocus

Spherical defocus alters the location of image point in front of or behind the image plane (Retina), known as myopic defocus or hyperopic defocus respectively which collectively are ametropia. To correct the ametropic eye, negative (diverging) lenses or positive (converging) lenses can be used. The power of the correcting lens (S) is the spherical refractive error, which is the spherical part of the eyeglasses prescription.

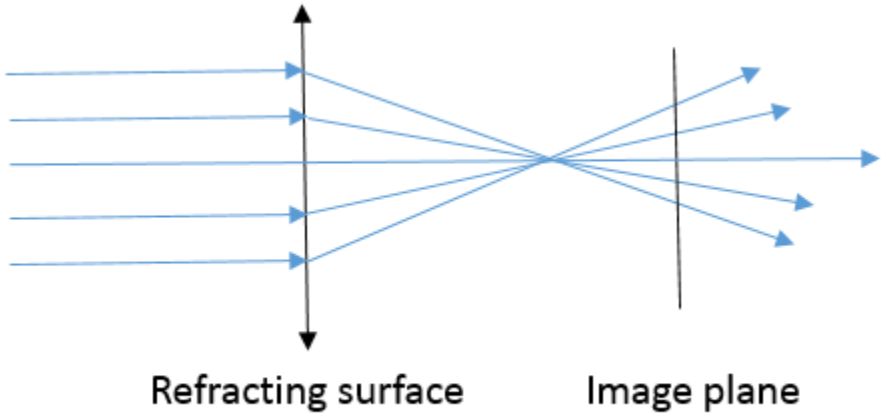

Figure 1. 5 Schematic of myopic defocus

Astigmatism arises due to different powers in different meridians of a refracting surface. The refracting surface can be modeled as a toroid with different curvatures and powers in two mutually perpendicular meridians. The power difference D between two meridians is termed as astigmatism. Therefore, two focal lines form. The pencil of rays from the highest power meridian converge to a single point closer to refracting surface and determine the position of the first focal line, the pencil of rays from the lowest power meridian determine the position of the second focal line. The disc of least confusion sits midway between these two lines dioptrically (not geometrically). This is the location of a circular blur, any other plane would present an elliptical blur with orientation dominated by the closer foci line.

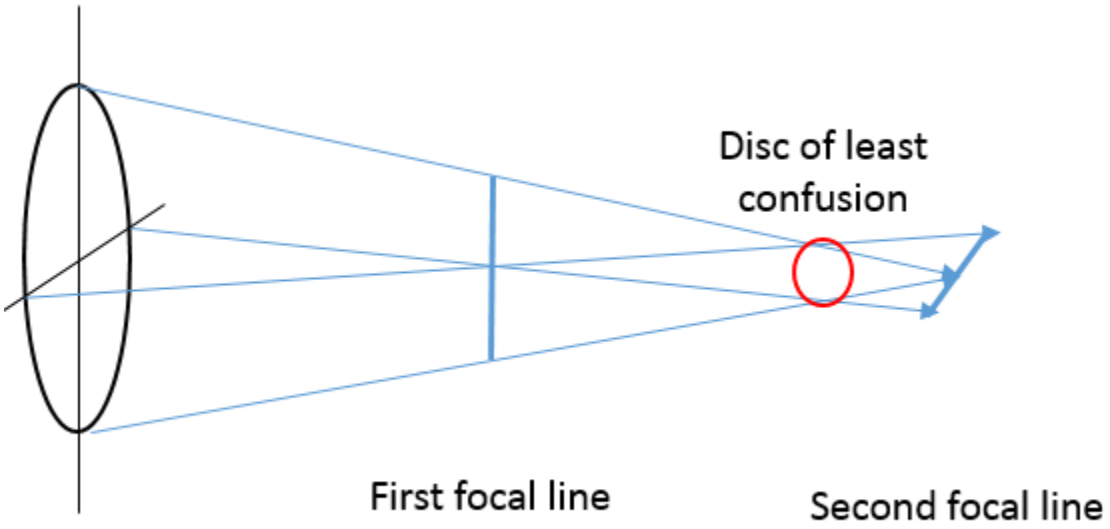

Figure 1. 6 Schematic of astigmatism, in this case, plotted as against the rule astigmatism where the high power meridian (maximum curvature) is in a horizontal direction.

Astigmatism can be corrected with a cylinder lens. The power of a cylinder can be denoted as the power (D) of meridian perpendicular to the cylinder axis which has zero power. θ ranging from 0° to 180° in a counter clockwise direction with respect to horizontal designates the cylinder axes position in a spectacle lens prescription (ISO 8429: standard 1997). If there is a spherical error as well as a cylinder error then a toroidal surface which is optically equivalent to a sphero-cylindrical lens with spherical power (S) for the weaker principle meridian and cylindrical power (C) which is the absolute power difference between two perpendicular meridians is needed. The mean power M of an astigmatic lens, termed as mean sphere is the mean of the two principle powers S and (S+C). In eye glasses prescription, the mean sphere is also known as the mean ocular refraction (MOR) which is the power needed to place the disc of least confusion on the retina when the eye is not accommodated:

$$MOR = S + \frac{C}{2}$$

Equation 1. 2

Accommodation, astigmatism and the retinal image

To better understand the resulting optical blur on the retina as the eye accommodates with both astigmatism and spherical defocus, it is important to know the position of the retina with respect to two foci lines and disk of least confusion. Accommodation is the process of increase in refractive power in the eye, which moves the disk of least confusion and two foci line closer towards the vitreous side of the eye.

Accommodation does not change the relative location and length of two foci lines, but the projection of the blur on the image plane can differ as it moves the position of these features with respect to the retina. Figure 1.7 shows an example of accommodation effects with initial hyperopic astigmatism where the blur changes with the amount of accommodation and decreases to a minimum when the disc of least confusion is on the retina. Note that accommodation, which increases eye power, does not improve the visual quality in myopic astigmatism when the second line focus is on or in front of the retina.

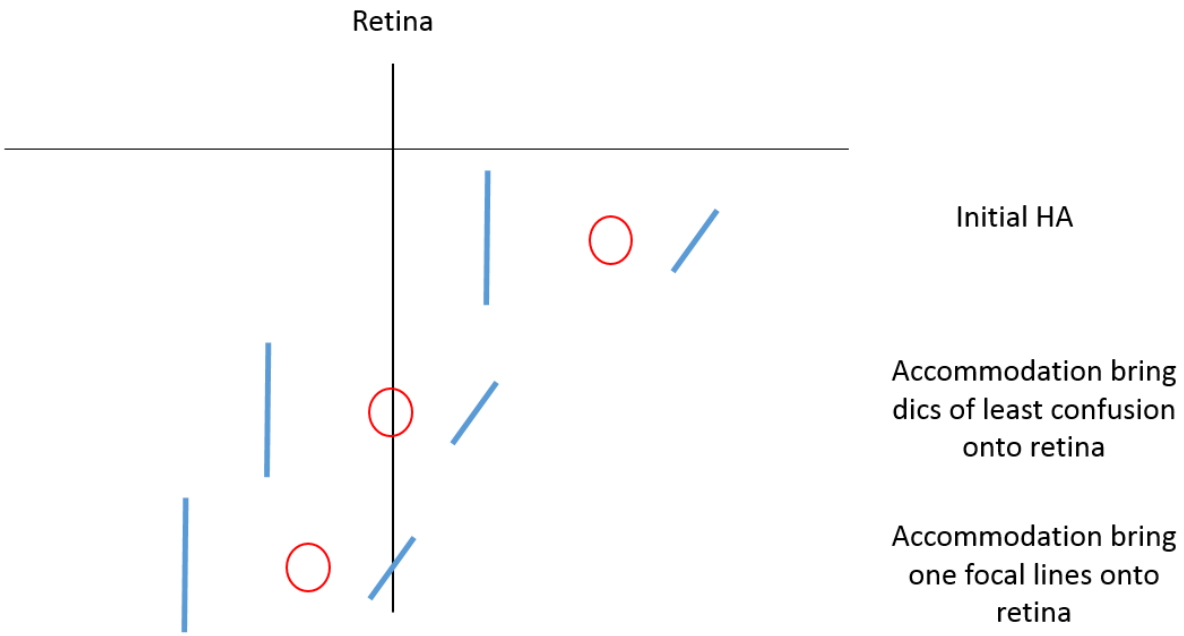

Figure 1.7 Schematic of accommodation effects on an example of initial hyperopic astigmatism. $\boldsymbol{Measured\ mean\ refraction, MR = S - \frac{C}{2}}$ **where C (Negative Cylinder) is unchanged in three cases, If the instantaneous mean refraction is measured is the dioptric distance of red circle from the retina, initially** $\boldsymbol{MR < 0}$**, then** $\boldsymbol{MR = 0}$**,** $\boldsymbol{MR > 0}$ **from top to bottom.**

Higher order aberrations

Higher order aberrations refer to the wavefront aberration terms of 3rd order and higher, such as trefoil, coma, spherical aberration, quadrofoil.

Spherical aberrations arise when marginal rays focus at a different location (marginal focus) along optical axis than paraxial rays (paraxial focus or Gaussian focus). The difference between marginal image and the paraxial image is the longitudinal aberration.

Spherical aberration is rotationally symmetric about the optical axis, resulting in a circular blur shape. There exists a minimum circular blur at the disk of least confusion. This disc may be shifted by spherical aberration from the position given by astigmatism alone. Coma produces an asymmetrical blur shape in the image plane and the amount of blur will remain asymmetrical no matter where the focal plane is placed. Other terms in the wavefront error expansion also exist (Wyant & Creath, 1992).

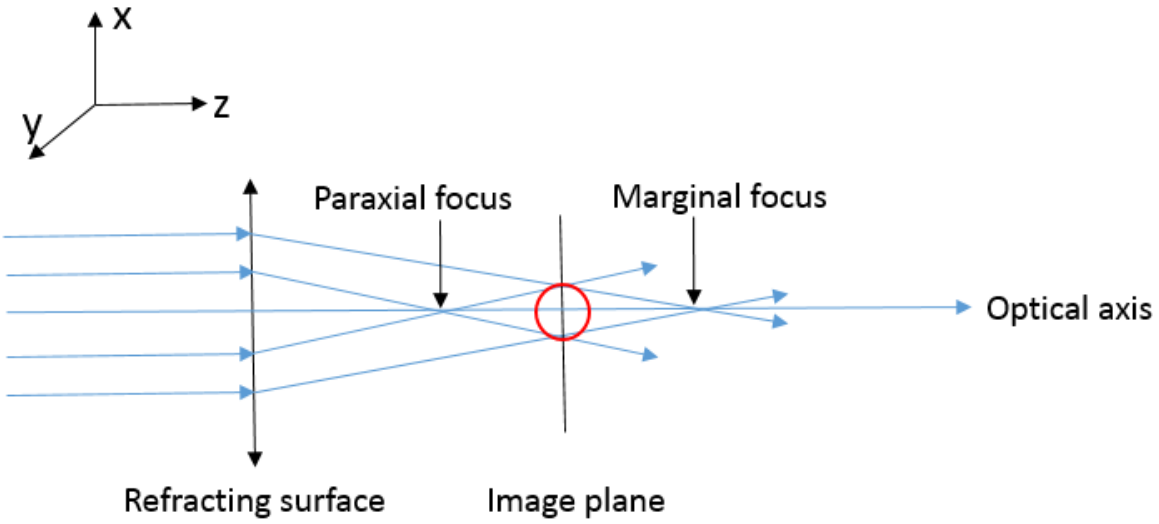

Figure 1. 7 Schematic of spherical aberrations, in this case, the disk of least confusion sits on the image plane (retina) if only spherical aberration is present in the Zernike expansion. The spherical defocus term tells you how far the disc of least is from the retina.

1.3 The Point spread function

Light from a point source at infinity propagates as plane waves. If it is incident on a screen containing an aperture, only a fraction of the plane wave propagates through the aperture, consequently, the image is never a perfect reconstruction of the point source but a diffraction pattern.

The point spread function (PSF) is the intensity distribution of an emitting point source at infinity after it has passed through a given optical systems onto a screen in image space. For a circular aperture in an optical system with no aberrations, the point spread function is a diffraction limited pattern, a highly compact spot image, known as an Airy disk. The final image is the convolution of the PSF with the intensity distribution of the object (Hecht, 2002). Thus, the PSF is an important concept to describe the blur created in an image by an optical system. When the system creates wavefront aberrations, the spread of PSF will be larger than the Airy disc and the observed image blur is larger.

The PSF is related to the wavefront aberrations $W(x,y)$ (W in Figure 1.2) by:

$$PSF(x,y) = K * \left| FT\left\{P(x,y) * e^{-\frac{2\pi i}{\lambda} * W(x,y)}\right\}\right|^2$$

Equation 1. 3

Where K is the constant usually neglected. $P(x,y) * e^{-\frac{2\pi i}{\lambda} * W(x,y)}$ is known as pupil function, $P(x,y)$ is part of the pupil function, defining the shape, size and transmission of the optical system. $W(x,y)$ is the wavefront aberrations. In a real eye, transmission varies due to the absorption of lens. The effective intensity of a ray reaching the photoreceptor layer can be modeled by incorporating Stiles Crawford effect (Snyder & Pask, 1973) which reflects the fact that obliquely incident rays are not waveguided as efficiently by the cone photoreceptors. If this effect is accounted for, the pupil function would take the form of a Guassian function (Artal, 1989).

In the case of diffraction limited system with circular aperture, the irradiance distribution is an Airy disk:

$$PSF(r) = I_0[\frac{2J_1(r)}{r}]^2$$

Equation 1. 4

1.4 Image metrics derived from wavefront aberrations

Although methods have been developed to accurately measure the aberrations of the eye, for years, people have searched for a single parameter that can best predict the image quality, i.e. when image quality is "better" or what the eye can 'see' given the amount of aberrations. In human, image metrics derived from wavefront aberrations have been well studied and their performance in predicting visual performance and acuity was compared to subjective measurement systematically (Thibos, Hong, Bradley, & Cheng, 2002; Thibos et al., 2004a). Image metrics can be categorized into two types depending on where they are calculated based on aberrations measurement, Firstly, image plane metrics are determined in retinal space such as from the point spread function in the spatial domain and the modulation transfer function in the Fourier domain. Secondly, pupil plane metrics are determined from measurements in the pupil plane of the wavefront aberrations. Most commonly root mean square wavefront aberration was used as a metric (See section 1.2.2 Equation 1.1). In particular, it has been shown that those metrics calculated from the PSF in the image space (image plane metrics) gave better predictions in normal human eye of subjective refraction and acuity than those calculated from pupil plane measurements of wavefront aberrations(pupil plane metrics) (Guirao & Williams, 2003).

This part will briefly introduce image plane metrics and a simple metric derived from the pupil plane metric which shows a good approximation of radial extent of image plane metrics calculated in the thesis. For details refer to Chapter 3 and 4.

1.4.1 Image plane metrics calculated from the Point spread function

Metrics which quantify the size of the PSF include half width at half height (HWHH), Strehl ratio in space domain (SRX) (Thibos, Hong, Bradley, & Applegate, 2004b).

HWHH is the half width at half maximum intensity of PSF, given by the average width of every cross section of the PSF (Equation 1.5), HWHH describes the compactness of PSF, and larger HWHH means more spread of PSF intensity.

$$HWHH = \sqrt{\frac{1}{\pi}\int C(x,y)dxdy}$$

Equation 1. 5

Where $C(x,y) = 1\ if\ PSF(x,y) > \max(PSF)/2$, otherwise, $C(x,y) = 0$.

Strehl ratio (SRX) is widely used which also correlates with the spread of PSF intensity and gives better indication of image quality variation for relatively good quality (W. J. Smith, 2000), it is defined as the ratio of actual peak intensity of the PSF divided by the maximum of a diffraction limit PSF with same pupil size.

$$SRX = \frac{\max(PSF)}{\max(PSF_{DL})}$$

Equation 1. 6

1.4.2 Pupil plane metrics: RMS wavefront aberration

The variance of any wavefront aberration can be described by the root mean square of the wavefront aberrations. Root mean square aberrations () gives a general indication of the image quality of the optical system (or the eye). It combines all the aberrations from pupil plane and reveals little about the actual image quality on the retina because some aberrations types cause greater degradation in the PSF than others for the same RMS value. That is the same magnitude of RMS from different terms of the Zernike polynomial do not result in equivalent loss in optical quality, Zernike modes having lower angular frequency (near the center of Zernike pyramid) affect the PSF and visual acuity more than the ones near the edge (Applegate, Sarver, & Khemsara, 2002). A metric derived from RMS wavefront error known as total equivalent blur was proposed in our lab (Kisilak et al., 2006). Despite giving equal weighting to the Zernike modes, total equivalent blur (EB) gives a good approximation of the radial extent of total angular blur (PSF radius) on the retina (Hunter, 2006).

$$EB = \frac{4\sqrt{3}\,RMS}{r}$$

Equation 1. 7

Where RMS is the root mean square of wavefront aberrations and r is the radius of the pupil size.

It is much simpler to calculate than calculating the PSF from the wavefront aberrations via Equation 1.3 followed by a calculation of the extent of the PSF from Equation 1.5.

1.5 Optical signals guiding emmetropization

For individuals, emmetropization is the mechanism to maintain the optimal refractive error in early life. A fundamental question in emmetropization is what signals are present to guide the eye to distinguish the sign of defocus (hyperopic blur or myopic blur) in order to direct the eye to achieve the optimal refractive state. The retina itself may perform image processing independently to derive the sign of defocus. Without connection to the brain, eyes with optic nerve surgery showed intact emmetropization, though the endpoint refractive state is shifted (C. F. Wildsoet, 1997a), suggesting the brain is necessary for finer emmetropization mechanism. Visual cues such as chromatic aberrations, monochromatic aberrations including astigmatism, accommodation and diurnal rhythm which directly or indirectly affect the blur on the retina have been hypothesized to play important roles in the determination of the direction of defocus.

Though chromatic aberrations cause a color dependent focus difference between red and blue light for hyperopes and myopes, chromatic aberrations have been proven to be unnecessary for emmetropization. Chicks raised in monochromatic light were shown to reduce defocus normally (C. F. Wildsoet, Howland, Falconer, & Dick, 1993).

Accommodation is not a sole signal in emmetropization. Chicks raised in a vertical drum allowing only one viewing distance showed good refractive compensation (Park, Winawer, & Wallman, 2003). However, it is possible that accommodation indirectly plays a role in emmetropization by altering the blur on the retina (Wallman, 1993).

Diurnal rhythm is another important factor. A diurnal light cycle is crucial in the normal ocular growth (Weiss & Schaeffel, 1993). Circadian rhythm has been found in axial length, choroid thickness, pupil sizes in chicks (Tian & Wildsoet, 2006), those ocular parameters contribute to the change of MOR. Diurnal variation in MOR was quantified and compared with the changes in pupil sizes and axial length in chicks for normal emmetropization (M. C. Campbell et al., 2012). Preliminary results show that the diurnal variation becomes larger in the presence of defocus, possibly giving an enhanced signal to the direction of defocus (M. C. Campbell, Bunghardt, & Irving, 2009).

Monochromatic aberrations, including astigmatism, are a possible signal to provide information about the sign of defocus because they generate the different shape of images on the retina. It has been shown that humans with training, are able to tell the direction of defocus through the differences in their point spread function (Wilson et al., 2002). The appearance of the PSF was examined in eye models with 0.125 to 0.5D defocus, the intensity distribution of the PSF were different with opposite

sign defocus, and astigmatism was shown to have induced asymmetries in the PSF with different defocus (M. C. W. Campbell, Priest, & Hunter, 2001).

1.6 Resolution theory

1.6.1 Optical resolution of imaging system: diffraction limit

Resolution is the finest ability to discriminate two equal irradiance adjacent point sources at a distance as seen through the optics. For an aberration-free system, each point object forms a blur referred to as a point spread function (PSF) with the width of an Airy disk. As the distance between two point objects reduces, the image spots come closer and overlap. The minimum separation the two point sources that can just be resolved given by Lord Rayleigh's criterion is the radius of one Airy disk (Hecht, 2002):

$$\Delta l_{min} = 1.22\frac{f\lambda}{D}$$

Equation 1. 8

Where f is the focal length, λ is the wavelength of light, D is the diameter of the aperture.
The minimum angular separation that is resolvable is given by:

$$\Delta\theta_{min} = 1.22\frac{\lambda}{D}$$

Equation 1. 9

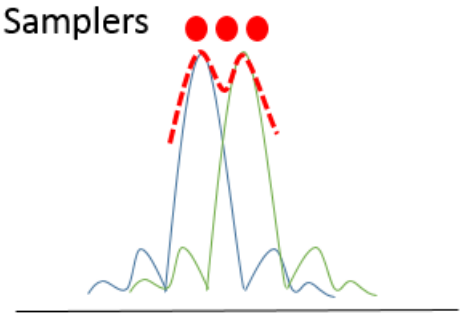

Figure 1. 8 Rayleigh optical criterion for distinguishing two point stimuli with equal intensity: they are resolved when the zero of one PSF coincides with the peak of the other PSF. Thus the separation of the two points that can just be resolved equals the redius of the Airy disc. The red dots represent the maximum cone spacing which will still sample the two point sources given by Shannon's sampling theorem. Each of two cones sample the peak of each stimulus and a third

cone samples the dip in between, so the two stimuli is resolved for a cone spacing that is twice the separation of the peaks.

In applying the Rayleigh criterion to get the optically defined minimum resolvable separation of 2 points, (figure 1.10A), there is a saddle in between two central peaks. Each peak falls on the position of the other's first minimum, so the minimum separation at which the two points can be optically resolved equals the radius of the PSF. When the system is no longer diffraction limited, we generalize the Rayleigh criteria as the closest approach at which two points can just be resolved is equal to the radius of the PSF.

1.6.2 Resolution of the eye: Nyquist limit

The fundamental limit of an image processing system is imposed by the ability to reconstruct the image. When there are insufficient receptors to match the optical resolution, sampling the stimuli determines the intrinsic resolution of the system. When there are enough receptors, the optical resolution determines the resolution. In a discrete signal processing system, sufficient samplers are required to reconstruct the image. Undersampling causes aliasing, resulting in incorrect reconstruction of the image. The baseline to match the optical resolution and have a reconstruction without aliasing is to have samplers at twice the frequency of the closest spacing of the point sources that can be resolved in optically. This is known as Nyquist limit, first proposed in communication technology by Harry Nyquist (National Research Council, 1990).

The retina is very much a sophisticated signal processing system which samples light and processes some information independently without connection to brain given that research shows animals with optical nerve severing still showed compensatory growth (C. Wildsoet, 2003). Cone photoreceptors are the first receptor cells on the retina responsible for light detection, thereby potentially determining the sampling limit of the eye. Therefore, the cone sampling frequency, calculated as the reciprocal of the spacing between two rows of presumed hexagonally packed (Kisilak, Bunghardt, Hunter, Irving, & Campbell, 2012; Kram, Mantey, & Corbo, 2010) cones, needs to be twice the frequency of the highest optical frequency that is resolved by the optics. In the spatial domain for a diffraction limited system, the spacing between two rows of cones has to be at most one half of the radius of one Airy disk. For example, in figure 1.10A, a third cone (red dot) is required to sample the dip in between two sampled peaks.

1.7 Adaptive optics aided retinal imaging

Adaptive optics is a cutting-edge technique to image the microstructure on the retina, particularly cone photoreceptors (Marcos et al., 2017).

The concept of adaptive optics was first proposed by Babcock to compensate the dynamic optical aberrations caused by atmospheric turbulence in astronomy (Babcock, 1953). Shortly after the invention of the Hartmann-Shack wavefront sensor which can accurately measure the wave aberrations, Liang &Williams combined the adaptive optics (a deformable mirror) with a Hartmann-Shack sensor and successfully obtained high-quality retinal images in Human, including the resolution of cone photoreceptors (Liang, Williams, & Miller, 1997). Previously, this had been difficult as the resolution of the retina did not increase with increasing pupil size as predicted by Equations 1.8 and 1.9 but decreased due to an increase in monochromatic aberrations of the eye with increasing pupil size, especially for pupil sizes larger than 3mm.

Nowadays, the application of adaptive optics in retinal imaging makes it possible to reveal microscopic structure at a cellular level. By shaping the wavefront to compensate for the aberrations in the eye, Adaptive optics (AO) aided retinal imaging enables transverse resolution close to the fundamental diffraction limit at larger pupil sizes. Groundbreaking work has been made with AO-OCT (three dimensional imaging of individual cone photoreceptors (Felberer et al., 2014)), AO flood illumination and AO scanning laser ophthalmoscope (AOSLO) (visualization of photoreceptors, retinal pigment epithelial cells, retinal ganglion cells (Rossi et al., 2017)). AO SLO is a state of art technology in vision science research, particularly in visualizing photoreceptors.

AO SLO is used in this project for cone photoreceptor imaging in living chick eyes. Below this technique is introduced.

1.7.1 Adaptive optics scanning laser ophthalmoscope

The conventional scanning laser ophthalmoscope was invented by Webb et al (Webb & Hughes, 1981), providing real-time imaging with axial sectioning of retina. As the image is formed point by point as scanners move a beam across the focal plane on the retina, the SLO has the advantage of providing video-rate imaging, giving rise to potential applications in visualizing metabolism changes such as blood flow. The limiting noise in a flood illumination imaging of the retina is the scattered light from retina structure other than the plane of interest. This problem was partially addressed by the limited size of the detector in the SLO and further addressed in the confocal SLO. In a confocal SLO,

a confocal pinhole blocks the unwanted wide-angle scattered and out of focus light. The fundamental working mechanisms of the confocal SLO (CSLO) are the same as the SLO with an additional confocal pinhole placed in front of the detector which restricts the light that can be collected by the photomultiplier (detector) used in the SLO. Thus, the combined confocal pinhole with a scanning laser source in a confocal scanning laser ophthalmoscope (CSLO) could produce a higher contrast image (higher signal to noise ratio) than flood illuminated imaging which illuminated the entire fundus and collected light scattered from the retina and other ocular structures as well as light reflected from all axial retinal layers (Webb, Hughes, & Delori, 1987). However, adaptive optics is needed so that the confocal pinhole can correct most of the light in the PSF focused on the pinhole.

The size of the confocal pinhole combined with the axial and lateral point spread functions governs the axial and lateral resolution in the CSLO. A small confocal pinhole will increase the resolution but reduce the amount of detected light. A proper size should be chosen considering both factors.

Conventionally, the size of the pinhole is defined in coordinates normalized to the Airy disk of the collection optics (Porter, Queener, Lin, Thorn, & Awwal, 2006):

$$1\ Airy\ disk\ raidus = 1.22\frac{\lambda f}{nd}$$

Equation 1. 10

Where λ is the wavelength of beam, f is the focal length, n is the refractive index in which the light is focused and d is the beam diameter. For example, in our AOSLO system, the imaging wavelength is 760 nm, the collector lens in front of the confocal pinhole (air, n = 1) has f= 150 mm, the beam diameter is ~3.5mm, the radius of the Airy disk at the pinhole is 39.7 um. The actual pinhole size is larger than this to increase the detected light levels because the actual point spread function at confocal pinhole is broader than an Airy disk due to residual aberrations following adaptive optical correction.

The resolution of the SLO was limited both laterally and in its ability to section retinal layers due to the aberrations in the eye. With AO included in the instrument design, the axial resolution was improved from 200 nm to 100nm and lateral resolution to 2.5 um (Roorda et al., 2002), making it possible to see the microscopic structures of the retina at a cellular scale.

An adaptive optics (AO) aided confocal scanning laser ophthalmoscope (AO SLO) provides a noninvasive method to study the normal or pathological retina at a microscopic scale at live video

rates. The first application of AO in a confocal scanning laser ophthalmoscope (CSLO) was proposed by Roorda et al, allowing axial retinal sectioning and visualization of cone photoreceptors, the nerve fiber layer, and flow of blood cells in human with improved lateral and depth resolution (Roorda et al., 2002). The novel design combines adaptive optics correction of the aberrations and defocus of the eye, a confocal pinhole and raster scanning at video rates, which had significant ramifications in revealing microscopic retinal structure.

1.7.2 Photoreceptor imaging with AOSLO

There was a long time debate on the possibility to resolve the photoreceptors using the optics of the eye itself. The sampling theory (Nyquist limit) states that the samplers can only interpret optical frequencies that are half of their own frequency. Therefore, in order for us to view the frequency corresponding to photoreceptor spacing (the object), one would need the eye's optics to transmit twice the spatial frequency of the photoreceptor spacing and then it needs to be sampled by an imaging system with sensors at a matched spatial frequency (Snyder, Bossomaier, & Hughes, 1986). However, for the cone photoreceptors to "see" all the information that the eye's optics transmit, the cut-off spatial frequency of the optics can be matched to the Nyquist sampling frequency of the cone photoreceptors. That is, the cone photoreceptors have twice the sampling frequency as the optics. Thus imaging of the cone photoreceptor mosaic requires optics that is better than that which exists if the cone sampling is matched to the optics (Snyder et al., 1986).

The first successful attempt in imaging the cone photoreceptor mosaic in a vertebrate was by Land & Synder on a live garter snake with a conventional ophthalmoscope (Land & Snyder, 1985). They extrapolated the argument to suggest the possibility to image the photoreceptors in living human. But unlike the snake, human optics degrade with increasing pupil size. However, with corrected aberrations over a large pupil, the optics improve and the AO SLO to date provides the best image of the cone photoreceptor mosaic in human (Roorda & Williams, 1999) and in animals such as chicks (Headington, Choi, Nickla, & Doble, 2011; Kisilak et al., 2012) . It is important however that the images be taken at pupil sizes larger than the pupil in normal viewing conditions, so that the cone photoreceptor array will be resolvable even if the cone sampling is matched to the optical resolution. The cones are of great importance because they act as the first neurons to sample the light and photoreceptor dysfunction is a major cause of blindness in adults (Wright, Chakarova, El-Aziz, & Bhattacharya, 2010).

1.7.3 Cone photoreceptors in Chicks

Chickens are typical diurnal birds with seven types of photoreceptor cells, rods, and six cone types. 4 cones with oil droplets, the droplets are located at the inner segment and act as wavelength filters. Two cones without oil droplets are closely paired and act as a single unit, known as double cones, to facilitate luminance detection for motion perception. The 4 types of single cone are responsible for tetrachromatic color vision due to the differing oil droplets, which act like spectrum filters and thus the cones are maximally responsive to violet (360-380nm), blue (430-445nm), green (500-520nm) and red light (~570nm) respectively (Bowmaker, Heath, Wilkie, & Hunt, 1997). Double cones are most prevalent, taking up 40.7%, following by green cones 21.1%, red cones 17.1%, blue cones 12.6%, and violet cones 8.5% for normal chick retina including in mid-peripheral fields at day 15 (Kram et al., 2010).

The spatial distribution of cone photoreceptors have shown a certain degree of regularity as photoreceptors of of like type tend to avoid the vicinity of each other, resulting in hexagonally packed submatrices which are interleaved. 39% (Kram et al., 2010) *in vitro* and 40% (Kisilak et al., 2012) *in vivo* of the cones were found to be hexagonally packed.

When the longitudinal development of cones was studied using a confocal scanning laser ophthalmoscope without adaptive optics for normal chick eyes, no differences were found with growth in the angular cone density from day 0 to day 14, giving the angular cone spacing 4.18 arcmin, 4.16 arcmin on day 0 and day 14, respectively (Kisilak et al., 2012). With Adaptive optics correction, a significant increase was reported with age and no significant difference was found in angular cone densities between control and goggled eyes (Kislak, 2015), the corresponding change in angular cone spacing was 15% lower in day 14 than day 0.

The first research comparing retinal cells (cone photoreceptors and ganglion cells) between normal chicks with emmetropic eyes and eyes with induced myopia used an Adaptive optics multiphoton microscopy (Bueno et al., 2014). They measured the spatial distribution of cone photoreceptors between eyes and found no difference in the density between emmetropes and myopes for chicks at 4-week of age but they found enlarged ganglion cells bodies in myopic eyes. With AOSLO, we are able to compare the longitudinal changes of cone photoreceptor density between control eyes and eyes with imposed positive and negative defocus.

Chapter 2: Methods

General procedures

Groups of mixed gender chicks (total number 21) were acquired at the local hatchery on the day of hatching. Right eyes were goggled with +10D or -15D lenses with Velcro rings (Irving, 1993) on the first day (day 0). Left eyes grew normally. Measurements were performed on day 0 and subsequent days up until day 21. Goggles were briefly removed on some days to clean them to avoid form deprivation.

The experiments carried out in this thesis include measurements of aberrations in the growing chick eye and imaging of cone photoreceptors on the chick retina in normal growing eyes and eyes treated with different powered lenses. This is mainly accomplished through two instruments: a Hartman-Shack aberrometer and an Adaptive optics scanning laser ophthalmoscope, which will be introduced in this chapter.

2.1 Wavefront aberration measurement

2.1.1 Wavefront aberration aberrometry

Optical aberrations of the eye degrade the image quality and limit high-resolution imaging through the eye. In order to obtain the best image of the retinal structure, it is necessary to compensate the aberrations within the eye. Different techniques have been developed based on four main principles: outgoing reflection aberrometry (Hartman-Shack wavefront sensor), retinal imaging aberrometry (Tscherning and ray tracing aberrometry), ingoing adjustable refractometry (spatially-resolved refractometry), and double pass aberrometry (slit skiascopy) (MacRae, Krueger, & Applegate, 2004). Hartman-Shack aberrometry has been the most popular choice for wavefront aberration measurement in various clinical applications such as post-laser in-situ keratomileusis (LASIK) surgery (Thibos & Hong, 1999) because of its advantages of simultaneous objective measurement across the entire pupil with high spatial resolution and high speed.

2.1.2 Hartman-Shack aberrometry

The first application of the Shack-Hartmann wavefront sensing technique in vision science was the aberration measurement in the human eye (Liang, Grimm, Goelz, & Bille, 1994). The principle

involves the measurement of local slopes of the local wavefront emerging from a spot on the retina and reconstruction of wavefront surface using Zernike polynomials.

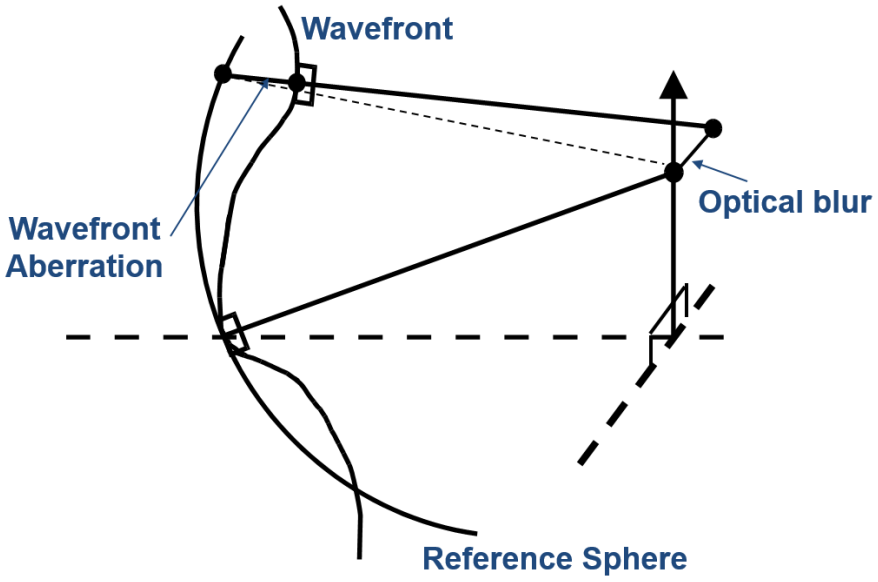

Figure 2. 1 Wavefront aberration (Used from Campbell labs with permission of Prof. Campbell)

2.1.3 Wavefront theory and image quality

In physical optics, light is described as a wave. Propagation of light can be described through either ray tracing, which is the actual optical path of the light or through wavefront, which are a surfaces perpendicular to ray propagation. In a eye with no aberrations focused on a point source, the incoming spherical wavefront would converge to a point on the image plane, the outgoing wavefront would be perfectly planar with boundary confined by the exit pupil. (Figure 2.1 reference sphere). In reality, the wavefront is not a perfect sphere, rays perpendicular to the wavefront will be focused at different locations because of aberrations. The distance from the paraxial focus to the actual intersection of the ray with the image plane is defined as the transverse aberration, resulting in additional optical blur. Longitudinal aberration is the separation along the optical axis from paraxial focus to the point of intersection with ray (figure 2.1). Wavefront aberration is the deviation of the intended wavefront shape from the reference wavefront. This wavefront error can be estimated by fitting the aberration with polynomials. The most popular choice is Zernike polynomials, a set of

basis function that is orthogonal to a unit circle. Each basis function represents a specific type of wave aberration.

In polar coordinate in the entrance pupil of the eye, the wavefront aberration is

$$W(\rho,\theta) = \sum_{m}\sum_{n} C_n^m N_n^m Z_n^m$$

Equation 2. 1

Where C_n^m shows the contribution of each aberration type present. As described in the proposed standard by OSA (Thibos, Applegate, Schwiegerling, & Webb, 2002), the Zernike polynomial contains three components, normalization Knoll's constant (N_n^m), and Z_n^m consists of a radial dependent component (R_n^m) and an azimuthal dependent component.

$$Z_n^m = \begin{cases} N_n^m R_n^{|m|}(\rho)\cos m\theta\,;\ for\ m \geq 0 \\ -N_n^m R_n^m(\rho)\sin m\theta\,;\ for\ m < 0 \end{cases}$$

Equation 2. 2

$$R_n^m(\rho) = \sum_{s=0}^{(n-|m|)/2} \frac{(-1)^s (n-s)!}{s!\,[0.5(n+|m|)-s]!\,[0.5(n-|m|)-s]}\rho^{n-2s}$$

Equation 2. 3

$$N_n^m = \sqrt{\frac{2(n+1)}{1+\delta_{m0}}}$$

Equation 2. 4

$$\delta_{m0} = \begin{cases} 1;\ for\ m = 0 \\ 0;\ for\ m \neq 0 \end{cases}$$

Equation 2. 5

Where ρ is the normalized radial distance in the pupil ranging from 0 to 1, θ is the angle from x axis along horizontal (nasal/temporal meridian) in a counter clockwise direction ranging from 0 to 2π, n is zero or positive integer represent the radial order of Zernike terms, m can only take the value as $-n, n+2, n+4, \ldots\ n$, representing the corresponding azimuthal frequency. Below shows the table of Zernike terms up to 4th order using right handed coordinate system, where z axis is along optical axis coming out of the eye.

n	m	Noll's constant N_n^m	Zernike basis Z_n^m	Aberration
0	0	1	1	Piston
1	-1	2	$\rho \sin\theta$	Tip
1	1	2	$\rho \cos\theta$	Tilt
2	-2	$\sqrt{6}$	$\rho^2 \sin 2\theta$	Astigmatism at axis $\pm 45°$
2	0	$\sqrt{3}$	$2\rho^2 - 1$	Spherical defocus
2	2	$\sqrt{6}$	$\rho^2 \cos 2\theta$	Astigmatism at axis 0° & 90°
3	-3	$\sqrt{8}$	$\rho^3 \sin 3\theta$	Trefoil
3	-1	$\sqrt{8}$	$(3\rho^3 - 2\rho) \sin\theta$	3rd Order Vertical Coma
3	1	$\sqrt{8}$	$(3\rho^3 - 2\rho) \cos\theta$	3rd Order Horizontal Coma
3	3	$\sqrt{8}$	$\rho^3 \cos 3\theta$	Trefoil
4	-4	$\sqrt{10}$	$\rho^4 \sin 4\theta$	Quadrafoil
4	-2	$\sqrt{10}$	$(4\rho^4 - 3\rho^2) \sin 2\theta$	2nd Order Astigmatism ± 45
4	0	$\sqrt{5}$	$6\rho^4 - 6\rho^2 + 1$	Spherical aberration
4	2	$\sqrt{10}$	$(4\rho^4 - 3\rho^2) \cos 2\theta$	2nd Order Astigmatism 0° & 90°
4	4	$\sqrt{10}$	$\rho^4 \cos 4\theta$	Quadrafoil

Table 2. 1 Zernike terms up to 4th order

Mathematically, the aberrations would be fit more precisely if more Zernike terms were used. The required number of Zernike coefficients (J) needed to effectively represent the true wavefront aberrations (surface function) including higher order aberrations and accurately measured by a Hartmann Shack for normal human eye is 42 (up to 8th order) (Liang & Williams, 1997). The maximum number of Zernike coefficients that can reliably calculate is approximately the same as the number of lenslets. This requires the number of lenslets (or Zernike coefficients J) in a Hartmann Shack to be at least 42 lenslets given by the equation below (Porter et al., 2006):

$$J = \frac{(N+1)(N+2)}{2} - 3$$

Equation 2. 6

Where J is the number of Zernike coefficients, N is the radial order of Zernike.

In chick analyzed in this thesis, where the pupil size which is smaller and has fewer aberrations than in humans, aberrations of chick eye are fitted up until the 4th order to at least 50 Hartmann spots. Therefore, the number of lenslets is sufficient to accurately measure the aberrations.

2.1.4 Hartman-Shack theory

The most important component in a Hartmann-Shack (H-S) apparatus is the use of a lenslet array. The lenslet array acts as many sub-apertures that divide the wave into segments and allow them to be focused as spots on the H-S image plane (Figure: 2.2). An ideal wavefront will form a regularly spaced grid where each spot of the grid is centered on the optical axis of the lenslet (Figure 2.2 top). This pattern is used as the reference pattern. A deformed wavefront will shift the image spots relative to reference image spots by an amount that is proportional to its local slope (Figure 2.2 bottom). In Cartesian coordinates, there exist a relationship between wavefront aberration ($W(x,y)$) and the local spot shift ($\Delta x\ \Delta y$) and the focal length (f) of lenslet in a material with refractive index n. (Liang et al., 1994):

$$\frac{\partial W(x,y)}{\partial x} = \mathrm{n}\frac{\Delta x}{f}$$
$$\frac{\partial W(x,y)}{\partial y} = \mathrm{n}\frac{\Delta y}{f}$$

Equation 2. 7

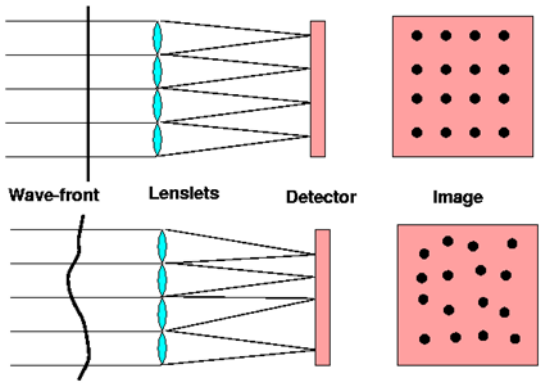

Figure 2. 2 Hartmann-Shack theory

The above equation in a matrix form is as following (Cubalchini, 1979):

$$\overline{C}(\overline{D})^T = \overline{S}$$

$\overline{D}$ is the derivatives of Zernike terms arranged in a matrix form, $\overline{S}$ is vector of the spots shift divided by the lenslet focal length for each spots (total number j) and $\overline{C}$ is a vector of the Zernike coefficients.

Equation 2. 8

$$\overline{D} = \begin{bmatrix} \frac{\partial Z_1^{-1}}{\partial x}(x,y)_1 \dots \frac{\partial Z_1^{-1}}{\partial x}(x,y)_j & \frac{\partial Z_1^{-1}}{\partial y}(x,y)_1 \cdots & \frac{\partial Z_1^{-1}}{\partial y}(x,y)_j \\ \vdots \quad \ddots \quad \vdots & \vdots \quad \ddots & \vdots \\ \frac{\partial Z_n^m}{\partial x}(x,y)_1 \dots \frac{\partial Z_1^{-1}}{\partial x}(x,y)_j & \frac{\partial Z_m^n}{\partial y}(x,y)_1 & \frac{\partial Z_m^n}{\partial y}(x,y)_j \end{bmatrix}$$

Equation 2. 9

$$\overline{S} = \frac{n}{f}\begin{bmatrix} \Delta x_1 \\ \Delta x_2 \\ \dots \\ \Delta x_j \\ \Delta y_1 \\ \Delta y_2 \\ \dots \\ \Delta y_j \end{bmatrix}$$

Equation 2. 10

Then the list of Zernike coefficients of the wavefront aberration, $\overline{C}$ can be decomposed as described below:

$$\overline{C} = (DD^T)^{-1}(\overline{D})(\overline{S})$$

Equation 2. 11

$$\overline{C} = \begin{bmatrix} C_1 \\ C_2 \\ \dots \\ C_j \end{bmatrix}$$

Equation 2. 12

Therefore, the component aberrations, W_{RMS} and PSF, can be derived can be derived.

2.1.5 Limitation on Hartmann-Shack

Potential problems may arise such as multiple spots, spots overlapped or crossed over or if the spacing of lenslet and the number of lenslets is not properly designed. As the spot displacement (Δd) is proportional to the focal length f and the wavefront slope θ (Figure 2.3), the dynamic range of Hartmann-Shack, defined as the maximum wavefront slope (θ_{max}) the system can measure (MacRae et al., 2004) is calculated as:

$$\theta_{max} = \frac{\Delta d_{max}}{f} = \frac{s/2}{f}$$

Equation 2. 13

Where s is the lenslet pitch (lenslet spacing).

Decreasing focal length can increase the dynamic range; however, this will reduce the measurement sensitivity (θ_{min}), which is defined as the smallest wavefront slope the system can measure:

$$\theta_{min} = \frac{\Delta d_{min}}{f} = \frac{2\Delta d_{min}\theta_{max}}{s}$$

Equation 2. 14

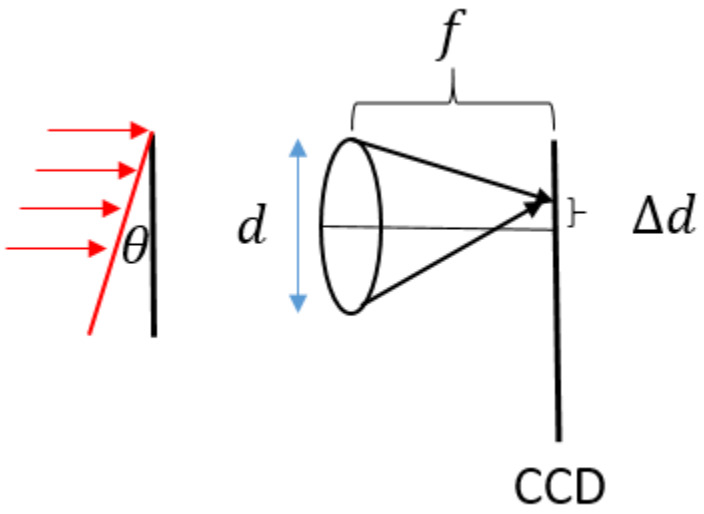

Figure 2. 3 Schematic showing wavefront slope θ, displacement Δd, focal length f and diameter of lenslet d .

2.1.6 Modified Hartmann-Shack for animal use

In a traditional Hartmann-Shack wavefront sensor, the pupil is conjugate with the lenslet array (LA), the retina is conjugate with the CCD camera, and the lenslet is placed at the focal point of the second lens. This design has been modified by our lab to make it more compact and appropriate for an animal with a small pupil size (Kisilak et al., 2006). In the modified setup, the lenslet array (LA) is placed against the final lens which is of a higher power (Figure 2.4). The specific design has been published (Kisilak, 2005).

In this thesis, the light source was a He-Ne laser source (633nm) rather than infrared used in commercial Hartmann-Shack for human.to aid alignment of the beam with the chick pupil and measure the aberrations for a more natural pupil size. The pupil is expected to constrict somewhat in response to the light. The lenslet array was composed of a square grid of 0.25 mm diameter lenslets with 19 mm focal length. Low room illumination was kept during the experiment to eliminate background light

A customized design ensures the balance between dynamic range θ_{max}, measurement sensitivity θ_{min} and spatial resolution across a small pupil for better image of Hartman-Shack spot. This design has been shown by our lab to be able to measure spherical defocus with a good agreement with

retinoscopy, a common subjective method on mean ocular refraction, with 1D systematic difference between the two measures. This 1D difference is mostly likely attributed to the chromatic aberration as wavelength used for the Hartmann-Shack and retinoscopy is 632.8 nm (red light) and white light respectively. There might be also be a small eye artefact (Glickstein & Millodot, 1970) which could change with wavelength with the possibility of the white light reflection not coming from photoreceptor layer but from the retinal vitreal interface.

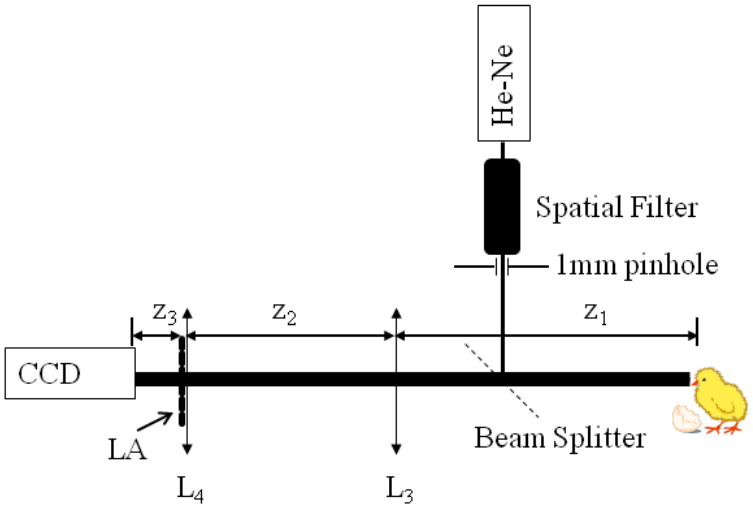

Figure 2. 4 Schematic of Hartman Shack, modified use for animal (Used from Campbell labs with permission of Prof. Campbell)

2.1.7 Hartmann-Shack pattern analysis

Satisfactory images were chosen for wavefront error analysis for larger pupils if all spots were visible, there were no reflections and a relatively even spot intensity across the pupil. Larger pupils were assumed to indicate less accommodation as pupillary and accommodative response are linked in chicks (Schaeffel, Howland, & Farkas, 1986). Images were then analyzed using the software Wavefront analyzer, developed in our lab to calculate the spot shift in the H-S images and to calculate the Zernike coefficients. To further exclude the errors from natural accommodation in chicks, mean ocular refractions (MORs) calculated from Zernikes were examined, more negative MORs from a given set of measurements were assumed to correspond to an accommodated state and were not used

in average values. When determining the range of refractive states on a given day (Chapter 4), values for all frames were used. Below shows sample images analyzed in the thesis (Figure 2.5).

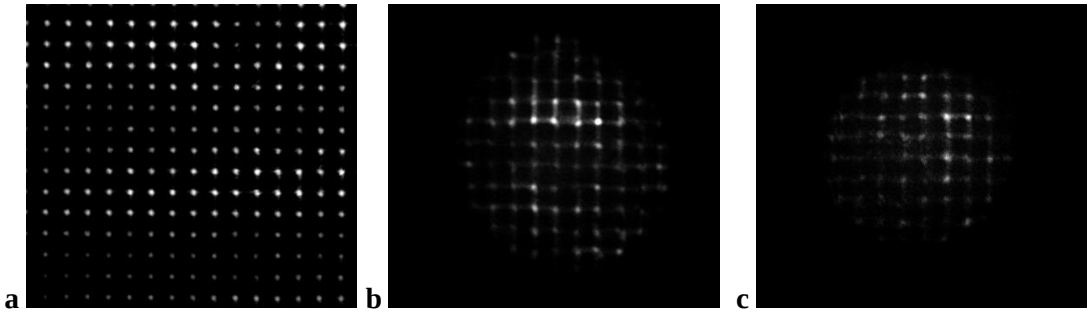

Figure 2. 5 Hartmann-Shack sample images a) a image taken through the apparatus with no eye present b) Control eye c) Goggled eye with negative trial lens correction. The reference image is taken when a mirror is placed at the position of the chick.

2.1.8 Image metrics calculated from Hartman-Shack measurement

Wavefront aberrations

The root mean square of wavefront aberration (W_{RMS}) is a measure of the variance of the wavefront aberrations, which gives a general description of image quality across the entire pupil. Large RMSW corresponds to poor image quality. Because individual Zernike polynomials are orthogonal and normalized, RMSW can be written as the square root sum of squares of all the Zernike coefficients:

$$W_{RMS} = \sqrt{\overline{W^2} - \bar{W}^2} = \sqrt{\sum \frac{1}{N_m^n} * Z_m^n} = \sqrt{(Z_0)^2 + (Z_2^{-2})^2 + (Z_2^2)^2 + \cdots}$$

Equation 2. 15

Retina blur calculation

In the calculation of the PSF (Equation 1.3 and chapter 1), transmission is equally weighted within pupil so P(x, y) is 1, and set to zero elsewhere outside.

The radial extent of angular spherical defocus PSF is well approximated by the new metrics proposed in Campbell lab (Kisilak et al., 2006) and is an exact calculation for the angular measure of blur assuming all blur is due to spherical defocus, known as equivalent blur (EB):

$$EB = \frac{4\sqrt{3}\, Z_2^0}{r}$$

Equation 2. 16

Geometric image blur is proportional to the first derivative of the wavefront aberration. It is possible to derive angular blur for individual aberration exactly. To combine different aberration types present, the constants from each aberration types are assumed to be the same as for spherical defocus (even though they aren't,) giving the more general calculation of EB as following:

$$EB(general) = \frac{4\sqrt{3}\sqrt{\sum \frac{1}{N_m^n} * Z_m^n}}{r}$$

Equation 2. 17

Total defocus equivalent blur (TDB) and total equivalent blur (TOB) calculated from above equation and previously gave a good approximation of the radial extent of the blur (Hunter et al., 2009) :

:

$$TDB = \frac{4\sqrt{3} \times RMS_{total\ defocus}}{r}$$

Equation 2. 18

$$TOB = \frac{4\sqrt{3} \times RMS_{total\ aberration}}{r}$$

Equation 2. 19

The extent of total optical blur and its components can be estimated well from the components of RMS aberrations and total RMS aberrations based on the definition of equivalent blur.

Refractive error calculation

Standard ophthalmic convention utilizes sphero-cylinder lenses correcting the refractive errors of the eye with its spherical power (S), cylinder power (C) and cylinder axis (φ) in a polar form, making it difficult for scalar analysis for population studies. In addition, as the cylindrical lens contains some spherical power, the dependence between cylinder power (C) and spherical power (S) makes the statistical analysis problematic. This issue is addressed by the Fourier analysis approach (Thibos, Wheeler, & Horner, 1997).

In a conventional method, the power profile of an arbitrary refracting surface $P(\theta)$ is written as following:

$$P(\theta) = S + C(\cos(\theta - (\varphi + 90°)))^2$$

Equation 2. 20

This can be shown (Thibos et al., 1997) to be equivalent to:

$$P(\theta) = S + \frac{C}{2} + \frac{C}{2}\cos(2(\theta - (\varphi + 90°))$$

Equation 2. 21

The constant term now is independent of the harmonic term.
This approach associates each term with physical lenses that are easily added up, the constant term is a spherical lens with power ($S + \frac{C}{2}$), the cosine term describes the power of a Jackson cross Cylinder with power $\frac{C}{2}$ and its axis angle inclined at $\varphi + 90°$. A JCC lens can be further written as two characteristic lenses, $JCC0$ at axis 0° and $JCC45$ at axis 45°.

$$JCC = \frac{C}{2}\cos(2(\theta - (\varphi + 90°)) = \frac{C}{2}\cos(2(\varphi + 90°)\cos 2\theta + \frac{C}{2}\sin(2(\varphi + 90°)\sin 2\theta$$

Equation 2. 22

$$JCC0 = \frac{C}{2}cos(2(\varphi + 90°)$$

Equation 2. 23

$$JCC45 = \frac{C}{2}\sin(2(\varphi + 90°)$$

Equation 2. 24

$$C = -2\sqrt{JCC0^2 + JCC45^2}$$

Equation 2. 25

Thus, the astigmatism of an optical system can be fully described by total Cylinder (C) and its components $JCC0$, and $JCC45$. JCC0 corresponds to horizontal/vertical astigmatism, JCC45 corresponds to oblique astigmatism. They can be calculated from the corresponding Zernike terms (Thibos et al., 2004a):

$$JCC0 = \frac{-2\sqrt{6}Z_2^2}{r^2}$$

Equation 2. 26

$$JCC45 = \frac{-2\sqrt{6}Z_2^{-2}}{r^2}$$

Equation 2. 27

Mean ocular refraction, defined as the mean refractive error of eye power, is aimed at placing disc of least confusion on the retina for an eye with refractive errors, which can be calculated from the spherical defocus Zernike term (Thibos et al., 2004a):

$$MOR = \frac{4\sqrt{3}Z_2^0}{r^2}$$

Equation 2. 28

2.2 In vivo cone photoreceptor imaging

2.2.1 Image formation of cone photoreceptor in AO SLO

Cone photoreceptors are both stimulated and imaged with light. Cone photoreceptors are known to waveguide light. The size and structure of cone photoreceptor enable it to behave similarly to an optical fiber. Figure 2.6 shows a simplified structure of cone photoreceptor. Primary reflections of a single cone photoreceptor come from two parts: 1) junction between inner and outer segments (OS), 2) posterior tips of the outer segment. Thus, reflectance from each cone photoreceptor is the sum of weighted intensity from two layers of point sources.

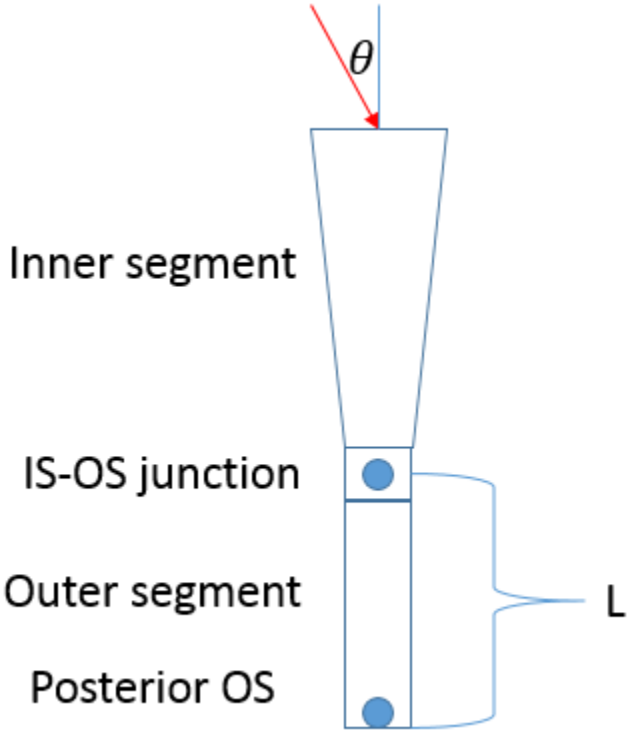

Figure 2. 6 Image formation of cone photoreceptors in AO SLO

2.2.2 Adaptive optics scanning laser ophthalmoscope

Waterloo AO CSLO

The Waterloo AO CSLO can be operated in a larger field of view in human as well as a smaller field of view in animal port to facilitate retinal imaging.

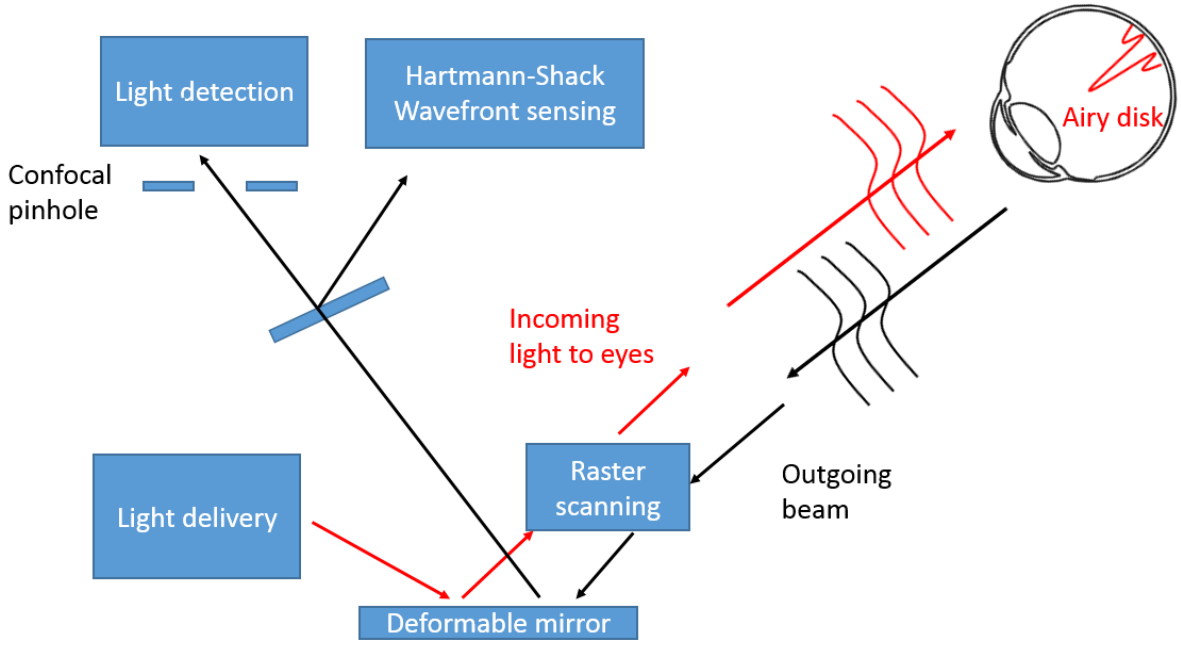

Figure 2. 7 Schematic of Adaptive optics scanning laser ophthalmoscopy

Figure 2.7 shows the schematic of Adaptive optics confocal scanning laser ophthalmoscopy. It is comprised of five major parts: 1) Light delivery; 2) Wavefront sensing; 3) Wavefront compensation; 4) Raster scanning 5) Confocal detection or light detection. The wavefront sensing is used to decide the shape needed on the deformable mirror.

Light delivery

A well-collimated single-mode optical fiber (FO) produces the beam of 760nm with bandwidth 15 nm for the SLO beam. Maximum permissible exposure (MPE) to laser light is governed by the American National Standards Institute (ANSI) standard. MPE for 760nm, 1 degree of raster scanning size with duration 900s, is 785 uW, this represents 63.6% of the ANSI threshold (Physical sciences institute, 2010).

Wavefront sensing

A Hartmann-Shack lenslet array is placed conjugate with the optical path of subject's pupil to measure the aberrations at the pupil plane of the eyes.

Wavefront compensation

A deformable mirror is placed before the raster scan to compensate the aberrations of both incoming light (red line) to reduce the spot on the retina, forming a near diffraction limit Airy disc and outgoing light to reduce the size of the spot on the confocal pinhole.

Raster scanning

Galvanometric scanners are placed conjugate to the entrance pupil. Horizontal scan (HS) produces a line on the retina and the vertical scan (VS) scans that line producing a square field. The line rate and frame rate (set by the HS) is 525 lines per frame and 30 frames per second (set by VS).

Light detection

A confocal pinhole (CP) is placed in front of a photomultiplier (PMT) to block the unwanted light from out of focus planes. The ideal pinhole size is about 39.7 um calculated in the above Equation 1.10 with wavelength 760nm, beam size 3.5mm, focal length 150mm. The actual pinhole is larger than this to increase the amount of detected light.

Animal imaging port in Waterloo AO CSLO

Field of View Measurement

When imaging chicks with a smaller pupil size than in humans, an additional mirror is added in the optical path to minify the beam to about 3.5 mm diameter. Given the measured pupil size (~2.5 mm naturally dilated under IR on day 0), the Rayleigh criterion gives optical resolution of 1.27 arcmin (Equation 1.8). In order to obtain the density of photoreceptors, the field of view was calibrated. Before the experiment, a +20D lens was placed at the pupil plane and a ruler was placed at the focal plane of the lens as an artificial retina. Images were then saved in best focus. The ruler was then moved close or away from the lens, images were saved in the two directions at the edge of the depth of focus when the image started to blur.

The field of view can be calculated as:

$$tan\theta = \frac{image\ size}{focal\ lenth}$$

Equation 2. 29

Best focus image is shown in the figure, the number of pixels of the total image is 1000 (width) times 1024 (height).

The focal length of the +20D lens was 50mm, since best-focused images were found at a back focal length of 45 mm, 45 mm was chosen as the effective focal length. The image size of the grey arrow (Figure 2.8) was calculated to be 4.92 mm as follows:

$$image\ size = \frac{grey\ arrow}{Total\ height}\frac{1024pixels}{208pixels} * 1mm$$

Equation 2. 30

Given Equation 2.35, the field of view is 6.22°. The field angle subtended by a single pixel is 0.37 minute of arc.

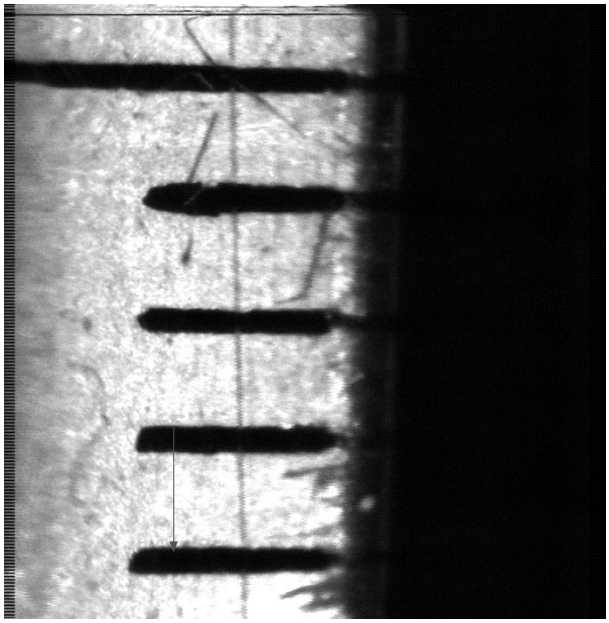

Figure 2. 8 Calibrating field of view in AO CSLO

To study the longitudinal changes of photoreceptors density with age, awake chicks were imaged under scotopic illumination to allow natural dilation to a larger pupil over which the ocular aberrations could be corrected. The chicks were not anesthetized so the chicks could blink to replenish the tear film naturally as dry eyes result in a degradation of image quality and scattered light

(Koh et al., 2002; Thibos & Hong, 1999). Alert chick measurements also avoid the use to lid retractors which has been shown to change the cornea shape as much as 5D by causing transient flattening in young chick eyes (Irving, 1993). Lid retractors could also induce astigmatism in the cornea and eye.

2.2.3 Cone analysis

An average of 1 and 23 frames were chosen for cone analysis for each eye. A window size of 160×160 pixels (59.2×59.2 minute of arc) with best image quality from each frame were chosen for cone density calculation.

A custom program written in MATLAB (copyright Roorda lab) automatically identified individual cones. Cone density was calculated by dividing the number of cones identified by the sampling window area.

$$D = \frac{\#\ Cones}{sampling\ area}$$

Equation 2. 31

Then density was averaged across frames for each eye, then averaged across birds for each day.

Angular cone row spacing was calculated assuming hexagonal packing (Headington et al., 2011; Kisilak et al., 2012). The mosaic was examined using Voronoi analysis (code written by Roorda lab).

$$Angular\ cone\ row\ spacing = \sqrt{\frac{\sqrt{3}}{2}} \times \frac{1}{\sqrt{D}}$$

Equation 2. 32

Chapter 3: Following emmetropization, residual optical blur matches cone photoreceptor resolution in chicks

3.1 Purpose

This chapter is written as an independent manuscript, the content was presented at the International Myopic conference 2017 and the Canadian Association of Physicists 2017. For coauthors' contributions, please see the Author's declaration at the beginning of the thesis. We wish to determine if there is an optical signal which stops the process of emmetropization before the refractive error reaches zero. We wish to determine the relationship between the endpoint of refractive error and the sampling frequency of the cone photoreceptors.

3.2 Introduction

The optical state of the eye is said to be emmetropic when the image of distant object forms a circle of least confusion at the photoreceptor layer of the retina without accommodation. Much has been reported in animal models such as tree shrews (Amedo & Norton, 2012; Zhu et al., 2013), primates(Hung et al., 1995; Zhu et al., 2013), and chicks (Irving et al., 2015; C. F. Wildsoet, 1997b) on ocular changes in response to imposed defocus errors, which supports the concept of active feedback control of eye growth. This control results in the eye coming into focus either during normal growth or growth in response to imposed defocus, known as emmetropization (C. F. Wildsoet, 1997b). The process of the reduction of at-birth defocus (prevalently hyperopic defocus) to emmetropia during early postnatal life occurs in most species including human and chicks (Wallman & Winawer, 2004a). Instead of straight emmetropia, a refractive error-free optical state, mild hyperopia (+0.5 to +2D) was suggested as the natural endpoint of refractive development in children (Morgan et al., 2010), a non-zero refractive error (+1.19D) was also reported for normal ocular development for 4-year old monkeys (Qiao-Grider et al., 2007), after this age, the ocular development for monkey is significantly slower (Qiao-Grider et al., 2007). Chick was shown to have non-zero refractive error at age 75 (Schaeffel & Howland, 1988). We would like to know why this mild hyperopia is the preferred endpoint in emmetropization and what optical signals could act as stop signals to emmetropization.

Chick with its rapid growth and accurate response to imposed defocus ranging from -10D to 20D (Irving et al., 2015) is a popular animal model for research on emmetropization and its mechanisms.

Systematic studies of ocular dimensions (axial length, corneal curvature, crystalline lens dimension and equatorial diameters (Irving, Sivak, Curry, & Callender, 1996)) in the eye have been carried out. The lens induced refractive error changes are mostly attributed to the change in vitreous chamber growth rates and secondarily to cornea changes (E. L. Smith 3rd, 2011). Emmetropization was shown to be driven by the retinal image (Kisilak et al., 2006), which is degraded by the optical aberrations of the eye and processed by the cone photoreceptors in the retina. Therefore, studying the optical aberrations in the eye and cone photoreceptor sampling can help us better understand the control of emmetropization, and the possible stop signals to emmetropization.

The effect of induced refractive error on optical quality has been studied in chicks (Coletta, Marcos, Wildsoet, & Troilo, 2003) as the full width at half height (FWHH) of the double pass point spread function. Here, we present single pass PSFs and a simple calculation of estimated optical blur derived from the wavefront error using the extended definition of equivalent blur (Kisilak et al., 2006). This measure gives a good approximation of the radial extent of the actual point spread function (PSF) (Hunter et al., 2009) to quantify the retinal image quality.

Studies on cone photoreceptor distribution with eccentricity *in vitro* have used bright field microscopy (Kram et al., 2010) and adaptive optics multiphoton microscopy (Bueno et al., 2014) and *in vivo* have used adaptive optics fundus imaging (Headington et al., 2011). Kislak et al have reported the longitudinal change of photoreceptors during normal refractive development using a confocal scanning laser ophthalmoscope (Kisilak et al., 2012) but this was not compared to the defocus blur.

Longitudinal changes of cones measured with an AO-corrected confocal scanning laser ophthalmoscope from the day of hatching up until day 21 of eyes with positive, negative and no lens are reported here and compared to the defocus blur at the same time points. We wish to determine the relationship between retinal image quality and cone photoreceptor density and sampling.

3.3 Methods

3.3.1 Experimental data

Chicks were obtained on the day of hatching. Measurements were performed on day 0 and subsequent days up to day 21. All experiments received ethics approval from the University of Waterloo Animal Care Committee.

Four groups of a total of 17 birds were goggled with -15D lenses on right eyes on day 0 and left eyes grew normally:

Group 1 (G1) of 4 birds, group 2 (G2) of 5 birds and group 3 (G3) of 4 birds were measured from day 0 and on subsequent days until day 14. Group 4 (G4) of 4 birds was measured from day 9 and on subsequent days until day 21. Cone density was measured starting on day 14 for Group 4. Group 5 (G5) of 4 birds was goggled with +10D lenses on the right eyes on day 0 and left eyes grew normally: They were measured on days 0 and 14.

3.3.2 Dioptric and aberration measurements

Axial length was measured using A-scan ultrasound. Aberrations and defocus were measured with a customized Hartmann-Shack aberrometer (Kisilak et al., 2006) with 633nm light on awake chicks under scotopic illumination while goggles were removed for a short period. Measurement was performed in the morning, at approximately the same time, each day to eliminate the effects of diurnal rhythm (M. C. Campbell et al., 2012). Trial lenses, with powers estimated from retinoscopy, were inserted at a known distance from the eye to give more focused Hartman-shack images. Calculations were corrected for lens vertex distances. Most research uses retinoscopy to measure the refractive error of the eye. The uncertainty in the measurement of the mean refractive error (MOR) (by retinoscopy) of the chick eyes during the first two weeks is about 0.7D (Kisilak, 2005). Alternatively, refractive errors can be measured with a Hartmann-Shack wavefront sensor with an uncertainty less than 0.5D (Kisilak, 2005).

3.3.3 Optical blur calculation

Point spread functions (PSFs) were calculated (Matlab) from aberration measurements (Hartmann-shack images). The complete PSF was calculated as well as PSF's which accounted for components of the wavefront aberration: spherical defocus PSF due solely to spherical defocus (Figure 3.1 A

Control eyes; D Goggled eyes for one subject at day 21) and the total defocus PSF due to spherical defocus and 1st order astigmatism (Figure 3.1 B Control eyes; E Goggled eyes for one subject at day 21). Total PSF was calculated including total defocus and higher order aberrations up to 4th order (Figure 3.1 C Control eyes; F Goggled eyes for one subject at day 21). The equivalent blur calculation for SDB is exact. The radial extents of the TDB and TOB PSFs are well approximated by the calculated (Equation 2.19-2.22 Chapter 2) equivalent blur (dashed line in Figure 3.1). The blur increases as effects of astigmatism in the TDB and higher-order aberrations in the TOB are considered.

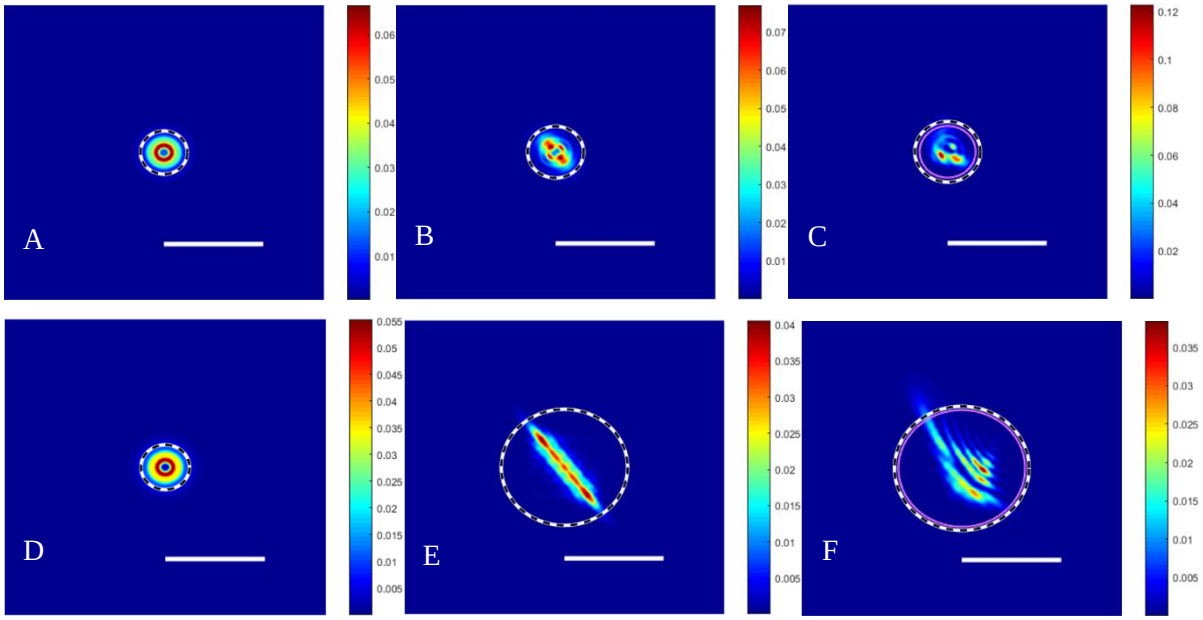

Figure 3. 1 Types of optical blur on the retina. Sample PSFs from one chick at Day 21 (control eye top, goggled eye (-15 D) bottom; dashed white circles represent corresponding estimation of the optical blur from equivalent blur calculations. A) and D) spherical defocus blur (SDB), B) and D) total defocus blur (TDB), C) and F) total optical blur (TOB) purple circles: TDB). Scale bar 15 arcmin.

For spherical defocus blur (SDB), an exact calculation of equivalent blur is defined as the angular radius of the blur due only to spherical defocus (Equation 3.1).

$$SDB = \frac{4\sqrt{3} \times Z_2^0}{r}$$

Equation 3. 1

Where r is the radius of pupil, and Z_2^0 is the spherical defocus Zernike term measured for control eyes. For goggled eyes, the spherical defocus term accounted (Equation 3.2) for the chick's view through the defocus imposed by goggles (power of lenses $P_{lenses} = -15D \; or \; 10D$). The blurs shown are therefore the residual blurs for the goggled eyes looking the through goggles.

$$Z_{2\,calibrated}^0 = Z_{2\,measured}^0 - (\frac{-P_{lenses} * r^2}{4\sqrt{3}})$$

Equation 3. 2

The radial extents of the total PSF and the PSF due to total defocus were also approximated as total defocus blur (TDB) (Equation 3.3) and total optical blur (TOB) (Equation 3.4).

$$TDB = \frac{4\sqrt{3} \times RMS_{total\,defocus}}{r}$$

Equation 3. 3

$$TOB = \frac{4\sqrt{3} \times RMS_{total\,aberration}}{r}$$

Equation 3. 4

The constant $(4\sqrt{3})$ is exact for SDB and an approximation when combining different aberration types for TOB and TDB.

The astigmatic equivalent blur is defined in terms of the two Zernike terms which represent defocus (or first order) astigmatism (Equation 3.5).

$$ASB = \frac{4\sqrt{3} \times RMS_{1st\,astigmatism}}{r}$$

Equation 3. 5

Where

$$RMS = \sqrt{\sum_m^n Z_m^n}$$

Equation 3. 6

Where Z_m^n are the Zernike terms of the wavefront aberration in the OSA double index standard (Thibos, Applegate, Schwiegerling, Webb, & VSIA Standards Taskforce Members. Vision science and its applications, 2002). For each of Equations 3.3 and 3.4, the corresponding range of m and n were chosen. Total aberration RMS was also calculated up to 4th order excluding the first three terms; total defocus RMS includes only second order Zernike terms, RMS of 1st astigmatism includes the second order Zernike terms excluding the spherical defocus term. The exact calculation for ASB uses a constant ($2\sqrt{6}$), giving values that are 30% less than those from equation 3.5. This difference does not affect the relative amount between control eyes and goggled eyes or with age.

The magnitude of estimated optical blur from equivalent blur quantifies the image quality of the eye, larger blur means poorer vision. The sign of the spherical defocus optical blur shows the position of the blur with respect to the retina. If the eye experience hyperopic defocus, the optical blur is positive (Figure 3.2 a), if the eye has myopic defocus, the optical blur is negative (Figure 3.2 b).

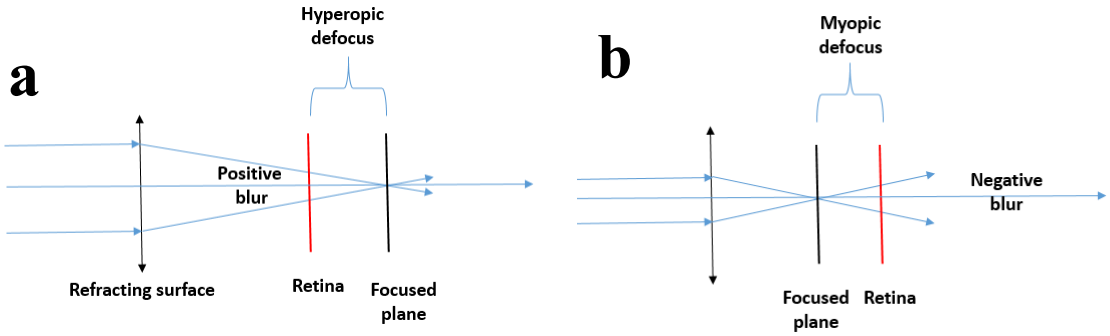

Figure 3. 2 Schematic of the relationship between blur sign and defocus of the eye, hyperopic defocus with positive blur; myopic defocus with negative blur.

SDB, TDB, TOB, ASB were calculated as function of age for both goggled and control (non-goggled) eyes. Optical blur was calculated as absolute values for each frame, then averaged for each eye and then averaged across eyes on each day within each group.

3.3.4 Measurement of cone densities

Awake chicks were imaged with an adaptive optics scanning laser ophthalmoscope (AO SLO) in a 6.6° field of view close to the area centralis. AO SLO images (1024 pixel×1000 pixel) were recorded with 760 nm light (Chapter 2).

3.3.5 Cone resolution calculation

Subregions of AO SLO images were analyzed with cone counting software [Coded by Kaccie Y. Li (2006), copyright Roordalab, used by permission]. Angular cone densities were calculated from the images.

Angular cone density (D) was calculated for each frame, then averaged for each eye and then averaged across eyes on each day within each group. Angular cone row spacing (RS) was calculated from angular cone density (Equation 3.8) assuming hexagonal packing (Headington et al., 2011; Kisilak, Hunter, Irving, & Campbell, 2007).

$$RS = \sqrt{\frac{\sqrt{3}}{2}} \times \frac{1}{\sqrt{D}}$$

Equation 3. 7

Where RS is angular row to row cone photoreceptor spacing.

Cone resolution (CR) was calculated as twice the angular cone row spacing (Equation 3.9) based on Shannon sampling theory (National Research Council, 1990).

$$CR = 2 \times RS$$

Equation 3. 8

3.4 Results

3.4.1 Cone densities

An ANOVA (Matlab) test on groups run at different times with a -15D lens treatment (G1, G2, G3, and G4) showed (Table 3.1) : 1) significant decrease of angular row spacing with age ($p < 0.001$) (Figure 3.3); 2) Non significant difference between groups with the same treatment or between treated and control eyes ($p > 0.1$); 3) Non significant interactions between age and treatment or group and treatment ($p > 0.5$); 4) A significant group difference ($p = 0.039$). Multi comparison showed that G4 measured over a different age range is different from the other 3 groups. An ANOVA test on G1, G2, and G3 (Table 3.2) showed a non-significant difference between these groups ($p > 0.05$). On day 14, the values in the first three groups were 2% higher than in G4.

Source of variations	**P value**
Age	0.0001
Treatment (Control or Goggled)	0.7139
Groups (G1, G2, G3, G4)	0.0391
Age*Groups	0.1205
Age*Treatment	0.6779
Group*Treatment	03603

Table 3. 1 ANOVA test on cone densities for Groups 1, 2, 3, 4 goggled with -15 D lenses. * means interaction term. $p < 0.05$ means significantly different.

Source of variation	P-value
Age	0.0001
Treatment (Control or Goggled)	0. 5193
Groups (G1, G2, G3)	0.0691
Age*Groups	0.1708
Age*Treatment	0.5725
Groups*Treatment	0.5395

Table 3. 2 ANOVA test on cone densities for Group 1, 2, 3 with -15D lenses. * means interaction term. p<0.05 means significantly different.

An ANOVA test on birds treated with +10D lenses (G5) (Table 3.3) showed: 1) significant decrease of RS with age ($p < 0.001$); 2) Non significant difference in treatment ($p > 0.05$); 3) Non significant interactions between age and treatment ($p > 0.1$).

Source of variation	P-value
Age	0.0001
Treatment (Control or Goggled with +10D lenses)	0.0698
Age*Treatment	0.3043

Table 3. 3 ANOVA test on cone densities for Group 5 with +10D lenses. * means interaction term. p<0.05 means significantly different.

Because of their non-significant differences, control and goggled eyes of G1, G2, G3 (goggled with -15D lenses) were pooled and compared with G5 (goggled with +10D lenses) on day 0 and day 14 to test the difference of goggling conditions. The ANOVA test showed no difference between differently treated eyes nor between treated eyes with control eyes on either day ($p > 0.1$).

As goggling does not significantly affect cone row spacing and there was no difference between control and goggled eyes for the groups raised from day 0-14, these 4 groups were pooled together for

regression analysis of cone row spacing (RS) with age. A significant better fit by an exponential with a constant (Equation 3.9, Table 3.4) is suggested by F statistics ($p < 0.005$) than the exponential model without a constant (Equation 3.9, c = 0) (Fig 3.3).

Parameter y takes the form of an exponential equation with a constant c, the value at infinity the endpoint), and decay constant b (Equation 3.9).

$$y = c + a * \exp(-b * Age)$$

Equation 3. 9

Rate of change for y, given by the derivatives of equation 3.9 is:

$$y = -ab * \exp(-b * Age)$$

Equation 3. 10

Row spacing fit	*a*	*Decay rate b*	*Endpoint c [arcmin]*	*Intial rate of change ab*
	0.32 ± 0.069	0.43 ± 0.23	3.46 ± 0.04	0.14 (0.05-0.26)

Table 3. 4 Constants of exponential equation for angular cone row spacing with age

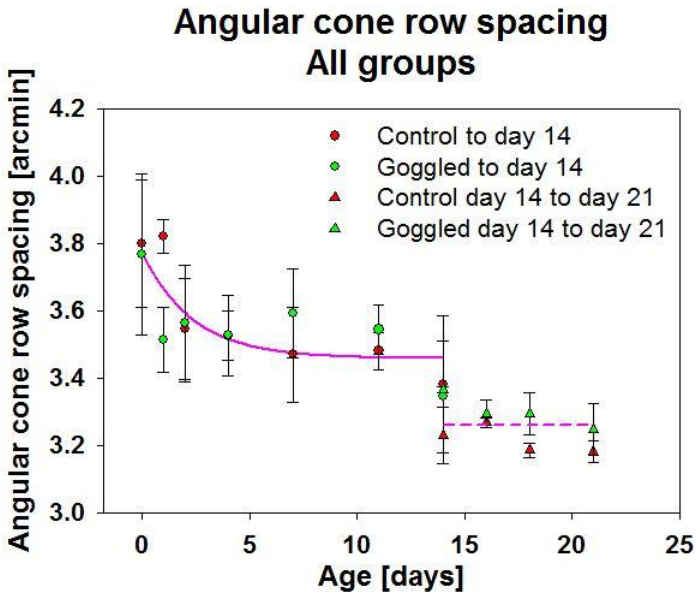

Figure 3. 3 Angular cone row spacing for all 5 groups, control eyes in red; goggled in green; circles are angular cone row spacing averaged across groups 1, 2, 3 with -15D lens and Group 5 with +10D lens; triangles are group 4 with -15D lens. Error bars are standard deviation. Solid line is best regression fit for the control and goggled eyes of the 4 groups (G1, G2, G3, G5) raised from day 0 to day 14. Dashed line is a line fit to group 4 (G4) measured on later days (days 14 to 21); control and goggled eyes were pooled. Multiple data points on day 14, were plotted to show overlapping days.

Figure 3.3 shows the change of angular cone row spacing with age for all 5 groups. Cone row spacing reduced quickly and reached $\frac{1}{e}$ of the day 0 value at day 2.3 (1/b). Endpoint cone resolution CR1, calculated from endpoint angular cone row spacing RS1 was $6.92 \pm 0.09\ /arcmin$. An ANOVA test on the older eyes with -15D lenses (G4) (measured from day 14 to day 21) showed no significant change with age ($p > 0.1$); control and goggled eyes showed no significant difference ($p > 0.05$). The pooled average across age of control and goggled eyes gives a second cone resolution CR2. The value for days 14-21 ($CR2 = 6.5 \pm 0.1\ arcmin$) is 6% lower than the value from the exponential fit extrapolated to infinity (Table 3.5).

Cone row spacing endpoints [arcmin]	*Cone resolution ednpoints [arcmin]*
$RS1 = 3.46 \pm 0.04$	$CR1 = 6.92 \pm 0.09$
$RS2 = 3.26 \pm 0.07$	$CR2 = 6.5 \pm 0.1$

Table 3.4 Endpoints for cone row spacing and cone resolution. RS1: endpoint of angular cone row spacing from the exponential fit. CR1: endpoint cone resolution calculated from RS1. RS2: pooled average across age of control and goggled eyes for birds measured from day 14-21. CR2: endpoint cone resolution calculated from RS2.

3.4.2 Optical blur

Total optical blur (TOB)

An ANOVA test on eyes goggled with -15D lenses and measured from day 0 to 21 (G1, G2, G3, G4, showed: 1) significant reduction of TOB with age ($p<0.0001$); 2) significant difference between treated and control eyes ($p<0.0001$); 3) Non significant difference between groups ($p>0.05$). Each of control and goggled eyes of G1, G2, G3, and G4 were then pooled together and averaged and as function of age as shown in figure 3.4.

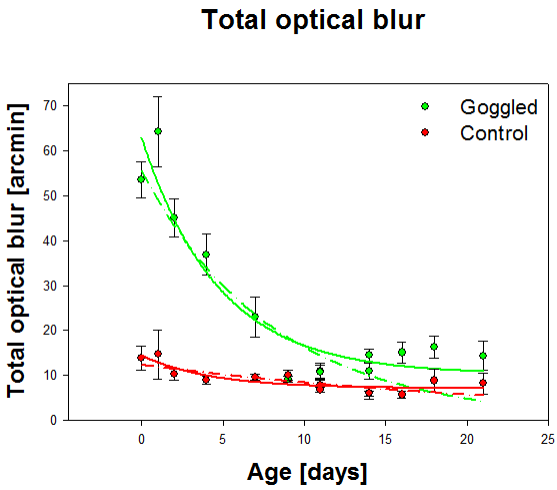

Figure 3. 4 Total optical blur with age for birds goggled with -15D lenses. Control eyes in red, Goggled eyes in green; Solid lines are better exponential fits with nonzero endpoints, than dashed lines which are exponential fits with zero endpoints. Multi data points on day 14, day11 were plotted to show overlapping days.

F statistics demonstrate a significantly better fit of TOB of an exponential with plateau (Equation 3.9; Table 3.8; Figure 3.4) than without the plateau (Figure 3.4 Equation 3.9 c=0) for control ($p < 0.05$) and goggled ($p<0.05$) eyes respectively.

An ANOVA test on total optical blur between day 14 and day 21 with age and between eyes (table 3.4) showed non-significant change with age ($p>0.5$), a significant difference between control and goggled eyes ($p=0.0001$). Paired-t-test was performed between control and goggled eyes on each day from day 14 to day 21, a significant difference between control and goggled eyes was found on day 14 ($p<0.001$) and day 16 ($P<0.01$).

Source of variation	**P-value**
Age	0.3375
Treatment (Control or Goggled with -15D lenses)	0.0001
Age*Treatment	0.8787

Table 3. 5 ANOVA test on total optical blur between day 14 to day 21 for birds goggled with -15D lenses. * means interaction term. p<0.05 means significantly different.

Total defocus blur (TDB)

For birds goggled with -15D lenses, when the contribution of the higher order aberrations to the blur is not considered, total defocus blur (TDB), an F test demonstrates a significantly better fit of an exponential with plateau (Equation 3.9; Table 3.8; Figure 3.5) than without the plateau (Equation 3.9 $c = 0$, Figure 3.5) for control ($p<0.05$) and goggled ($p<0.05$) eyes.

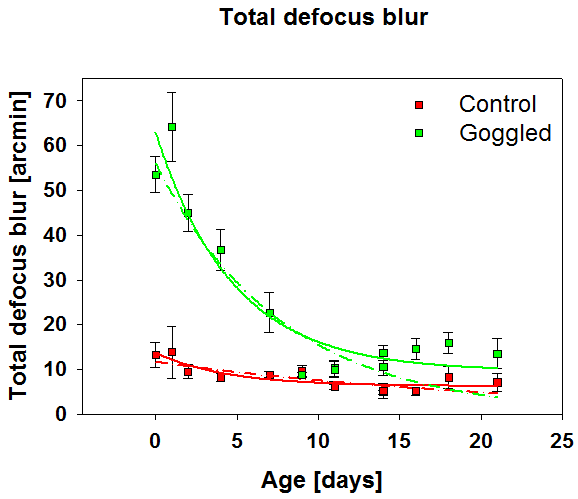

Figure 3. 5 Total defocus blur with age for birds goggled with -15D lenses. Control eye in red, Goggled eye in green; Solid lines are better exponential fits with nonzero endpoints, than dashed lines which are exponential fits with zero endpoints. The fits of total defocus blur had significant nonzero endpoints as demonstrated by F tests for both eyes. Multi data points on day 14 were plotted to show overlapping days.

An ANOVA test on total defocus blur between day 14 and day 21 with age and between eyes showed non-significant change with age ($p>0.5$), a significant difference between control and goggled eyes ($p<0.0002$).. Paired t-test was performed between eyes on each day from day 14 to day 21, a significant difference between control and goggled eyes on day 14 ($P<0.001$) and day 16 ($P<0.05$).

Spherical defocus blur (SDB)

For birds goggled with -15D lenses, when the contribution of the higher order aberrations and astigmatism to the blur are not considered, although an F test did not show a significance to the constant term, spherical defocus blur was fitted with exponential decay with a constant as in total defocus blur and total optical blur for control eyes (Table 3.8, regression fit $p<0.005$, Figure 3.6) and goggled eyes respectively. Spherical defocus blur exponentially reduced in both control and goggled eyes. From day 14 to 21, no significant difference was found for spherical defocus blur between eyes and with age as suggested by an ANOVA test (table 3.7). The effect of treatment was borderline ($p=0.077$).

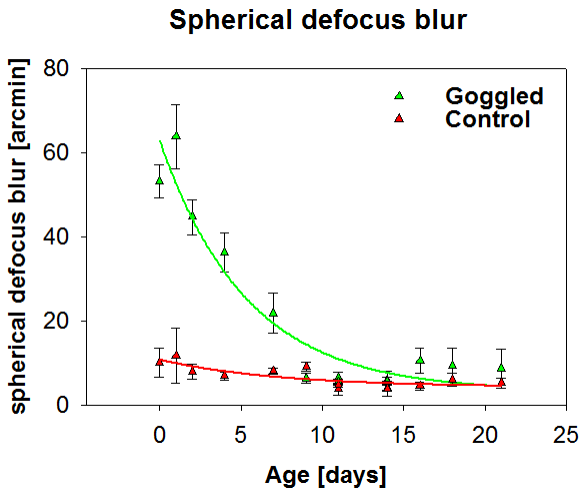

Figure 3. 6 Spherical defocus blur with age for birds goggled with -15D lenses. Control eye in red, Goggled eye in green; Solid lines are exponential fits with nonzero endpoints. Multi data points on day 14, day 11were plotted to show overlapping days.

Source of variation	P-value
Age	0.7663
Treatment (Control or Goggled with -15D lenses)	0.0766
Age*Treatment	0.8592

Table 3. 6 ANOVA test on spherical defocus blur between day 14 to day 21 for birds goggled with -15D lenses. * means interaction term. p<0.05 means significantly different.

Birds goggled with +10D lenses were limited to two data points (day 0 and day 14). Paired-t-test showed non-significant differences between control eyes and goggled eyes looking through goggles on the last measurement day 14 for total optical blur (p>0.05), total defocus blur (p>0.05), and spherical defocus blur (p>0.05). As expected, the blur did not differ between eyes on day 0 (p>0.05) prior to goggling.

Comparison of TOB TDB and SDB

Optical blur (TOB), total defocus blur (TDB) and spherical defocus blur (SDB) fits (Equation 3.9) are shown for control and goggled eyes with -15D lenses in Table 3.8.

Optical blur fit	*a*	*Decay rate b*	*Endpoint c [arcmin]*	*Intial rate of change ab*
TOB_Control_-15D	7 ± 1	0.2 ± 0.1	7.1 ± 0.8	1.4 (0.6-2.4)
TOB_Goggled_-15D	53 ± 6	0.21 ± 0.07	10 ± 4	11.1(6.6-16.5)
TDB_Control_-15D	7 ± 1	0.2 ± 0.1	6.3 ± 0.9	1.4 (0.6-2.4)
TDB_Goggled_-15D	53 ± 6	0.21 ± 0.07	10 ± 4	11.1(6.6-16.5)
SDB_Control_-15D	7 ± 2	0.1 ± 0.1	4 ± 2	0.7(0-1.8)
SDB_Goggled_-15D	60 ± 6	0.19 ± 0.06	3 ± 5	11.4(7.0-16.5)

Table 3. 8 Constants of exponential equation (Equation 3.9) for optical blur with age for birds goggled with -15D lenses.

For birds goggled with -15D lenses, adding astigmatism and then higher order aberrations increases the amount of blur (c in Table 3.8). The endpoints of TOB and TDB were larger than SDB. Initial rate of change (ab from equation 3.10 when Age = 0) is significantly larger in goggled eyes than control eyes (Table 3.8).

For birds goggled with +10D lenses (Group 5), the measurement was limited to two days (day 0 and day 14). Assuming the same decay constant b which was not significantly different for TOB, TDB and SDB in control and goggled eyes for birds goggled with -15D lenses, regressions for change in retinal blurs with age were calculated from measured data points taking the exponential form with a

constant (Equation 3.9). Adding astigmatism and then higher order aberrations increases the amount of blur (c in Table 3.9).

Table 3.6 is the summary of the time constants and their ranges calculated from the standard deviation for birds goggled with -15D lenses. Time constant for component retinal blur (spherical defocus blur, total defocus blur) and total optical blur did not differ significantly from each other. With similar time constant between control and goggled eyes, goggled eyes exponentially reduced optical blur at a faster initial rate (ab) because of larger initial value of a.

Optical blur fit	*a*	*Decay rate b*	*Endpoint c [arcmin]*	*Intial rate of change ab*
TOB_Control_+10D	7.15	0.24	7.25	1.7
TOB_Goggled_+10D	3.91	0.21	7.29	0.8
TDB_Control_+10D	7.19	0.23	6.91	1.7
TDB_Goggled_+10D	3.91	0.21	7.09	0.8
SDB_Control_+10D	8.53	0.14	5.42	1.2
SDB_Goggled_+10D	6.58	0.19	4.57	1.3

Table 3. 9 Constants of exponential equation (Equation 3.9) for optical blur with age for birds goggled with +10D lenses. Regression fits were calculated from two measured data points (Day0 & Day14) assuming same decay rate b as the birds goggled with -15D lenses for control and goggled eyes respectively.

Figure 3.7 demonstrates the comparison of three types of estimated optical blur with age for birds goggled with -15D lenses, and +10D lenses, Total optical blur (TOB), total defocus blur (TDB) and spherical defocus blur (SDB) are shown. In all eyes, adding astigmatism and then higher order aberration terms increases the amount of blur as shown by the regression fits.

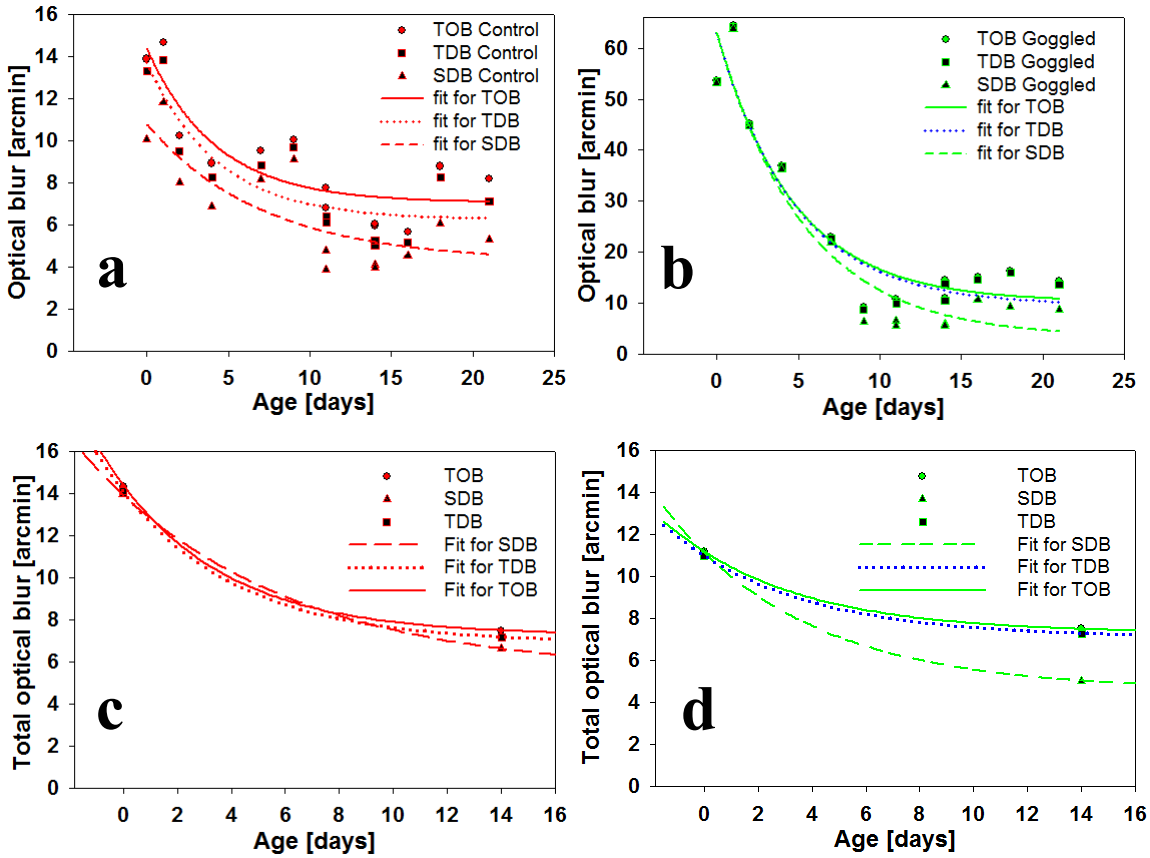

Figure 3. 7 Comparison of 3 types of estimated optical blur with age. For birds treated with -15D lenses. (a) Control & (b) Goggled eye, solid, dashed, dotted lines are the best fit for estimated total optical blur, total defocus blur and spherical defocus blur respectively. For birds goggled with +10D lenses, (c) Control & (d) Goggled eyes, solid, dashed, dotted lines are regression fits (Equation 3.9, Table 3.9) calculated from measured data points assuming the same decay rate b as for birds treated with -15D lenses(Table 3.8) for total optical blur, total defocus blur and spherical defocus blur respectively.

	$\frac{SDB}{TOB}$	$\frac{TDB}{TOB}$
Goggled eyes [+10D] day 14	64% (34%-90%)	96% (94%-99%)
Control eyes [+10D] day 14	88% (82%-96%)	95% (90%-98%)
Goggled eyes [-15D] day 14 to 21	55% (50%-66%)	95% (94%-97%)
Control eyes [-15D] day 14 to 21	64% (52%-70%)	89% (84%-96%)

Table 3. 7: Ratio of spherical defocus blur and total defocus blur, total defocus blur and total optical blur and their range across birds on and after day 14.

Table summarizes the ratio of spherical defocus blur and total defocus blur with total optical blur and their range across birds on and after day 14 for birds goggled with -15D lenses or +10D lenses. Total defocus blur including spherical defocus and astigmatism is the main component of retinal blur.

Comparing endpoint optical blurs for birds goggled with different lenses

Endpoints estimated from regression fits for the same type of optical blur were not significantly different between control eyes and goggled eyes or for different lens treatments (table 3.10). There also appears to be no significant difference between the end points for birds goggled with -15D and +10D lenses.

Subject	*Estimated optical blur*	*Birds with -15D lenses endpoints [arcmin]*	*Birds with +10D lenses endpoints [arcmin]*
Control	Total optical blur (TOB)	7.1 ± 0.8	7.25
Control	Total defocus blur (TDB)	6.3 ± 0.9	6.91
Control	Spherical defocus blur (SDB)	4 ± 2	5.42
Goggled	Total optical blur (TOB)	10 ± 4	7.29
Goggled	Total defocus blur (TDB)	10 ± 4	7.09
Goggled	Spherical defocus blur (SDB)	3 ± 5	4.57

Table 3. 8 Comparison endpoints from regression fits of 3 types of blur for birds goggled with different lenses

Blur due to 1st order astigmatism (horizontal/vertical and oblique astigmatism)

An ANOVA test was performed to compare control eyes and goggled eyes for astigmatic blur (ASB) (Equation 3.5) with age and within the 4 measured groups. The ANOVA test showed: 1) significantly larger astigmatic blur in goggled eyes than control eyes ($p<0.05$); 2) a significant difference in astigmatic blur with age ($p<0.05$); 3) no significant difference between groups ($p>0.05$); 4) Significant interaction between age and treatment ($p<0.05$); 5) a non-significant difference for the interaction between age and group or between group and treatment. Astigmatic blur was separately pooled across the 4 groups for control eyes and goggled eyes. Figure 3.8 a) shows the comparison of astigmatic blur with age between control eyes and goggled eyes for the pooled data. Astigmatic blur in control eyes significantly exponentially reduced (exponential fit $p<0.05$). Astigmatic blur in goggled eyes significantly linearly increased (linear fit $p<0.005$).Figure 3.8 b shows the difference in astigmatic blur between eyes with age, astigmatic blur is significantly larger in the goggled eyes than control eyes and the difference significantly linearly increased (Significant linear regression fit $p<0.05$).

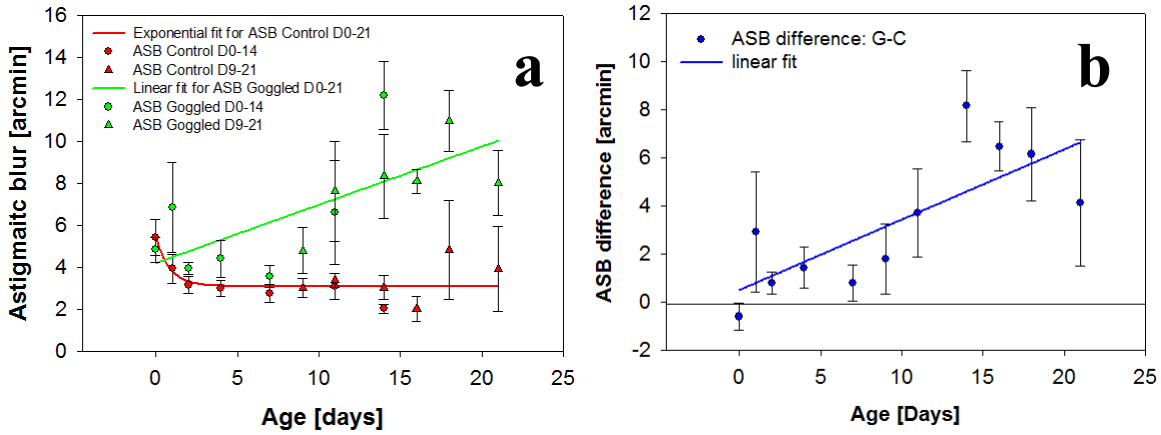

Figure 3. 8 a) Astigmatic blur with age for birds goggled with -15D lenses. Control eyes in red, Goggled eyes in green. Circles are 3 groups measured from day 0 to 14, triangles are one group measured on later days from day 9 to 21. Significant decrease and increase in control eyes (red

solid line: exponential fit) and goggled eyes (green solid: linear fit) line respectively are shown. b) Astigmatic blur difference between eyes with age for birds goggled with -15D lenses. Circles represent astigmatic blur of goggled eyes minus control eyes. An increasingly significant larger astigmatic blur in the goggled eyes than control eyes is shown by a linear fit from day 2 (blue line).

3.4.3 MOR and optical blur with age

Figure 3.9 shows the change of average MOR (Equation 2.31in Chapter 2) during emmetropization to lenses for birds goggled with -15D lenses and birds goggled with +10D lenses. Though F stats were not significant, significant exponential decays with a constant were fit for control eyes and goggled eyes for birds with -15D lenses as a nonzero refractive error has been reported for chick at day 75 (Schaeffel & Howland, 1988). As shown in figure 3.9, MOR in goggled eyes with -15D lenses after day 14 (red triangles) agrees better with the exponential fit for control eyes (dashed red line), which has a non-zero endpoint. On day 14, MOR for goggled eyes with either +10D lenses or -15D lenses is not significant different and not significantly different from control eyes ($p>0.1$).

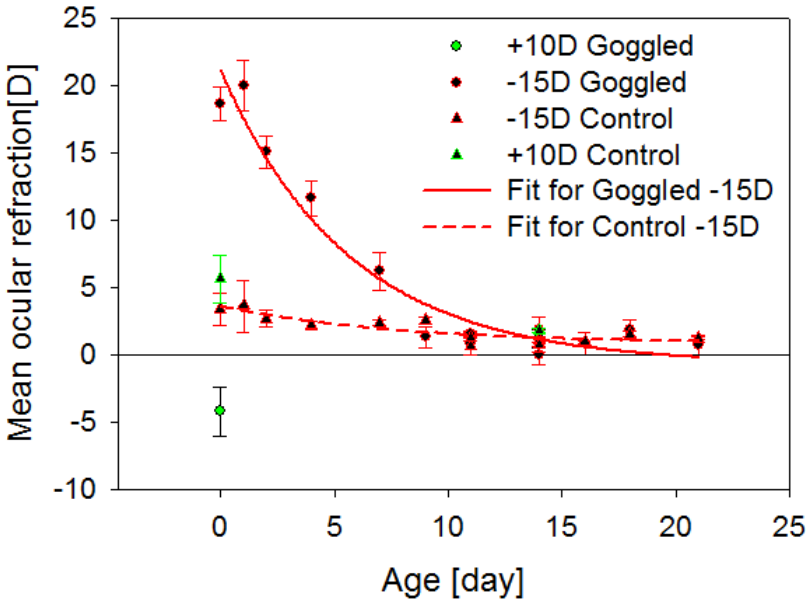

Figure 3. 9 Mean ocular refraction with age. Birds goggled with -15D lenses in red, birds goggled with +10D lenses in green. Control eyes are triangles, Goggled eyes are circles. Solid

line is significant fit with constant for goggled eyes with -15D lenses: $\boldsymbol{MOR_{-15Dcontrol} = (0.8 \pm 0.6) + (2.8 \pm 0.6) * \exp[-(0.13 \pm 0.08) * Age]}$**;** $\boldsymbol{MOR_{-15Dgoggled} = (-0.7 \pm 1) + (22 \pm 2) * \exp[-(0.18 \pm 0.04) * Age]}$**. Dashed line is a significant fit for control eyes of birds with -15D lenses.**

Figure 3.10 shows individual eyes' MOR and individual eyes' total optical blur for birds goggled with -15D lenses between day 14 and day 21 (figure 3.10A: individual MOR; figure 3.10C: individual total optical blur) and birds goggled with +10D lenses on day 14 (figure 3.10B: individual MOR; figure 3.10D: individual total optical blur). Total optical blur stays significantly above zero as MOR varies close to zero.

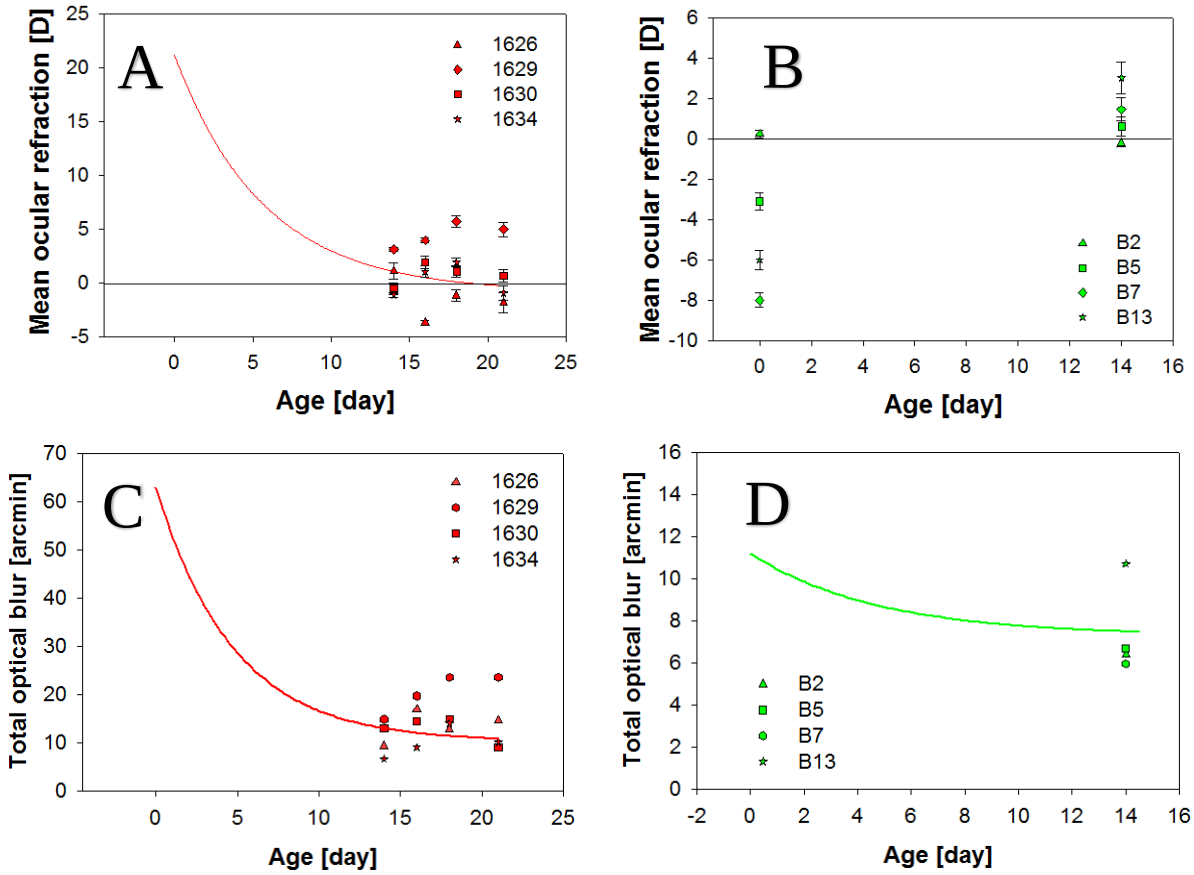

Figure 3. 10 Individual goggled eyes' average MORs and total optical blur for day14 to day 21. Different symbols represent different birds. A: MOR for birds goggled with -15D lenses; B:

MOR for birds goggled with +10D lenses. Error bars are standard deviation across frames for averages of MOR, taken from the most hyperopic frames with larger pupil sizes. C: Total optical blur for birds goggled with -15D lenses; B: Total optical blur for birds goggled with +10D lenses. Fitted lines are regression fits for MOR in A (Figure 3.9) and total optical blur in C, D (Table 3.9).

3.4.4 Comparing cone resolution with optical blur

Figure 3.11 shows the comparison of total optical blur estimated from equivalent blur with cone resolution based on Shannon sampling theory for birds goggled with -15D lenses: In all four cases, total optical blur exponentially reduced to match the cone resolution. All optical measurements were well above the diffraction limit.

For the birds goggled with -15D lenses from day 14 to day 21, an ANOVA test on control eyes (Figure 3.11 a) showed no difference between TOB and CR ($p>0.1$). An ANOVA test showed a difference in goggled eyes with -15D lenses (Figure 3.11 b) between TOB and CR from day 14 to day 21 ($p<0.05$). A paired-t-test showed no difference between TOB and CR on day 21 ($p>0.05$) but a significantly larger TOB than CR on day 14, day 16, and day18 ($p<0.001$). For birds goggled with +10D lenses, a paired-t-test found no significant difference between TOB and CR on day 14 d in either control eyes ($p>0.05$) (Figure 3.11 c) or Goggled eyes ($p>0.05$) (Figure 3.11 d).

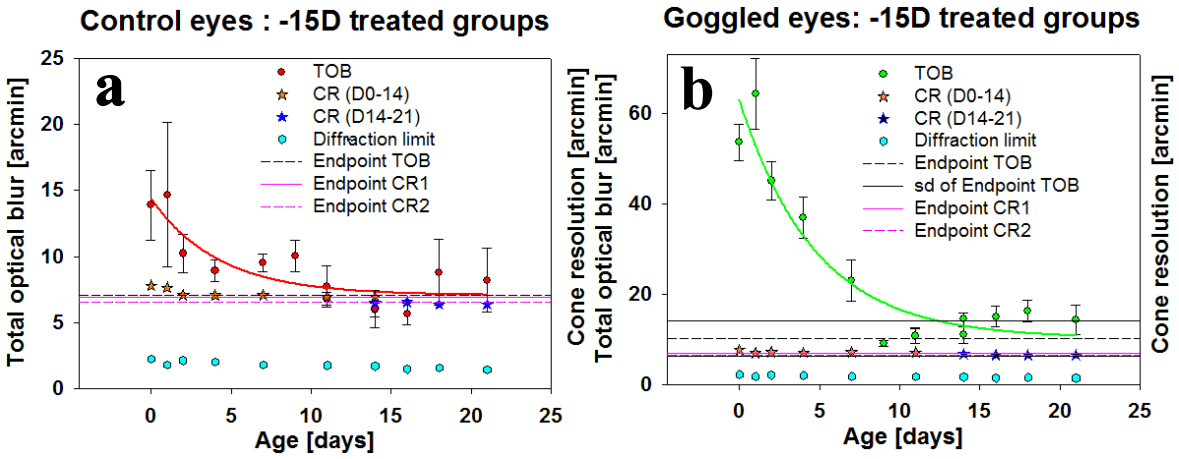

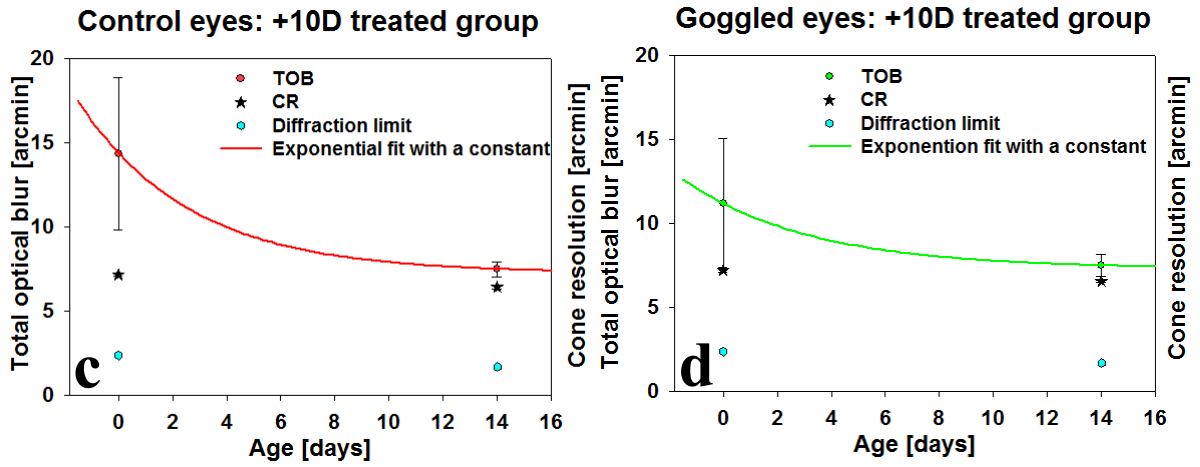

Figure 3. 11: Comparison of total optical blur with cone resolution (CR) (a) Control eyes & b) Eyes goggled with -15D lenses, (c) Control eyes & (d) Eyes goggled with +10D lenses. Light blue dots: diffraction limit for optical blur. Orange star: cone resolution measured from day 0 to day 14. Dark blue star: con resolution measured from day 14 to day 21. Purple line: estimated endpoint cone resolution from exponential fit (CR1), dashed purple line: averages of control and goggled eyes from days 14 to 21 (CR2). Dashed black line: estimated endpoint of total optical blur from the exponential fit. Black line: stand deviation of the estimated endpoint of TOB. Error bar is standard error. The endpoint cone resolution and TOB endpoints are in agreement.

Endpoint comparison

Endpoints for total optical blur and cone resolution were plotted as a straight lines in Figure 3.9 and summarized in table 3.11 for birds goggled with -15D lenses, +10D lenses and control eyes. The estimated endpoint from Equation 3.10 of angular cone row spacing gives the first estimated endpointof cone resolution, $CR1$. The second endpoint was estimated from pooled measurements from day 14 to day 21 which gives an endpoint, CR2, significantly lower by 6% from CR1. The estimated endpoints of total optical blur estimated in the same manner were not significantly different from the endpoint cone resolutions for -15D birds. For +10D birds, the endpoint total optical blur from regression fit is within 5% of endpoint cone resolution.

	Endpoint Total optical blur TOB [arcmin]		*Cone resolution CR1 [arcmin]*	*Cone resolution CR2 [arcmin]*
Subjects	Birds with -15D lenses	Birds with +10D lenses	Birds with -15D or +10D lenses	Birds with -15D lenses
Control	7.1 ± 0.8	7.25	6.92 ± 0.09	6.5 ± 0.1
Goggled	10 ± 4	7.29		

Table 3. 9 Endpoints summary for total optical blur estimated from regression fits and cone resolution CR1 estimated from regression fits for cone densities measured between day 0 to day14 and cone resolution CR2 for cone densities measured between day 14 to day 21.

3.5 Discussion

Cone densities

Changes in cone photoreceptors density were studied with age using adaptive optics (Figure 3.3). An initial decrease of angular row spacing is possibly due to cone migration proceeding in chick, in addition, it has been reported that cone differentiation does not finish until day 15 (López, López-Gallardo, Busturia, Anezary, & Prada, 2005). Cone row spacing reduced exponentially which implies a rapid decrease during the first 2 days and little change after day 14 possibly involving the combination of cone migration and expansion of the eye. We found no difference in angular cone row spacing between differently goggled eyes or between goggled and control eyes, suggesting the goggling does not affect the change of angular cone row spacing with age. Retinal images taken *in vitro* using Adaptive optics multiphoton microscopy between form deprived myopic eyes treated at later age and its normal sighted eyes in chicks (Bueno et al., 2014) found 13% lower linear cone density at central retina area and 13% lower linear ganglion cell density in -10D form deprived myopic eyes than control eyes, which is mostly explained by the 18% increase in the axial length. This implies that the angular cone densities are relatively unchanged by the form deprivation, in agreement with our result of no change in angular cone densities with lens treatment.

Different sets were used for analysis in this project, average cone row spacing for group 5 measured on later days was 6% lower than the endpoint cone row spacing, possibly due to small sample size of 4 subjects.

Compared to cone densities measured in confocal scanning laser ophthalmoscope (confocal SLO) (Kisilak et al., 2012) without adaptive optics, we were able to resolve more cones with an AO correction and larger naturally dilated pupil size, that gave a 22% smaller on average angular cone row spacing (3.4 arcmin on day 14) than their results (4.16 arcmin on day 14). Like us they reported no difference between control and goggled eyes in cone densities for central retina in chicks. Pupil sizes increased with age, the naturally dilated pupil size (~2.5) on day 0 gives the Rayleigh criterion for the minimum separation at which cones can be resolved of 1.27 arcmin. At this age we measured a cone separation of 3.89 arcmin so were not limited by the AO corrected optical resolution. The optical resolution improves with age as the pupil increases. On the last measurement day (day21), we resolve cone separations of 3.18arcmin which are again not limited by the optical resolution. We are able to resolve spacings much closer than the smallest like type spacing, calculated by Kisilak from Kram's data of 2.5 arcmin assuming that the ocular aberration was well corrected. Our measured cone

row spacing is higher because it is the average of all like and unlike type cone spacing. Previously, without adaptive optics the smallest unlike cone separation on day 14 (which will be smaller than that for like cones was 4.16 arcmin on day 14 (Kisilak et al., 2012). Therefore, as previously postulated AO correction across a large pupil is needed to get an accurate measurement of cone spacing. With AO, Headington (Headington et al., 2011) was able to resolve the row spacing of cones for two 6-week old chicks as 2.69±0.2arcmin. The 10% difference with our endpoint cone row spacing is probably due to the small sample size in their study or a stain difference.

Optical blur

MOR which contributes to the spherical blur only makes up part of retinal blur (approximately 60% after day 14), total defocus including spherical defocus and astigmatism predominates in the total optical blur (approximately 92% after day 14) (Table 3.10). When considering the image quality of the eye, one should take spherical defocus, astigmatism and higher order aberration into consideration. Considering just spherical defocus greatly underestimates the blur present and the overestimates the optical resolution of the eye. Therefore, our calculation of optical blur based on the definition of equivalent blur is a better indicator of refractive development with age than MOR alone. It is also necessary to consider the total blur when comparing with the cone resolution.

Hartman-Shack measurement was taken for goggles eyes while goggles removed assuming the large radius of goggles relative to pupil size contributes little to the higher-order aberrations, the image quality was calculated from the HS of the eye and the spherical defocus term of the goggles.

For birds goggled with -15D lenses, the initial rate of change optical blur (SDB, TDB, TOB) was significantly larger in goggled eyes than control, because the rate of change is proportional to the amount of blur present (Table 3.8).This is consistent with findings that the eye requires a longer time to compensate for -30D lenses than -15D lenses (Kisilak, Hunter, Huang, Campbell, & Irving, 2007). Initially, the amount of blur present in the goggled eye was larger looking through defocus lenses than in the control eyes, once the blur reduced to a similar amount, the rate of change became similar between eyes (slopes in Figure 3.4 3.5 3.6). During emmetropization, average optical blur (TOB, TDB, SDB) exponentially reduced in all eyes, and plateaus after day 14 (Figure 3.7). After day 14, spherical defocus blur was not significantly different between control eyes and goggled eyes consistent with normal emmetropization and emmetropization of spherical defocus. However total defocus blur and total optical blur was larger in goggled eyes than control eyes on days 14 and 16

respectively, this is likely due to the increase in astigmatic blur in goggled eyes compared to control (Figure 3.8). It is possible that increased astigmatism in the goggled eyes is then reduced in order to be not different from control eyes, suggested by homeostasis (Wallman & Winawer, 2004c), as TOB was not different between eyes on day 18, day 21. Birds goggled with +10D birds were measured on only two days. Regression analysis was based on a reasonable assumption that the rate of change (b) which was not significantly different in control and eyes goggled with -15D lenses would be the same in eyes goggled with +10D lenses.

Endpoints for estimated optical blur (spherical defocus blur, total defocus blur, total optical blur) were not significantly different between control eyes and goggled eyes with different powered goggles as shown in table 3.11 suggesting that goggling condition affects the endpoint blur due to the refractive state and aberrations very little. Some increase in the astigmatic blur was shown in goggled eyes. Initially, birds at hatching had an average of 6.5±4.5 D hyperopic defocus. Looking through -15D lenses gives approximately 20D of blur with the focus sitting behind the retina, much larger than the ~+5D of myopic blur with the focus in front of the retina when looking through +10D lenses. The fact that the endpoints did not differ between eyes may suggest that neither the magnitude nor sign of blur has much effect on the endpoint of optical blur. Instead it may be primarily influenced by the cone density (see next section).

Astigmatic blur significantly differed between control eyes and goggled eyes and with age (Figure 3.8), astigmatic blur exponentially reduced in control eyes, consistent with the emmetropization of astigmatism in normal growth (Kisilak et al., 2006). The eyes with imposed defocus saw opposite changes, astigmatic blur in goggled eyes linearly increased (Equation 3.31), which is similar to the findings in chick goggled with high power negative lenses (Kisilak et al., 2007). For more discussion of astigmatism, see Chapter 4.

MOR changes

During refractive development, eyes actively compensate to the imposed positive or negative defocus in response to lenses, consistent with normal emmetropization and emmetropization to lenses. Though F stats were not significant when comparing an exponential fit with a constant endpoint to an exponential fit without a constant (with a zero endpoint), significant exponential decays with a constant were fit for control eyes and goggled eyes for birds with -15D lenses as nonzero refractive

error was reported for chick at day 75 (Schaeffel & Howland, 1988). On day 14, average MOR were about 0.8D and not significantly different between control eyes and differently goggled eyes. The nonzero endpoints for the total defocus blur and total optical blur were consistent with a nonzero more hyperopic MOR

Comparing cone resolution with optical blur

Initially, the optical blur was larger than cone resolution, thus, the young eye was able to resolve the blur present. Optical blur exponentially reduced during emmetropization to match the amount of blur that can be resolved by cone photoreceptors on the retina. For the birds goggled with -15D lenses, total optical blur in control eyes reduced to the value which was not significantly different from cone resolution starting day 14 nor on day 14 in goggled eyes. But optical blur was significantly larger than cone resolution on days 16, 18 and 21, which is likely due to larger astigmatic blur in the goggled eyes than control. The endpoint total optical blur for -15D control and goggled eyes (given by the exponential fit) including residual spherical defocus, astigmatism and higher order aberration on average across birds was not significantly different from endpoint cone resolution. For the eyes goggled with +10D lenses measured on day 0 and day 14, total optical blur was not significantly different from cone resolution on last measurement day. When the optical blur is fitted to exponential curves, we have first found a match between the endpoints of optical blur and the endpoint cone resolutions in all eyes, suggesting that the minimum blur achieved may be determined by cone photoreceptor sampling. The match between optical blur with cone resolution is likely the stop signal to emmetropization, subsequent growth may be a uniform scaling of the eye, which would keep both angular optical bur and cone photoreceptor density constant (Hunter et al., 2009). It is likely that the non-zero endpoint of refractive error found in children (Morgan et al., 2010), monkeys (Qiao-Grider et al., 2007) near the end of normal refractive development are determined by the retinal resolution, in other words, the final optimal refractive state is achieved once the minimum blur cannot be resolved by cone photoreceptors on the retina.

Chapter 4 Cone photoreceptors and optical signals to defocus following emmetropization to lenses in chicks

4.1 Purpose

We have previously shown that retinal blur reduces to a non-zero endpoint, which matches endpoint cone photoreceptor resolution, and this match is likely a stop signal to emmetropization. Following emmetropization, if the eye drifts from the optimal refractive error, an optical signal or signals are required to re-establish optimal focus. Astigmatism was proposed as one potential optical signal to the direction of eye growth required to bring the eye back into focus. This is because it generates focus dependent asymmetry in retinal image (Wallman, 1993). Here, we wish to determine whether astigmatism can provide a cue to sign of defocus following emmetropization when the retinal blur has plateaued to a value not different from cone resolution. This chapter is written as an independent manuscript, the related content has been accepted for presentation at the Association of Vision and Ophthalmology Annual Meeting (ARVO 2018, for author's contribution, please see declaration at the beginning of the thesis.

4.2 Introduction

Chicks show excellent compensatory growth to imposed defocus ranging from -30D to +20D. When placing lenses on the eye with myopic defocus or hyperopic defocus, the eye growth can be slowed or accelerated and hence bring the image into focus so that when the lens is removed, the eye becomes hyperopic or myopic respectively. Hyperopia develops faster than myopia (Irving et al., 2015). It is believed that the young eye can completely compensate the spherical refraction for imposed lenses of powers between -30D and +20D, but complete compensation to higher powered lenses takes longer and astigmatism is increased in the presence of high defocus blur (Kisilak et al., 2007). In human, a decrease in refractive error, a decrease in its variability, and a decrease in mean astigmatism are three main components in normal emmetropization (Hirsch & Weymouth, 1990). The reduction in spherical error and a decrease in its variability has also been found in chicks either emmetropizing normally or responding to lenses with lower power (Kisilak, 2005). Astigmatism decreases in chick eyes as a function of normal emmetopization but increase in the presence of higher powered lenses (Kisilak, 2005) as it does in monkeys with lens treatments(Kee, Hung, Qiao-Grider, Ramamirtham, & Smith, 2005).

Astigmatism is the presence of differential refractive powers along different ocular meridians, this causes two distinct line foci that cannot be corrected through accommodation or with a spherically symmetric lens. Spherical defocus (myopia or hyperopia) produces a symmetric blur along the optical axis of the eye, while away from the disc of least confusion, astigmatism contributes a blur which changes its orientation with position between two foci planes. The coexistence of spherical defocus, astigmatism and higher order aberrations degrade the image on the retina.

One fundamental question in emmetropization is how the eye discerns the sign of defocus to achieve the optimal refractive state. Visual cues such as chromatic aberrations, accommodation, higher order monochromatic aberrations, astigmatism and diurnal rhythm have been hypothesized to play important roles. Animal research ruled out the necessity of chromatic aberrations in emmetropization as chicks raised in monochromatic light can reduce defocus normally (C. F. Wildsoet, Howland, Falconer, & Dick, 1993). Accommodation is unlikely to be a sole signal as chicks raised in drum permitting only one viewing distance showed good refractive compensation (Park, Winawer, & Wallman, 2003). It is possible that accommodation indirectly plays a role by altering the amount of blur on the retina (Wallman, 1993). Diurnal variation of MOR associated with changes in pupil size and axial length contributes to a diurnal variation in retinal blur and thus may be important in

determining the direction of eye growth needed to bring the eye into focus (M. C. Campbell et al., 2012). In addition, monochromatic aberrations including astigmatism generate differences in PSF with opposite signs of defocus (M. C. W. Campbell, Priest, & Hunter, 2001, (Wallman, 1993).

We have previously shown that average retinal blur across birds plateaus between day14 to day 21 for birds goggled with -15D lenses and the average retinal blur is not significantly different from cone resolution at this time. For birds goggled with +10D lenses (measured on two days), retinal blur is not significantly different from cone resolution on the last measurement day (14). We would like to know, once the magnitude of retina blur is just resolved by the cone photoreceptor sampling, i.e. when the amount of blur no longer decreases, what optical cues could be present to help the eye to maintain the optimal refractive state. We wish to determine whether astigmatism gives a difference in the retinal image with accommodation (as characterized by the point spread function) that could provide a signal to the direction of defocus if refraction drifts after emmetropization is almost complete.

.

4.3 Methods

Ross Ross chicks of mixed gender (same birds as the previous chapter) were goggled with either +10D (4) or -15D lenses (17) at hatching. Left eyes grew normally acting as controls. Measurements were taken on day 0 and subsequent days up to day 21 on awake birds of different sets. 4 birds goggled with +10D lenses were measured on day 0 and day 14. 4 birds goggled with -15D lenses were measured from day 9 to day 21. Additional sets of birds (total number 13) goggled with -15D lenses were measured from day 0 to day 14.

Aberrations were measured using Hartmann Shack aberrometry (Chapter 2) under dim light which allows natural pupil dilation and in the morning, at approximately the same time, each day to eliminate the effects of diurnal rhythm (M. C. Campbell et al., 2012).

Instantaneous ocular refraction (IR), calculated as spherical defocus through the goggles for HS frames taken of the chicks viewing a visible laser beam, assumed to vary with accommodation, is the dioptric distance between the disc of least confusion and the retina. This was calculated from the Zernike spherical defocus term for individual frames which allows us to study its changes with natural accommodation (Equation .4.1). The astigmatism was calculated from the other 2nd order Zernike terms (see below).

$$IR = \frac{-4\sqrt{3}Z_2^0}{r^2}$$

Equation 4. 1

In chapter 3, when determining mean ocular refraction (MOR), we measured refractions associated with the largest pupils and most hyperopic frames which are expected to represent the unaccommodated state. Here we measured refractions (including sphere and cylinder) at a wider range of pupil sizes which would represent the variation in accommodative state during the Hartmann Shack measurement and the amount of astigmatism present. During the measurement, the chick was viewing a red diode beam incident with zero vergence. MOR for each bird was averaged from frames with larger pupil sizes and most hyperopic measured instantaneous refraction (IR), which corresponded to unaccommodated state. For goggled eyes, MOR is calculated as the residual refractive errors looking through the goggles.

Astigmatism (total cylinder, C) and its component Jackson cross cylinders (JCC0, JCC45) were calculated for each frame from Zernike aberration terms as following (Thibos et al., 2004b):

$$JCC0 = \frac{-2\sqrt{6}Z_2^2}{r^2}$$

Equation 4. 1

$$JCC45 = \frac{-2\sqrt{6}Z_2^{-2}}{r^2}$$

Equation 4. 2

$$C = -2\sqrt{JCC0^2 + JCC45^2}$$

Equation 4. 3

Point spread functions and contributions to the optical blur of spherical defocus, total defocus including astigmatism and total blur including astigmatism and higher order aberrations were calculated exactly and their radial extents were approximated from equivalent blur for each frame as described in chapter 3. PSFs were calculated for individual H-S measurements for 4 birds unilaterally goggled with -15D lenses measured from days 14 to 21and 4 birds goggled with +10D lenses were measured on day 14, which additionally sampled more frames with wider range of measured accommodation.

Cone photoreceptors were imaged close to the area centralis using an AO scanning laser ophthalmoscope. Cone resolution was calculated from the images (Chapter 3). Endpoint cone resolutions were obtained (Chapter 3).

We analyze the changes in MOR, astigmatism and its components, retinal blur for individual birds after average retinal blur starts to stabilize at day 14. Statistical analysis was performed using sigmaplot 12.0 (Systat Software, San Jose, CA) to study the difference between groups and parameters.

4.4 Results

4.4.1 Astigmatism changes

Total astigmatism with age and between eyes

Figure 4.1 a shows the changes in total cylinder with age for control eyes and goggled eyes for birds goggled with -15D lenses. In the birds goggled with -15 D lenses, total cylinder (C) significantly exponentially reduced in control eyes ($p<0.01$) and significantly increased linearly in goggled eyes from day 0 to day 18 ($p<0.05$). The linear increase fit was not significant from day 0 to 21 ($p=0.09$). Figure 4.1 b shows the difference in total cylinder between eyes with age. Total cylinder was significantly larger in goggled eyes than control eyes and the difference was increased linearly significantly (linear fit $p<0.05$).

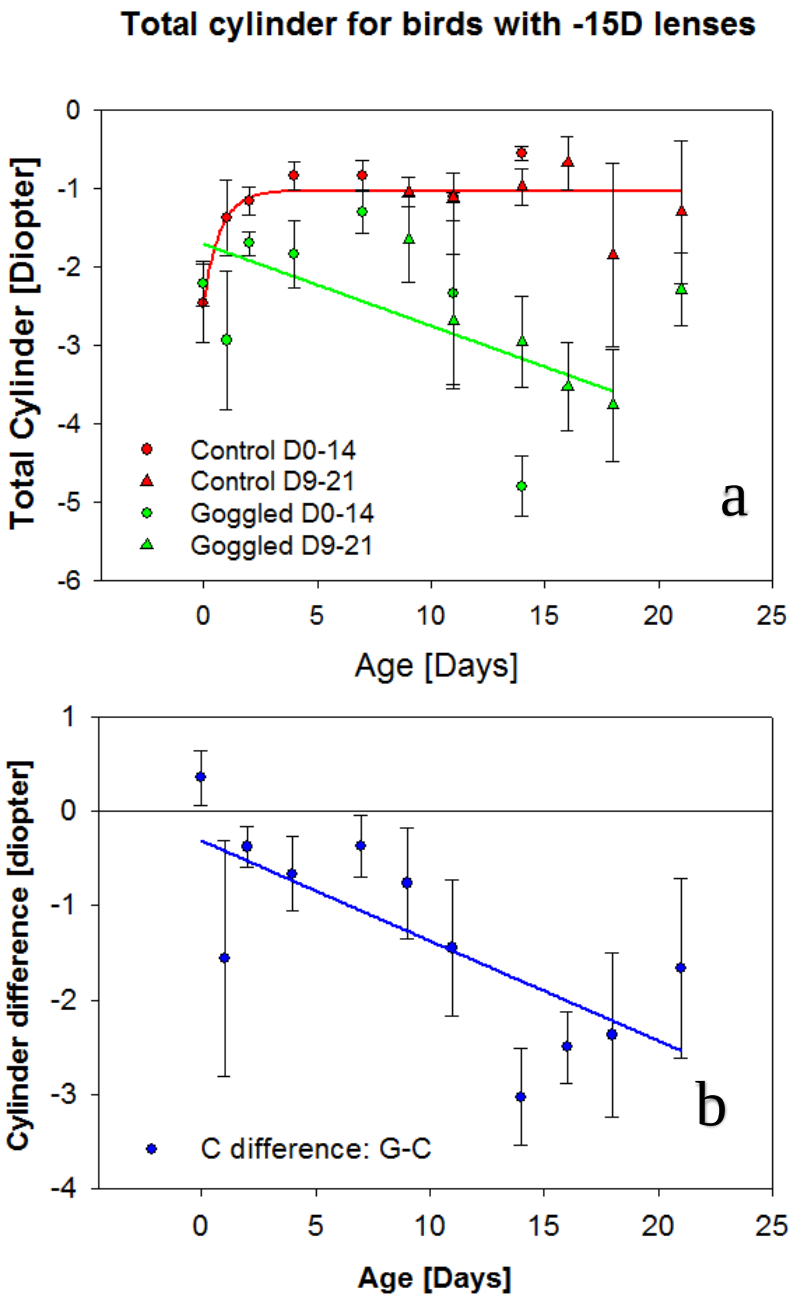

Figure 4. 1 a) Total cylinder for birds goggled with -15D lenses aged day 0 to day 21. Control eyes in red, goggled eyes in green. Red line: significant exponential fit ($p<0.01$) for control eyes. Green line: Significant linear fit to day 18 for goggled eyes ($p <0.05$). b) Cylinder difference between eyes with age. Blue circles: Total Cylinder of goggled eyes minus control eyes. Blue line: significant linear fit ($p<0.05$).

In the 4 birds goggled with +10D lenses (table 4.1), There is a non-significant decrease in Cylinder in control eyes ($p>0.05$) and a non-significant increase in Cylinder in goggled eyes ($p>0.05$). The total cylinder was not statistically significantly larger in goggled eyes than in control eyes on either day 0 or day 14 ($p>0.05$).

Total Cylinder ±SD [D]	**Day 0**	**Day 14**	**Paired-t-test p between Day 0 and Day 14**
Control [+10D]	-1.2±0.44D	-1.1±0.39D	P=0.13
Goggled [+10D]	-1.35±0.46D	-1.81±0.68D	P=0.18

Table 4. 1 Average astigmatism (Total Cylinder) changes with age in the birds goggled with +10D lenses

Astigmatic components with age and between eyes

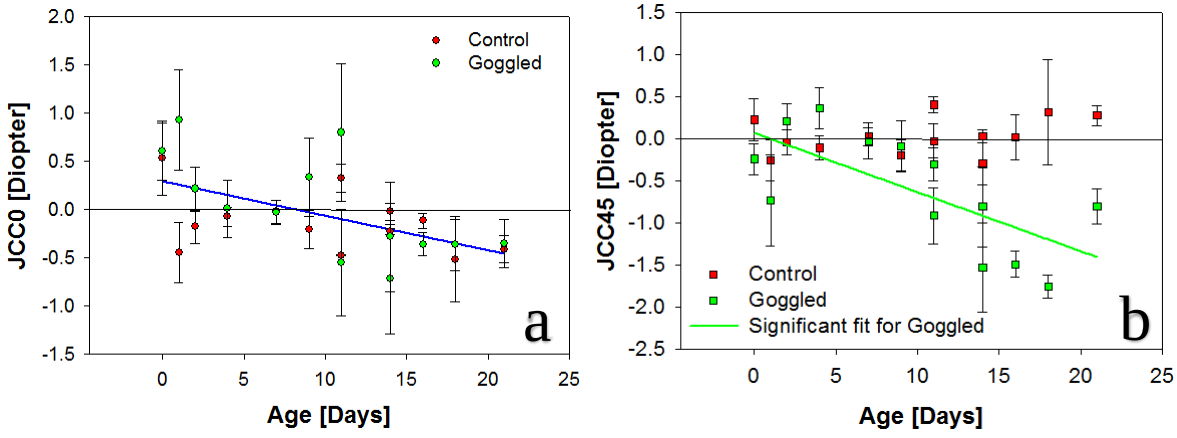

Figure 4. 2 Jackson cross-cylinders components with age for birds goggled with -15D lenses: JCC0 (a), JCC45 (b). Control eyes in red, goggled eyes in green. JCC0 is not significantly different between control eyes and goggled eyes (ANOVA: p=0.019). The blue line shows a

significant decrease in JCC0 for control and goggled eyes when pooled ($p<0.005$). The green line shows a significant linear increase in JCC45 in goggled eyes with age ($p<0.05$).

Source of variation	P-value
Age	0.019
Treatment (Control or Goggled with +10D lenses)	0.200
Age*Treatment	0.364

Table 4. 2 ANOVA test on JCC0 for birds goggled with -15D lenses. * means interaction term. $p<0.05$ means significantly different.

Figure 4.2 shows Jackson cross-cylinders versus age. An ANOVA test on JCC0 (Table 4.2; Figure 4.2a) showed 1) significant difference with age; 2) Non significant difference between control eyes and goggled eyes and 3) Non significant interaction between age and treatment. A significant linearly decrease was found for control and goggled eyes when pooled ($p<0.005$). The absolute value of JCC0 is not significantly different between day 0 and day 21 (t test: $p=0.178$). JCC45 (Figure 4.2b) significantly linearly increased (Equation 4.7) in goggled eyes. JCC45 did not significantly change with age in control eyes ($p>0.1$).

Figure 4.3 shows that Jackson cross cylinders (JCC0 plotted as x-axis, JCC45 plotted as y-axis) on day 0 and day 14 for birds goggled with -15D lenses (A and B) and +10D lenses (C and D). Control eyes in red, goggled eyes in green, the circles symbolize the results on day 0, triangles symbolize the results on day 14. The distance of each data point from zero (origin) represents the absolute value of half Cylinder (equation 4.2, 4.3, 4.4), revealing the changes of mean astigmatism.
For birds goggled with -15D lenses (Figure 4.3A, 4.3B), there is a decrease in the distance of the data points from zero (half the value of total cylinder) in control eyes and an increase in the in the goggled eyes from day 0 to day 14, consistent with the significant decrease in the cylinder value in control

eyes and an increase in cylinder in goggled eyes, (Fig 4.1) which was confirmed in paired-t-test as summarized in table 4.3.

For birds goggled with +10D lenses (Figure 4.3C, 4.3D), the decrease in the cylinder in control eyes (table 4.3). and increase in the goggled eyes was not significant. The change in JCC0 and JCC45 or their absolute values with age were not significant ($p>0.05$). On day 14, JCC0 was not different between eyes ($p>0.5$) but JCC45 was significantly larger in goggled eyes than control ($p=0.036$). On day 14, JCC45 was not significantly larger in eyes goggled with -15D lenses than eyes goggled with +10D lenses ($p>0.5$).

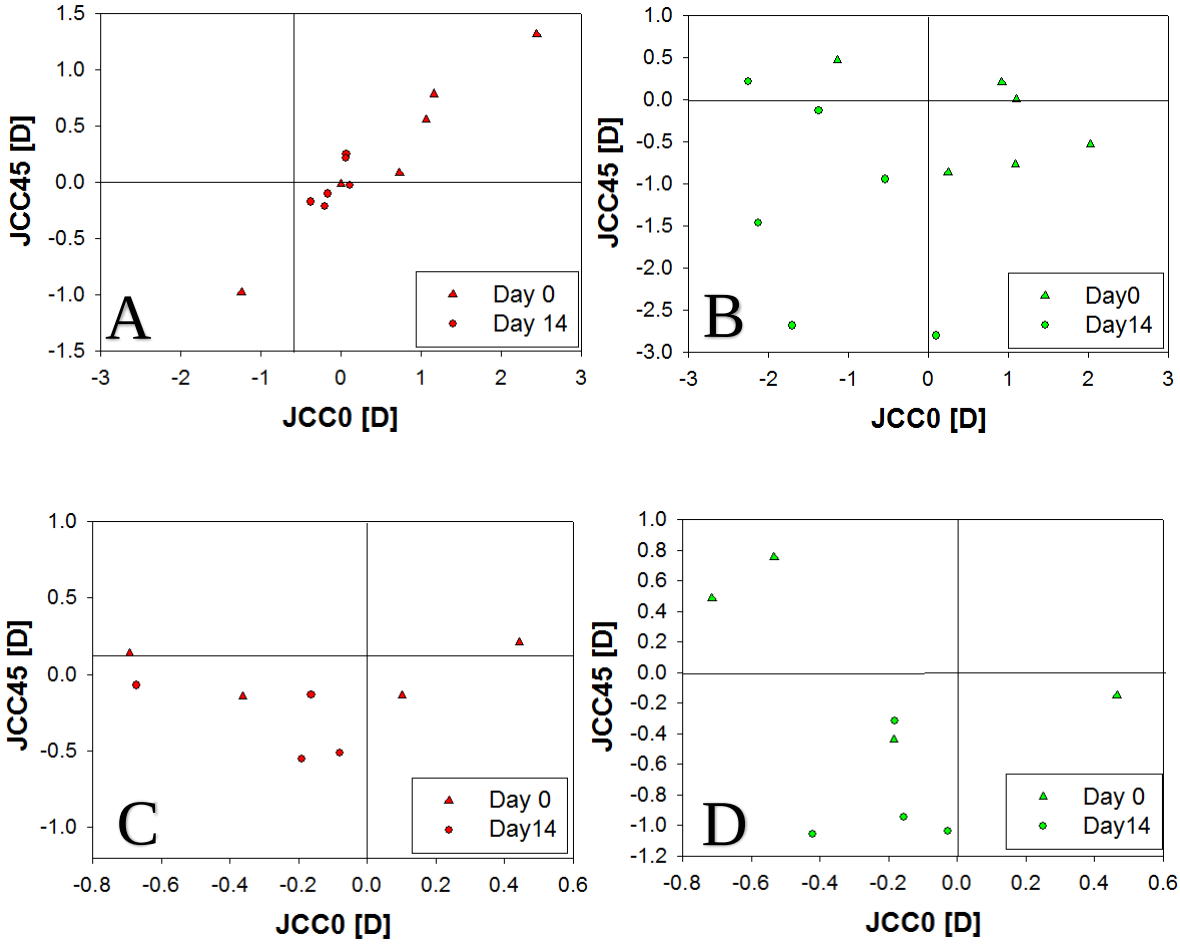

Figure 4. 3 JCC0 vs JCC45: for birds goggled with -15D lenses A and B and for birds goggled with +10D lenses C and D. Control eyes in red, goggled eyes in green. Triangles represent data from day 0 and circles represent data from day 14. Total cylinder significantly reduced in

control (A) eyes ($p<0.05$) and increased in goggled eyes (B) ($p<0.05$) for birds goggled with -15D lenses. For eyes goggled with +10D lenses, the change in JCC0 and JCC45 or their absolute values are not significant (paired-t test; $p>0.05$).

Total Cylinder ±SD [D]	Day 0	Day 14	Paired-t-test between day 0 and day 14
Control [-15D]	-3±2D	-0.7±0.2D	<0.05
Goggled [-15D]	-2.7±0.9D	-5±2D	<0.05
Control [+10D]	-1.2±0.4D	-1.1±0.4D	P=0.13
Goggled [+10D]	-1.4±0.5D	-1.8±0.7D	P=0.18

Table 4. 3 Average astigmatism (Total Cylinder) on day 0 and day 14. 6 birds with -15D goggles and 4 for +10D goggles are included.

4.4.2 Refraction variation and Cylinder value in individual birds day 14 to day 21

Instantaneous measured refraction (IR), calculated as spherical defocus looking through goggles, is zero if the disc of least confusion sits on the retina, IR is positive when the disk of least confusion sits behind the retina and negative when the disk of least confusion sits in front of the retina (Figure 4.4).

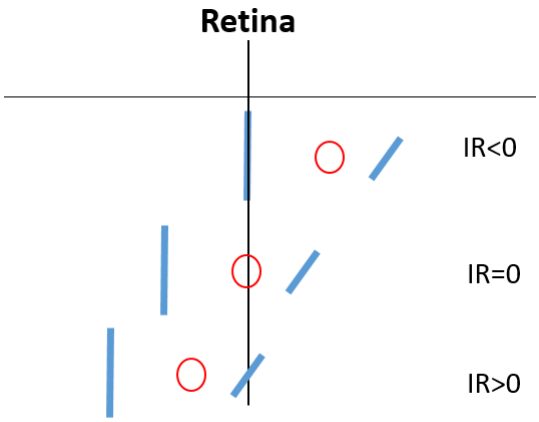

Figure 4. 4 Variation of measured refraction with respect to retina. Blue lines: two foci lines determined by astigmatism. Red circle: disc of least confusion. From top to bottom, IR<0, disc of least confusion is behind the retina (in this case, most myopic foci line sits on the retina); IR=0, disc of least confusion sits on the retina; IR>0, disc of least confusion is in front of the retina (in this case, most hyperopic foci line sits on the retina).

	ΔIR [D]	Cylinder $\lvert C \rvert$ [D]	Half Cylinder $\lvert \frac{C}{2} \rvert$ [D]	T test ΔIR and $\lvert C \rvert$	T test ΔIR and $\lvert \frac{C}{2} \rvert$
Goggled [+10D] day 14	3±2	1.8±0.7	0.9±0.3	0.46	0.17
Goggled [-15D] day 14 and 21	5±1	3.3±0.8	1.6±0.4	0.15	<0.05
Control [+10D] day 14	1.4±0.4	1.1±0.4	0.5±0.2	0.5	0.07
Control [-15D] day 14 and 21	4±1	1.4±0.9	0.7±0.5	<0.05	<0.05

Table 4. 4 Changes in measured instantaneous refraction IR across frames and comparison with the Cylinder and half Cylinder value.

Within each measurement day, individuals have a variation of measured ocular refraction IR across frames, which tracks the instantaneous position of disk of least confusion, likely associated with measured accommodation. Chicks' accommodative range is about 20D (Schaeffel et al., 1988). On average, the accommodation inferred from the range of IR is significantly larger than at least half cylinder value for birds goggled with -15D lenses and larger (with borderline significance) for control eyes of birds goggled with +10D lenses (Table 4.4), allowing the eye to change focus from one line foci to another.

For birds goggled with -15D lenses, though the average sampled frame number is significantly higher in the control eyes than the goggled eyes, the average change in measured ocular refraction (IR) across day 14 to day 21 is not significantly different between eyes. For birds goggled with +10D lenses, variation in measured ocular refraction is not significantly different between eyes and the number of sampled frames are not different (Table 4.5).

	ΔIR_i [D]	**Cylinder Absolute $\lvert C \rvert$ [D]**	**Sampled frames each day each eye#**
Goggled eyes [+10D] day 14	2.6±2.0	1.8±0.68	9±4
Goggled eyes [-15D] day 14 to 21	4.5±1.2	3.3±0.79	8±2
Control eyes [+10D] day 14	1.4±0.4	1.1±0.4	5±2
Control eyes [-15D] day 14 to 21	4±1	1.4±0.9	17±2

Table 4. 5 Changes in measured instantaneous refraction IR across frames, the cylinder value of refraction and average frame numbers sampled for analysis. Chicks' accommodative range is about 20D (Schaeffel et al., 1988).

4.4.3 Individual's retinal blur day 14 and after

Summary

Retinal blur corresponding to mean ocular refraction at day 14 is not significantly different from cone resolution as previously shown (Chapter 3). Astigmatism in this period was shown to be larger in the eyes goggled with -15D lenses than in control eyes. We then study the changes of PSF and their radial approximation for each bird goggled with -15D lenses or +10D lenses within individual day (across measurement time) at this time period. 4 out of 8 goggled eyes showed characteristic different elongation directions in their total PSF as a function of instantaneous refraction even with higher order aberrations present for measured Hartman-Shack frames. The orientation of PSF long axis appears in the majority of eyes to be dominated by oblique astigmatism (JCC45, which corresponds to Zernike term Z_2^{-2}). Given the ~20D accommodative range (Schaeffel et al., 1988), in control eyes and goggled eyes for those which orientation changes were not observed in the measured Hartman-Shack frames, PSFs were calculated with IR moved (<1D) beyond line foci evident in the Hartman-Shack frames assuming higher-order aberrations do not change. Orientation changes dominated by oblique astigmatism of total PSFs were observed in those goggled eyes which changes were not observed in the measured Hartman-Shack frames when the instantaneous refraction was moved less than 1D beyond line foci. Orientation changes were also observed in the total defocus PSFs of control eyes and the differences persist when including higher-order aberrations (See example for Control eyes section).

Orientation of PSF on the retina as function of change in refraction: Goggled eyes

The measured ocular refraction across all frames (IR) gives the position of the disk of least confusion with respect to the retina and tracks the presumed variations in accommodation. As IR changed, likely due to accommodation, the long axis of the total defocus PSF flipped its orientation as characterized by the two line foci in oblique astigmatism in goggled eyes (Figure 4.5 4.6 4.7 4.8). For most eyes, line foci pointed counter clockwise at approximately 45° when the sphere was positive and at 135°

when the sphere went negative. When higher order aberrations are considered in the total PSF, the direction of orientation of the PSF as a function of refraction is unchanged for those goggled eyes which observed orientation changes in total defocus PSF.

As measured ocular refraction IR changed during the limited measurement time, orientation changes of the long axes for the total defocus PSF were observed in 2 out 4 eyes goggled with +10D lenses (Figure 4.5, 4.6) and 2 out of 4 eyes goggled with -15D lenses (Figure 4.7, 4.8) within a single day's measurements (Table 4.6). The PSFs for the most hyperopic and most myopic measured ocular refractions are shown. The long axis of total defocus appears to be dominated by oblique astigmatism in all eyes, and the line length is above the cone resolution. When adding higher-order aberrations, this orientation of long axes (total PSF) were not obscured in goggled eyes with -15D lenses or goggled eyes with +10D lenses.

	Subject	**ΔIR within a day [D]**	**Cylinder C Absolute [D]**	**Orientation flip in total PSF**
Goggled +10D	B2	2.4 (-1.4 to 1.0)	2.0	Yes
Goggled +10D	B13	5.5 (-2.0 to 3.5)	2.2	Yes
Goggled -15D	B1634	3.0 (-1.1 to 1.9)	2.8	Yes
Goggled -15D	B1630	2.6 (-1.3-1.2)	2.3	Yes

Table 4. 6 Example of orientation flip observed in frames captured for birds goggled with -15D lenses or +10D lenses. ΔIR is variation of the measured ocular refraction during limited measurement time, brackets shows the range of measured ocular refraction.

Goggled eyes for birds with +10D goggles

Birds goggled with +10D lenses were measured on day 14, total defocus PSFs and total PSFs were examined for all frames for individual birds. Examples of PSFs are shown below.

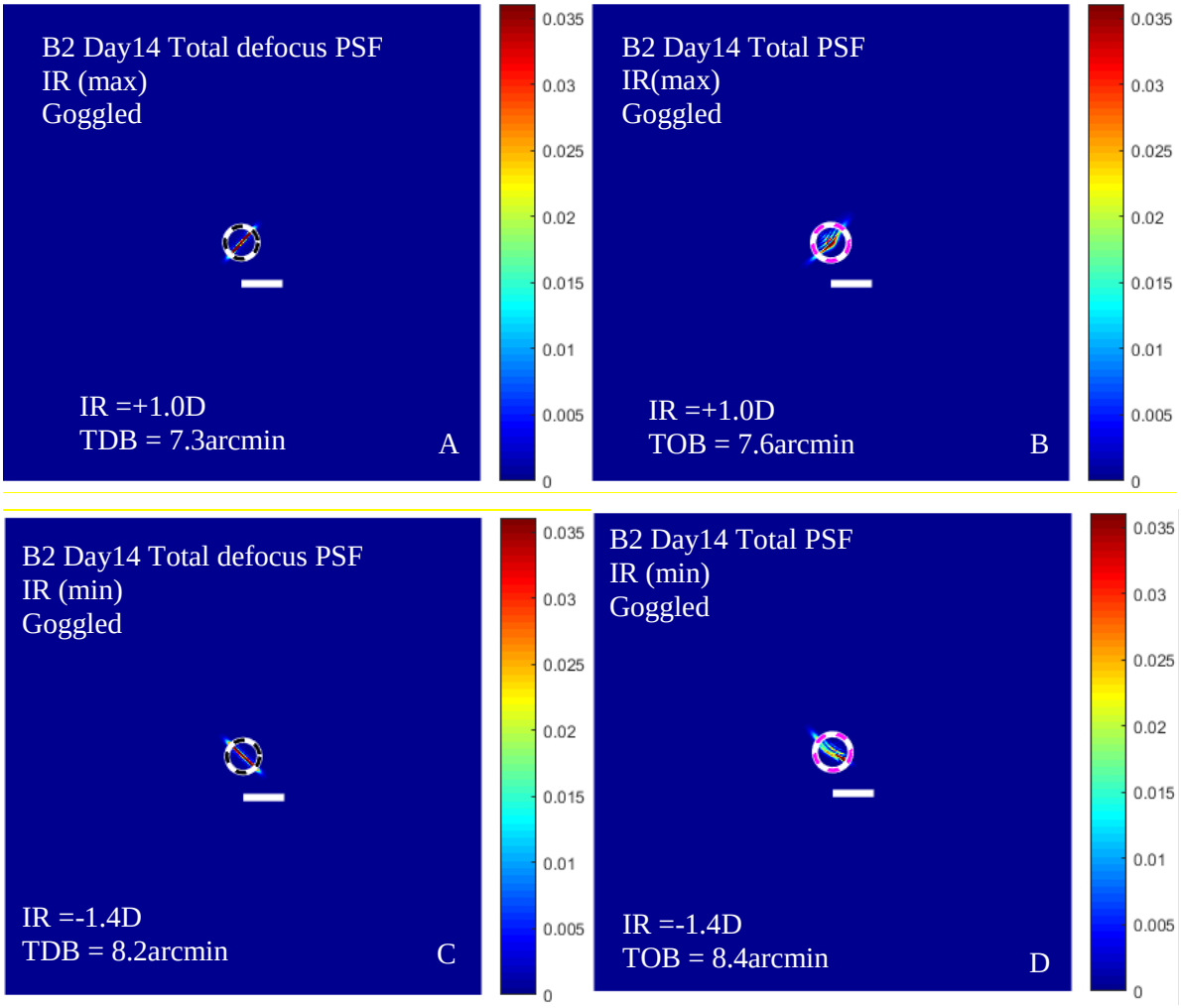

Figure 4. 5 Goggled eyes' PSFs on day 14 for Bird B2 goggled with +10D lenses: PSF for the most positive instantaneous refraction IR (likely an unaccommodated state): A total defocus PSF, B total PSF. PSF for the most negative IR (likely an accommodated state): C total defocus PSF, D total PSF. The radii of the dashed black circles and purple circles represent the total defocus blur (TDB) and total optical blur (TOB) respectively, calculated from the equivalent blur approximation. Cone resolution is 6.5arcmin. As measured, ocular refraction went from +1.0D to -1.4D, the long axis of PSFs rotated from about 45° counterclockwise to 135° counter clockwise (total defocus PSF Figure 4.7A and C; total PSF Figure 4.7B and D). Long axes orientation was not obscured by higher-order aberrations present in Figure 4.7B and 4.7D.

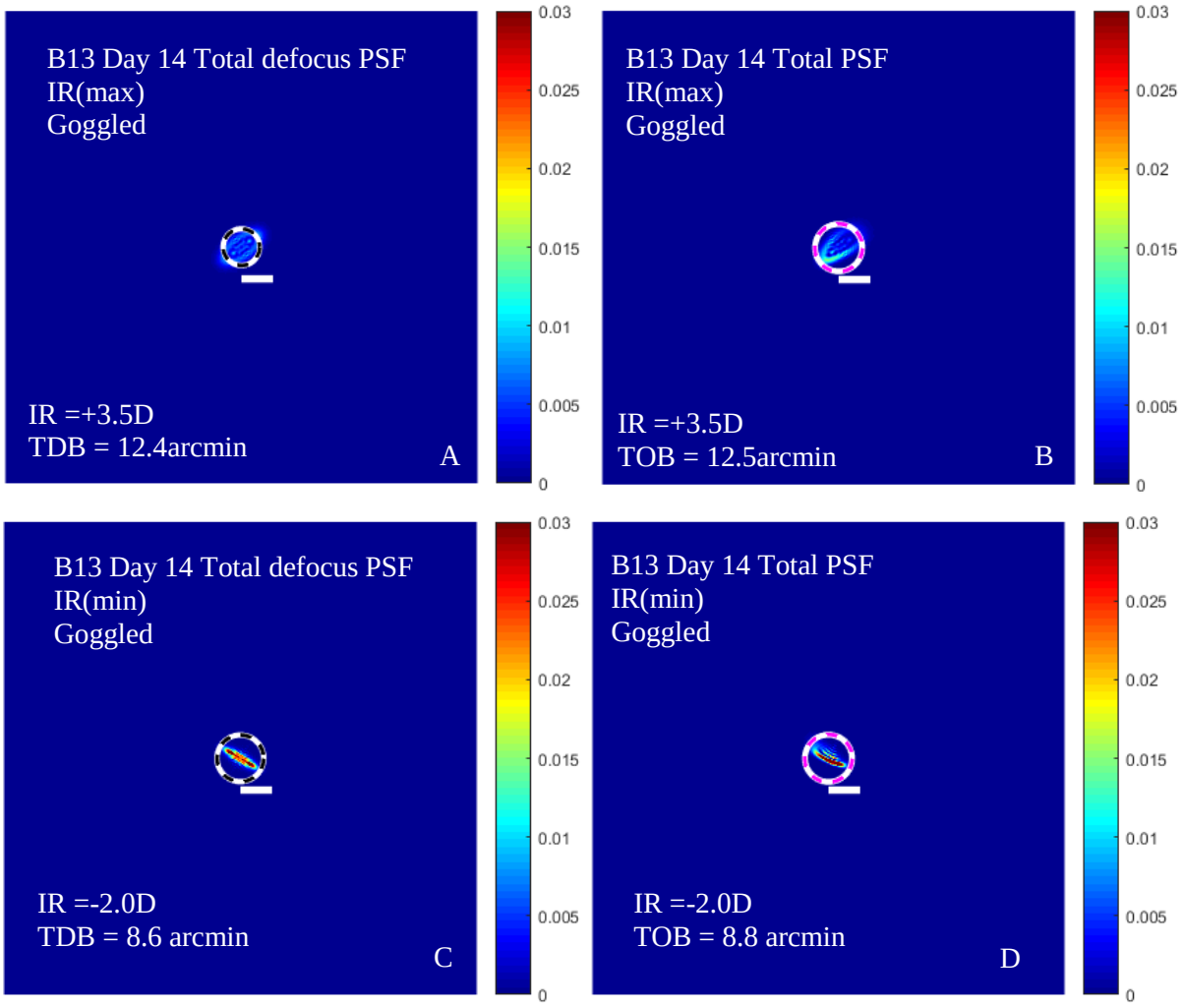

Figure 4. 6 Goggled eye's PSFs on day 14 for Bird B13 goggled with +10D lenses: PSF for the most positive IR (likely an unaccommodated state): A total defocus PSF, B total PSF. PSF for the most negative IR (likely an accommodated state): C total defocus PSF, D total PSF. The radii of the dashed black circles and purple circles represent the total defocus blur (TDB) and total optical blur (TOB) respectively, calculated from the equivalent blur approximation. Cone resolution at this time point is 6.5arcmin, for 4.6B, the radius of the short axis is 4.6 arcmin. As measured, ocular refraction went from +3.49D to -2.01D, the long axis of PSFs rotated from about 45° to 135°. Long axes orientation was not obscured by higher-order aberrations present in Figure 4.8B and 4.8D.

Goggled eyes for birds with -15D goggles

Birds goggled with -15D lenses were measured between day 14 to day 21, total defocus PSFs and total PSFs were examined for all frames measured on each day for individual birds. Examples of PSFs are shown below.

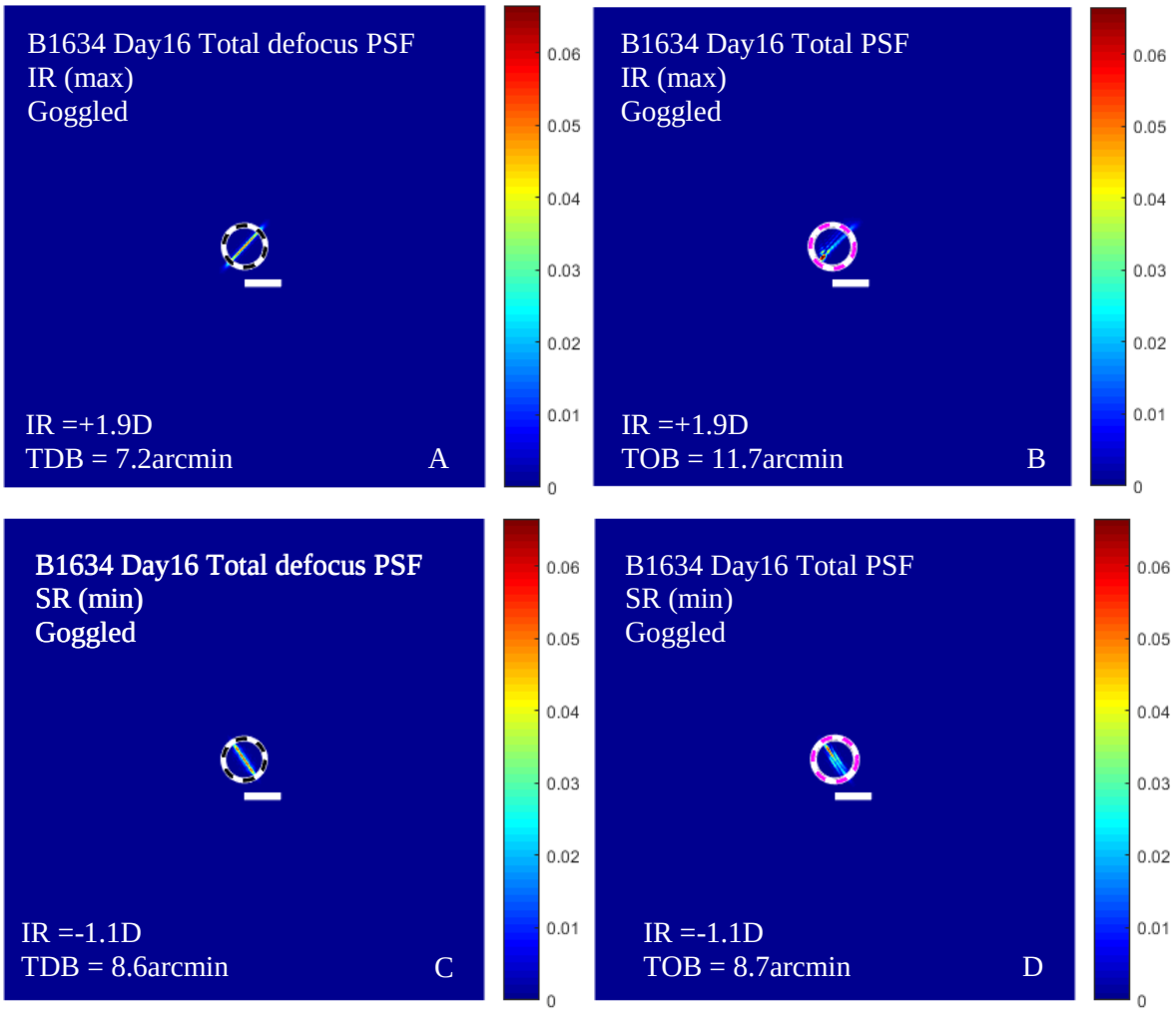

Figure 4. 7 Goggled eye's PSFs on day 16 for Bird B1634 goggled with -15D lenses: PSF for the most positive IR (likely an unaccommodated state): A total defocus PSF, B total PSF. PSF for the most negative IR (likely an accommodated state): C total defocus PSF, D total PSF. The

radii of the dashed black circles and purple circles represent the total defocus blur (TDB) and total optical blur (TOB) respectively, calculated from the equivalent blur approximation. Cone resolution at this time point is 6.53 arcmin. As measured, ocular refraction went from +1.9D to -1.1D, the long axis of PSFs rotate from about 45° to 135°. Long axes orientation was not obscured by higher-order aberrations present in Figure 4.7B, 4.7D.

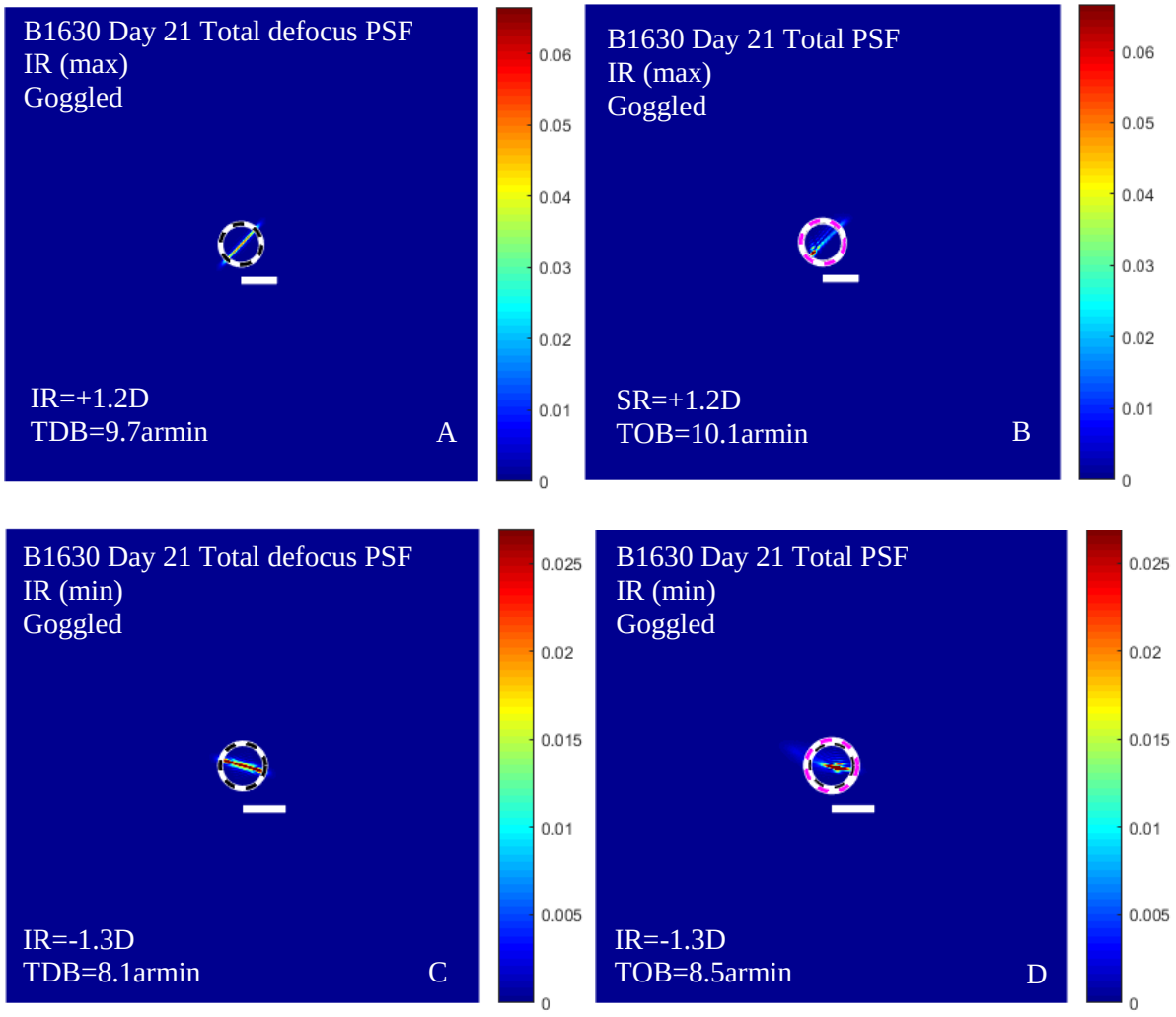

Figure 4. 8 Goggled eye's PSFs on day 21 for Bird B1630 goggled with -15D lenses: PSF for the most positive IR (likely an unaccommodated state): A total defocus PSF, B total PSF. PSF for the most negative IR (likely an accommodated state): C total defocus PSF, D total PSF. The

radii of the dashed black circles and purple circles represent the total defocus blur (TDB) and total optical blur (TOB) respectively, calculated from the equivalent blur approximation. Cone resolution at this time point is 6.49arcmin. As measured, ocular refraction went from +1.2D to -1.3D, the long axis of PSFs rotate from about 45° to 135°. Long axes orientation was not obscured by higher-order aberrations present in Figure 4.8B, 4.8D

Orientation of PSF on the retina as function of change in refraction: Control eyes

In the limited sampled frames, 2 out 4 control eyes of birds goggled with -15D lenses had observable orientation changes in the total defocus PSF, none of the control eyes of birds goggled with +10D lenses had observable changes in the total defocus PSF for the measured Hartman-Shack frames. When adding higher-order aberrations to produce the total PSF, the orientation of the long axes (evident in the defocus PSF) appears to be blurred out in control eyes. One example of the PSFs is shown below.

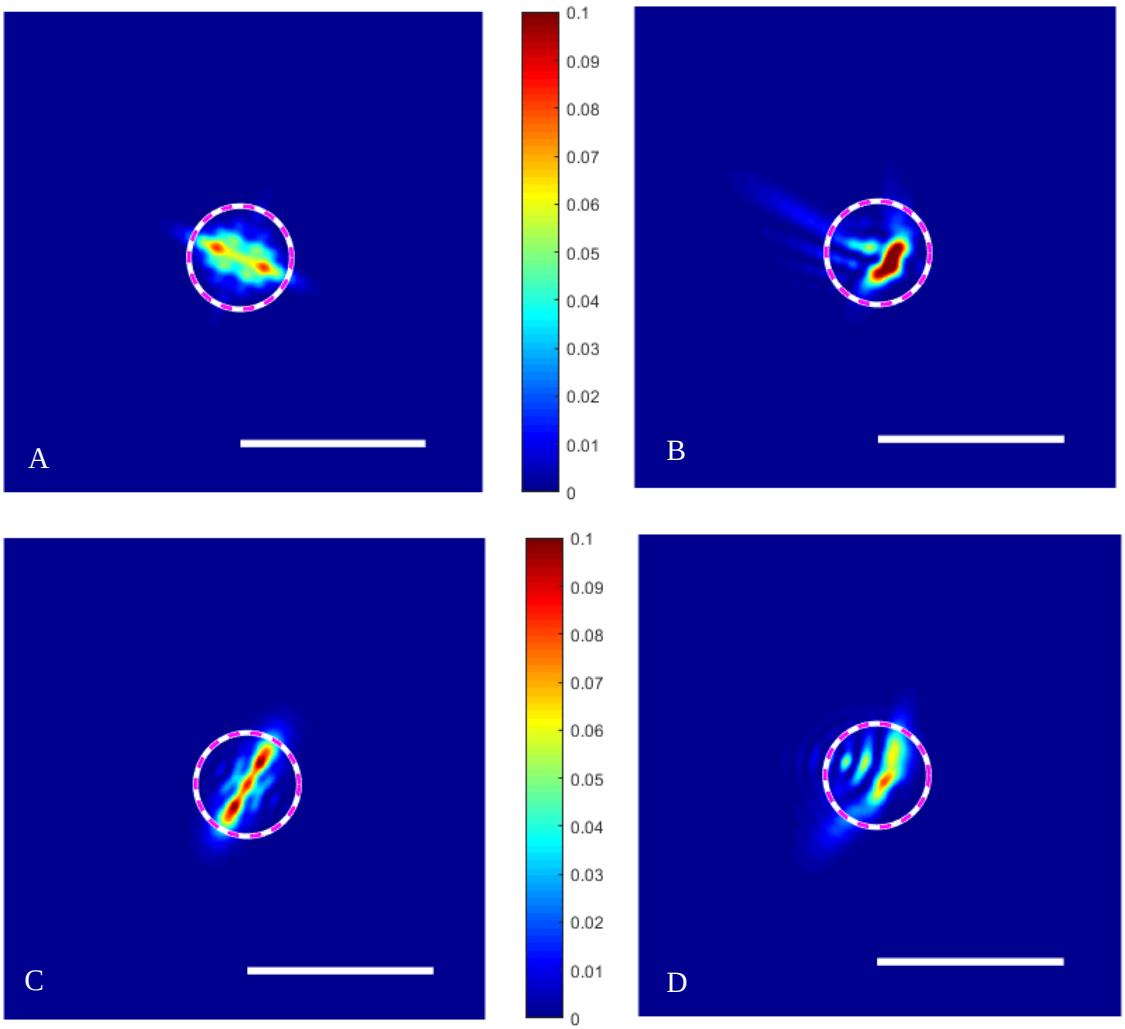

Figure 4. 9 Control eye's PSFs on day 14 for Bird B1634 goggled with -15D lenses: PSF for the most positive IR (likely an unaccommodated state): A total defocus PSF, B total PSF. PSF for the most negative IR (likely an accommodated state): C total defocus PSF, D total PSF.

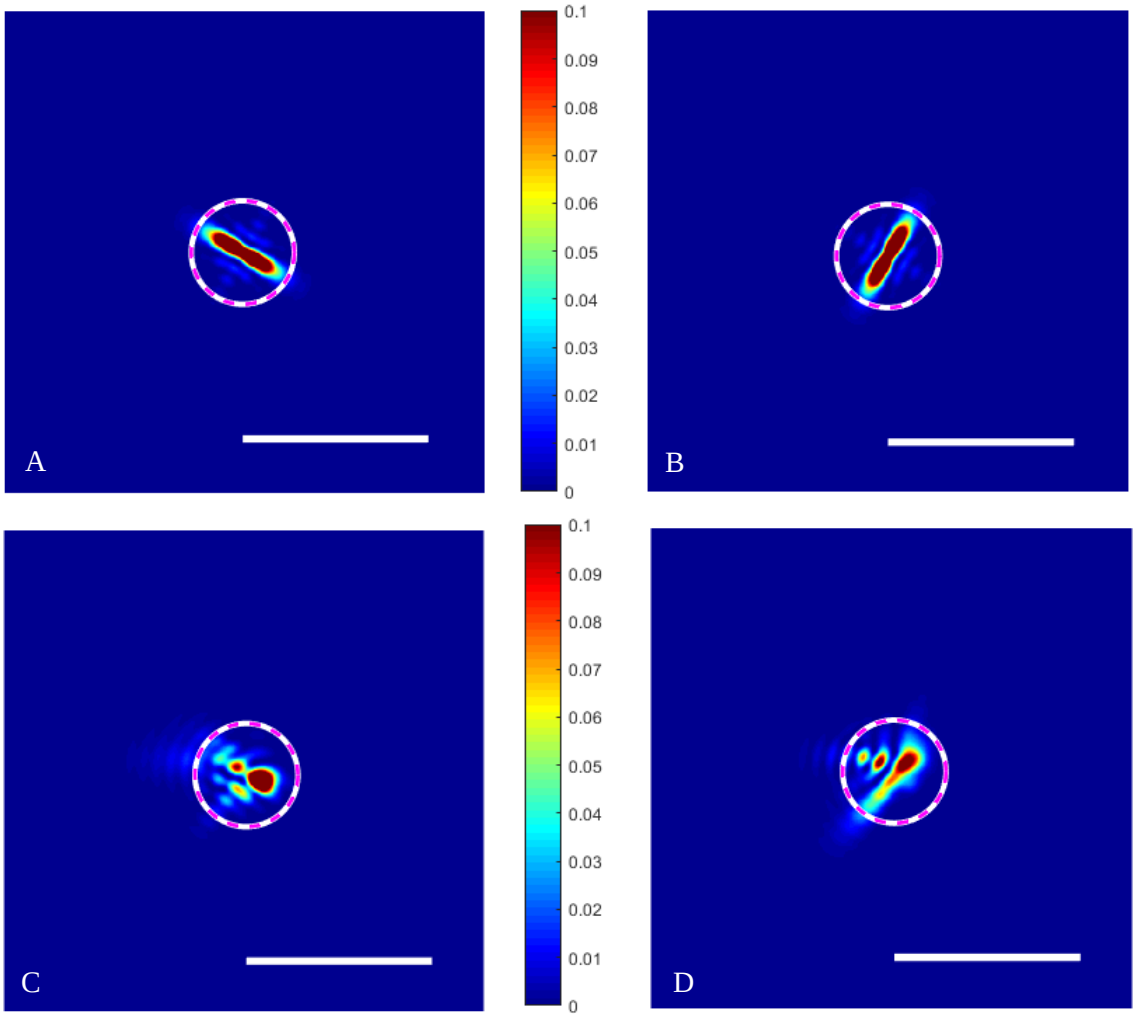

Figure 4. 10 Control eye's modeled PSFs on day 14 for Bird B1634 goggled with -15D lenses. In this particular case: A total defocus PSF when most myopic line foci sits on the retina ($IR = +\frac{|C|}{2}$), B total defocus PSF when most hyperopic line foci sits on the retina ($IR = -\frac{|C|}{2}$), C, D total PSF for A, B respectively.

4.5 Discussion

Astigmatism changes

In the birds goggled with -15D lenses (Figure 4.1a), cylinder values were significantly reduced in control eyes, consistent with emmetropization of astigmatism in normally growing eyes (Kisilak et al., 2006). Cylinder values in goggled eyes linearly increased up to day 18, similar to the birds goggled with higher powered negative lenses (-30D) (Kisilak et al., 2007). The difference in total cylinder between control and goggled eyes increased significantly linearly to day 21, suggesting continuing increase in astigmatism in the goggled eyes (Figure 4.1b). Since the pupil size was larger, the astigmatic blur was significantly larger on day 21 than on day 0 as previously shown in Chapter 3. Astigmatism in the goggled eyes may continue to increase until it reaches the physical limitation of ocular dimensions, or cylinder in the goggled eyes may reduce possibly on days later than measured here to be not different from control eyes (Figure 4.1b) as suggested by homeostasis growth (Wallman & Winawer, 2004b). To determine this, we would need to extend the measurement time beyond day 21. JCC0 significantly linearly reduced in control eyes and goggled eyes (Figure 4.2 a), the magnitude of JCC0 was not significantly different between day 0 and day 21, suggesting the change in sign rather than magnitude in JCC0. These results are consistent with another study (Schmid & Wildsoet, 1997)). Goggling appears to not affect the change of JCC0 with age (Figure 4.2 a). JCC45 (oblique astigmatism) significantly increased with age in the goggled eyes and varied little with age in the control eyes (Figure 4.2 b), the change in JCC45 likely explains the change in total cylinder, similar to the results previously found in the chick eyes goggled with -30D lenses. In this study, the emmetropization of astigmatism was interrupted and oblique astigmatism was increased in goggled eyes (Kisilak et al., 2007). The increase in oblique astigmatism may be a side effect of large ocular expansion, secondary to the large length changes due to defocus blur. Astigmatism may be induced by physical limitation of the eye growth in one dimension (Kisilak et al., 2007).

In the 4 birds goggled with +10D lenses (table 4.1), Cylinder was not statistically significantly larger with age nor was the increase in cylinder in goggled eyes than in control eyes. Following emmetropization, the total optical blur was also not significantly higher in the goggled eyes, possibly due to the smaller sample size, or the amount of increase was smaller than in eyes goggled with -15D lenses due to the lower power lenses. There was a non-significant decrease in cylinder with age in the corresponding control eyes, likely due to small sample size as reduction in astigmatism in normally

growing eyes is one aspect in emmetropization (Kisilak et al., 2006). No significant change with age was observed in JCC45 or JCC0 in the either control eyes (Figure 4.4 c) or eyes goggled with +10D lenses (Figure 4.4 d) from day 0 to day 14. However, JCC45 was significantly larger in goggled eyes than control on day 14. The oblique component is significantly larger but the total Cylinder is not. In the Cylinder measurement, the change in JCC45 may be masked by the lack of change in the JCC0. Change in astigmatism maybe associated with the power of inducing lenses as cylinder increases in the eyes goggled with -30D lenses (Kisilak et al., 2007) and more than -15D lenses and decreases in the control eyes (-15D goggled birds). It would be interesting to increase the sample size of +10D birds and to test additional lens powers to see if the change in oblique astigmatism is dependent on lens power As reported in Chapter 3, the increased astigmatism in eyes goggled with -15D lenses likely explains the higher total optical blur present on days 9-21 in goggled eyes compared to control eyes for birds goggled with -15D lenses.

Astigmatism signals to the direction of defocus

At the time period between day 14 and day 21(when retinal blur plateaus), average retinal blur is not significantly different from cone resolution as previously shown in Chapter 3. When the magnitude of retinal blur can just be resolved by cone photoreceptor array, it is expected to be a stop signal to emmetropization as previously proposed. If refractive error drifts after emmetropization, and the magnitude of blur increases, how does the eye tell the direction of the focusing error? Changes in retinal blur (shape of the PSF) with accommodation may provide a signal to the direction of the change in refractive state (M. C. W. Campbell, Priest, & Hunter, 2001, (Wallman, 1993). For this to occur, the instantaneous refraction (IR) of the eyes must vary from positive to negative with a variation larger than the cylinder distance during the measurement. In the goggled eyes with increased astigmatic blur, the orientation of the long axes of the PSF alters as accommodation varies. Oblique astigmatism was observed in 4 of 8 eyes (figures 4.5, 4.6, 4.7, 4.8) as providing a signal to the direction of defocus in goggled eyes As ocular refraction varies across frames, indicating an accommodative change, the distance of disc of least confusion from the retina changes, an orientation change in total PSF can be observed in goggled eyes if only the defocus (spherical and astigmatism) is considered. Chick can accommodate up to 20D (Schaeffel et al., 1988). This accommodation range will provide the possibility for the eye to shift focus from the most myopic meridian to the most

hyperopic meridian and beyond. The lack of observation of two line foci in those goggled eyes was likely due to the limited frames sampled. However, in those eyes which have variation in IR smaller than the Cylinder distance, when the instantaneous refraction was moved less than 1D beyond the foci line, changes in the orientation of the blur were observed which could provide a signal to the direction of defocus. The line foci observed are consistent with predominantly oblique astigmatism which generates the asymmetry in PSF orientation with changing instantaneous refraction (assumed to be due to accommodation). In all then the goggled eyes, this change in PSF orientation was still present in the presence of higher order aberrations. Thus, near the completion of emmetropization, oblique astigmatism provides a signal which could assist the eye to maintain the optimal refractive error. In addition, over a short time period, accommodative fluctuations allow the retina to sample this signal.

In the limited frames sampled, some control eyes changed their instantaneous refraction from positive to negative and an orientation change was observed in total defocus PSF. As control eyes have smaller astigmatism than goggled eyes, the orientation signal in the total defocus PSF is weaker, and maybe to be obscured by the higher-order aberration present in the total PSF. This does not rule out the possibility that there is a signal present due to astigmatism in control eyes. In the 8 control eyes with modeled IR beyond the line foci, an orientation change was observed in the total defocus. The difference in PSFs' orientation persists when adding higher-order aberrations. Thus, it is possible that control eyes accommodate beyond line focus in order to present an elongated blur on the retina with a larger orientation signal that are visible even with higher order aberration present. More frames were sampled in control than goggled eyes, which indicated the increased accommodation in the goggled eyes. Longer sample videos might indicate that accommodative fluctuations are larger and more frequent in goggled eyes in the later stages of emmetropization than in control eyes.

Other cues to the direction of defocus such as diurnal rhythm in MOR (M. C. Campbell et al., 2012), which varies the amount of blur on the retina may play a role in providing a signal to the direction of defocus in both control and goggled eyes. Our results support the idea that the larger astigmatism signal in the goggled eyes represents an upregulated signal to allow the eye to achieve and maintain an optimal refractive state. The actual accommodative range in chicks provides a possibility for the eye to shift focus from the most hyperopic line to the most myopic line, suggesting astigmatism may act as one potent signal to help the eye tell the drift in refractive errors. Our results might suggests that the goggled eye with higher astigmatism and the control eyes have a tendency to emmetropize to

the more hyperopic line focus instead of the mean sphere as the MOR is close to the refraction of the line focus, in agreement with an early study (Schmid & Wildsoet, 1997).

4.6 Conclusion

During emmetropization, mean astigmatism significantly increases in the goggled eyes with -15D lenses, likely due to the increase in oblique astigmatism. As ocular instantaneous refraction varies, which moves the disc of least confusion and foci lines determined by astigmatism with respect to the retina, orientation flip was observed between two line foci with orientation dominated by oblique astigmatism, the orientation of PSF is above the cone resolution. This may allow the chick to distinguish the directional change of defocus from the PSF in the eyes goggled previously with positive or negative lenses. In other words, oblique astigmatism is one potential signal to the fluctuation of refractive error in goggled eyes to help maintain optimal refractive state after emmetropization.

Chapter 5 Conclusions

General conclusion

Chicks raised with positive (+10D) or negative lenses (-15D) showed active emmetropization in response to the imposed defocus blur. Spherical defocus blur, total defocus blur and total optical blur all exponentially reduced in eyes goggled with positive lenses or negative lenses as did the control, non-goggled eyes. Total defocus blur and total optical blur reduced to non-zero endpoints (significantly above the diffraction limit), which were not significantly different between control and goggled eyes as suggested by the overlapping standard deviations. Astigmatism contributed significantly to the total optical blur which cannot be predicted from spherical defocus alone.

Cone row spacing exponentially reduced with age and was not different between control eyes and eyes goggled with different signed lenses. It varied much less with age than the optical blur. That is the cone resolution at younger ages was much better than the optical resolution. The endpoint cone row spacing in turn gives an endpoint of cone resolution based on Shannon sampling. The value of endpoint total optical blur (including residual spherical defocus, astigmatism and higher order aberrations) on average across birds reduces to match the endpoint cone resolution in all eyes, goggled and control. This indicates that cone photoreceptor sampling determines the endpoint refractive state. The amount of optical blur that can just be resolved by the cone photoreceptors is likely a stop signal to the further emmetropization of the refractive error.

As previously found with higher powered lenses, mean astigmatism increased significantly with age in eyes goggled with -15D lenses and decreased significantly in of the corresponding control eyes. In eyes goggled with +10D lenses, the overall astigmatism did not change significantly with age but the JCC45 component was larger in goggled eyes on day 14 than in control eyes. The significant increase in astigmatism in the eyes goggled with negative lenses is attributed to the significant increase in the oblique astigmatism. After day 14, total retinal blur averaged across birds plateaus; the component, spherical defocus blur, is reduced to a similar value between goggled and control eyes. Total defocus blur and total optical blur are well matched to the cone resolution in control eyes and is slightly (significantly) larger (on some days) in the eyes goggled with negative lenses, which is likely attributed to larger astigmatism in these goggled eyes than control eyes. When the optical blur is fitted with an exponential, the endpoint optical blur in the goggled and control eyes is not significantly different.

The presence of increased astigmatism, particularly oblique astigmatism, produces an orientation change in the long axes of the total defocus PSF as a function of variation in instantaneous refraction. This orientation and its change can be resolved by the cones. Adding higher-order aberrations, these characteristic orientation flips in total PSF were not obscured in some eyes goggled with positive or negative lenses, this orientation flips were not visible for control eyes in the measured range of instantaneous refraction. As the measured ocular refraction varies, the disc of least confusion and pairs of foci lines move with respect to retina, and a change of the orientation of the PSF could be detected by some goggled eyes. Chick can accommodate up to 20D (Schaeffel et al., 1988), changes in the orientation of the blur were observed for the rest control and goggled eyes which could provide a signal to the direction of defocus when the instantaneous refraction was moved less than 1D beyond the foci line. This oblique astigmatism may be one potential signal to help the goggled eyes detect fluctuations of the refractive state or any drift away from emmetropia. The increased astigmatism in goggled eyes may make the eye more sensitive to the change in defocus in order to maintain the optimal refractive state at the end of emmetropization.

Future interesting work would include:

1) Increase the sample size and number of time points sampled for birds goggled with +10D and compare the astigmatism change with different powers of lenses to ascertain if the change of astigmatism is proportional to the amount of the initially imposed blur.

2) Compare the cone sampling in children to the retinal blur to determine if the minimum blur near the endpoint of normal emmetropization is determined by cone photoreceptor resolution. Also determine whether children with higher spherical ametropia in childhood develop more astigmatism as they age analogous to the results in chicks.

References

References

Amedo, A. O., & Norton, T. T. (2012). Visual guidance of recovery from lens-induced myopia in tree shrews (tupaia glis belangeri). *Ophthalmic & Physiological Optics : The Journal of the British College of Ophthalmic Opticians (Optometrists), 32*(2), 89-99. 10.1111/j.1475-1313.2011.00875.x [doi]

Applegate, R. A., Sarver, E. J., & Khemsara, V. (2002). Are all aberrations equal? *Journal of Refractive Surgery (Thorofare, N.J. : 1995), 18*(5), S556-62.

Artal, P. (1989). Incorporation of directional effects of the retina into computations of optical transfer functions of human eyes. *Journal of the Optical Society of America.A, Optics and Image Science, 6*(12), 1941-1944.

Baba, T., Ohno-Matsui, K., Futagami, S., Yoshida, T., Yasuzumi, K., Kojima, A., . . . Mochizuki, M. (2003). Prevalence and characteristics of foveal retinal detachment without macular hole in high myopia. *American Journal of Ophthalmology, 135*(3), 338-342. S0002939402019372 [pii]

Babcock, H. W. (1953). The possibility of compensating astronomical seeing. *Publications of the Astronomical Society of the Pacific, 65*(386), 229-236.

Bowmaker, J. K., Heath, L., Wilkie, S., & Hunt, D. (1997). Visual pigments and oil droplets from six classes of photoreceptor in the retinas of birds. *Vision Research, 37*(16), 2183-2194.

Buehren, T., & Collins, M. J. (2006). Accommodation stimulus-response function and retinal image quality. *Vision Research, 46*(10), 1633-1645.

Bueno, J. M., Palacios, R., Giakoumaki, A., Gualda, E. J., Schaeffel, F., & Artal, P. (2014). Retinal cell imaging in myopic chickens using adaptive optics multiphoton microscopy. *Biomedical Optics Express, 5*(3), 664-674. 10.1364/BOE.5.000664 [doi]

Campbell, M. C., Bunghardt, K., & Irving, E. (2009). Potential optical signals to the direction of defocus change rapidly following an increase in defocus blur.

Campbell, M. C., Bunghardt, K., Kisilak, M. L., & Irving, E. L. (2012). Diurnal rhythms of spherical refractive error, optical axial length, and power in the ChickDiurnal variation of MOR, OAL, and power in chick. *Investigative Ophthalmology & Visual Science, 53*(10), 6245-6253.

Campbell, M. C. W., Priest, D., & Hunter, J. J. (2001). The importance of monochromatic aberrations to detecting defocus in retinal images. *Investigative Ophthalmology & Visual Science, 42*(4), S98-S98.

Coletta, N. J., Marcos, S., Wildsoet, C., & Troilo, D. (2003). Double-pass measurement of retinal image quality in the chicken eye. *Optometry and Vision Science, 80*(1), 50-57.

Cubalchini, R. (1979). Modal wavefront estimation from phase derivative measurements. *Journal of the Optical Society of America, 69*(7), 973-977.

Felberer, F., Kroisamer, J., Baumann, B., Zotter, S., Schmidt-Erfurth, U., Hitzenberger, C. K., & Pircher, M. (2014). Adaptive optics SLO/OCT for 3D imaging of human photoreceptors in vivo. *Biomedical Optics Express, 5*(2), 439-456.

Glickstein, M., & Millodot, M. (1970). Retinoscopy and eye size. *Science, 168*(931), 605-606.

Guirao, A., & Williams, D. R. (2003). A method to predict refractive errors from wave aberration data. *Optometry and Vision Science : Official Publication of the American Academy of Optometry, 80*(1), 36-42.

Headington, K., Choi, S. S., Nickla, D., & Doble, N. (2011). Single cell imaging of the chick retina with adaptive optics. *Current Eye Research, 36*(10), 947-957. 10.3109/02713683.2011.587934 [doi]

Hecht, E. (2002). Optics, 4th. *International Edition, Addison-Wesley, San Francisco, 3*

Hirsch, M. J., & Weymouth, F. W. (1990). Prevelance of refractive anomalies. (pp. 15-38). Boston: Butterworth-Heinemann.

Hopf, S., & Pfeiffer, N. (2017). Epidemiology of myopia. [Epidemiologie der Myopie] *Der Ophthalmologe : Zeitschrift Der Deutschen Ophthalmologischen Gesellschaft, 114*(1), 20-23. 10.1007/s00347-016-0361-2 [doi]

Hung, L. F., Crawford, M. L., & Smith, E. L. (1995). Spectacle lenses alter eye growth and the refractive status of young monkeys. *Nature Medicine, 1*(8), 761-765.

Hunter, J. J. (2006). *Image quality in ocular development and fundus imaging* (PhD).

Hunter, J. J., Campbell, M. C., Kisilak, M. L., & Irving, E. L. (2009). Blur on the retina due to higher-order aberrations: Comparison of eye growth models to experimental data. *Journal of Vision, 9*(6), 12.1-20. 10.1167/9.6.12 [doi]

Irving, E. L., Callender, M. G., & Sivak, J. G. (1991). Inducing myopia, hyperopia, and astigmatism in chicks. *Optometry and Vision Science, 68*(5), 364-368.

Irving, E. L., Sivak, J. G., & Callender, M. G. (2015). Refractive plasticity of the developing chick eye: A summary and update. *Ophthalmic & Physiological Optics : The Journal of the British College of Ophthalmic Opticians (Optometrists), 35*(6), 600-606. 10.1111/opo.12253 [doi]

Irving, E. L., Sivak, J. G., Curry, T. A., & Callender, M. G. (1996). Chick eye optics: Zero to fourteen days. *Journal of Comparative Physiology A-Sensory Neural and Behavioral Physiology, 179*(2), 185-194.

Irving, E. L. (1993). *Optically induced ametropia in young chickens* (Ph.D.).

Kee, C. S., Hung, L. F., Qiao-Grider, Y., Ramamirtham, R., & Smith, E. L.,3rd. (2005). Astigmatism in monkeys with experimentally induced myopia or hyperopia. *Optometry and Vision Science : Official Publication of the American Academy of Optometry, 82*(4), 248-260.

Kisilak, M. L. (2005). *Optical aberrations in growing eyes and in eyes with lens-induced myopia* (MSc).

Kisilak, M. L., Bunghardt, K., Hunter, J. J., Irving, E. L., & Campbell, M. C. (2012). Longitudinal in vivo imaging of cones in the alert chicken. *Optometry and Vision Science : Official Publication of the American Academy of Optometry, 89*(5), 644-651. 10.1097/OPX.0b013e31825489df [doi]

Kisilak, M. L., Campbell, M. C., Hunter, J. J., Irving, E. L., & Huang, L. (2006). Aberrations of chick eyes during normal growth and lens induction of myopia. *J.Comp.Physiol.A.Neuroethol Sens.Neural Behav.Physiol.,*

Kisilak, M. L., Hunter, J. J., Huang, L., Campbell, M. C. W., & Irving, E. L. (2007). In chicks wearing high powered negative lenses, spherical refraction is compensated and oblique astigmatism is induced. *Journal of Modern Optics,* , In press.

Kisilak, M. L., Hunter, J. J., Irving, E. L., & Campbell, M. C. W. (2007). In vivo imaging of photoreceptors in the alert chicken. *Investigative Ophthalmology and Vision Science, 48*, 1191.

Kislak, M. (2015). Adaptive optics measurements of cone density in chick eyes during lens induced myopia.

Koh, S., Maeda, N., Kuroda, T., Hori, Y., Watanabe, H., Fujikado, T., . . . Mihashi, T. (2002). Effect of tear film break-up on higher-order aberrations measured with wavefront sensor. *American Journal of Ophthalmology, 134*(1), 115-117.

Kram, Y. A., Mantey, S., & Corbo, J. C. (2010). Avian cone photoreceptors tile the retina as five independent, self-organizing mosaics. *PloS One, 5*(2), e8992. 10.1371/journal.pone.0008992 [doi]

Land, M. F., & Snyder, A. W. (1985). Cone mosaic observed directly through natural pupil of live vertebrate. *Vision Research, 25*(10), 1519-1523.

Liang, J., Williams, D. R., & Miller, D. T. (1997). Supernormal vision and high-resolution retinal imaging through adaptive optics. *Josa A, 14*(11), 2884-2892.

Liang, J., Grimm, B., Goelz, S., & Bille, J. F. (1994). Objective measurement of wave aberrations of the human eye with the use of a hartmann-shack wave-front sensor. *Journal of the Optical Society of America.A, Optics, Image Science, and Vision, 11*(7), 1949-1957.

Liang, J., & Williams, D. R. (1997). Aberrations and retinal image quality of the normal human eye. *Journal of the Optical Society of America. A, Optics, Image Science, and Vision, 14*(11), 2873-2883.

Lim, R., Mitchell, P., & Cumming, R. G. (1999). Refractive associations with cataract: The blue mountains eye study. *Investigative Ophthalmology & Visual Science, 40*(12), 3021-3026.

López, R., López-Gallardo, M., Busturia, I., Anezary, L., & Prada, C. (2005). Spatial and temporal patterns of growth and differentiation of cone oil droplets in the chick retina. *Journal of Neuroscience Research, 79*(3), 401-411.

MacRae, S., Krueger, R., & Applegate, R. (2004). *Wavefront customized visual correction*. Thorofare, NJ: SLACK Incorporated.

Marcos, S., Werner, J. S., Burns, S. A., Merigan, W. H., Artal, P., Atchison, D. A., . . . Yoon, G. (2017). Vision science and adaptive optics, the state of the field. *Vision Research, 132*, 3-33.

Mitchell, P., Hourihan, F., Sandbach, J., & Wang, J. J. (1999). The relationship between glaucoma and myopia: The blue mountains eye study. *Ophthalmology, 106*(10), 2010-2015.

Morgan, I. G., Rose, K. A., Ellwein, L. B., & Refractive Error Study in Children Survey Group. (2010). Is emmetropia the natural endpoint for human refractive development? an analysis of population-based data from the refractive error study in children (RESC). *Acta Ophthalmologica, 88*(8), 877-884. 10.1111/j.1755-3768.2009.01800.x [doi]

National Research Council. (1990). *Advances in photoreception: Proceedings of a symposium on frontiers of visual science* National Academies Press.

Park, T. W., Winawer, J., & Wallman, J. (2003). Further evidence that chick eyes use the sign of blur in spectacle lens compensation. *Vision Research, 43*(14), 1519-1531.

Physical sciences institute. (2010). Multimodel AO retinal imaging system user manual.

Porter, J., Queener, H., Lin, J., Thorn, K., & Awwal, A. A. (2006). *Adaptive optics for vision science: Principles, practices, design and applications* John Wiley & Sons.

Qiao-Grider, Y., Hung, L., Kee, C., Ramamirtham, R., & Smith, E. L. (2007). Normal ocular development in young rhesus monkeys (macaca mulatta). *Vision Research, 47*(11), 1424-1444.

Roorda, A., Romero-Borja, F., Donnelly III, W. J., Queener, H., Hebert, T. J., & Campbell, M. C. (2002). Adaptive optics scanning laser ophthalmoscopy. *Optics Express, 10*(9), 405-412.

Roorda, A., & Williams, D. (1999). The arrangement of the three cone classes in the living human eye. *Nature, 397*(6719), 520-522.

Rossi, E. A., Granger, C. E., Sharma, R., Yang, Q., Saito, K., Schwarz, C., . . . Williams, D. R. (2017). Imaging individual neurons in the retinal ganglion cell layer of the living eye. *Proceedings of the National Academy of Sciences of the United States of America, 114*(3), 586-591. 10.1073/pnas.1613445114 [doi]

Schaeffel, F., & Wildsoet, C. (2013). Can the retina alone detect the sign of defocus? *Ophthalmic and Physiological Optics, 33*(3), 362-367.

Schaeffel, F., Glasser, A., & Howland, H. C. (1988). Accommodation, refractive error and eye growth in chickens. *Vision Research, 28*(5), 639-657.

Schaeffel, F., & Howland, H. C. (1988). Visual optics in normal and ametropic chickens. *Clinical Vision Sciences, 3*(2), 83-98.

Schaeffel, F., Howland, H. C., & Farkas, L. (1986). Natural accommodation in the growing chicken. *Vision Research, 26*(12), 1977-1993. 0042-6989(86)90123-9 [pii]

Schmid, K., & Wildsoet, C. F. (1997). Natural and imposed astigmatism and their relation to emmetropization in the chick. *Experimental Eye Research, 64*(5), 837-847.

Shao, Z. (2015). *Optical changes during normal emmetropization, lens-induced myopia and its recovery in the young chick eye*

Smith, E. L.,3rd. (2011). Prentice award lecture 2010: A case for peripheral optical treatment strategies for myopia. *Optometry and Vision Science : Official Publication of the American Academy of Optometry, 88*(9), 1029-1044. 10.1097/OPX.0b013e3182279cfa [doi]

Smith, W. J. (2000). *Modern optical engineering*. Toronto: McGraw-Hill.

Snyder, A. W., Bossomaier, T. R., & Hughes, A. (1986). Optical image quality and the cone mosaic. *Science, 231*, 499-502.

Snyder, A. W., & Pask, C. (1973). The stiles-crawford effect--explanation and consequences. *Vision Research, 13*(6), 1115-1137.

Stirpe, M., & Michels, R. G. (1990). Retinal detachment in highly myopic eyes due to macular holes and epiretinal traction. *Retina (Philadelphia, Pa.), 10*(2), 113-114.

Thibos, L. N., Applegate, R. A., Schwiegerling, J. T., & Webb, R. (2002). Standards for reporting the optical aberrations of eyes. *Journal of Refractive Surgery, 18*(5), S652-S660.

Thibos, L. N., Applegate, R. A., Schwiegerling, J. T., Webb, R., & VSIA Standards Taskforce Members. Vision science and its applications. (2002). Standards for reporting the optical aberrations of eyes. *Journal of Refractive Surgery (Thorofare, N.J.: 1995), 18*(5), S652-60.

Thibos, L. N., & Hong, X. (1999). Clinical applications of the shack-hartmann aberrometer. *Optometry and Vision Science : Official Publication of the American Academy of Optometry, 76*(12), 817-825.

Thibos, L. N., Hong, X., Bradley, A., & Applegate, R. A. (2004a). Accuracy and precision of objective refraction from wavefront aberrations. *Journal of Vision, 4*(4), 329-351.

Thibos, L. N., Hong, X., Bradley, A., & Applegate, R. A. (2004b). Accuracy and precision of objective refraction from wavefront aberrations. *Journal of Vision, 4*(4), 329-351. 10.1167/4.4.9 [doi]

Thibos, L. N., Hong, X., Bradley, A., & Cheng, X. (2002). Statistical variation of aberration structure and image quality in a normal population of healthy eyes. *Journal of the Optical Society of America. A, Optics, Image Science, and Vision, 19*(12), 2329-2348.

Thibos, L. N., Wheeler, W., & Horner, D. (1997). Power vectors: An application of fourier analysis to the description and statistical analysis of refractive error. *Optometry and Vision Science : Official Publication of the American Academy of Optometry, 74*(6), 367-375.

Tian, Y., & Wildsoet, C. F. (2006). Diurnal fluctuations and developmental changes in ocular dimensions and optical aberrations in young chicks. *Investigative Ophthalmology & Visual Science, 47*(9), 4168-4178.

Troilo, D., Gottlieb, M. D., & Wallman, J. (1987). Visual deprivation causes myopia in chicks with optic nerve section. *Current Eye Research, 6*(8), 993-999.

Wallman, J. (1993). Retinal control of eye growth and refraction. *Progress in Retinal Research, 12*, 133-153.

Wallman, J., & Winawer, J. (2004a). Homeostasis of eye growth and the question of myopia. *Neuron, 43*(4), 447-468. 10.1016/j.neuron.2004.08.008 [doi]

Wallman, J., & Winawer, J. (2004b). Homeostasis of eye growth and the question of myopia. *Neuron, 43*(4), 447-468.

Wallman, J., & Winawer, J. (2004c). Homeostasis of eye growth and the question of myopia. *Neuron, 43*(4), 447-468. 10.1016/j.neuron.2004.08.008 [doi]

Webb, R. H., & Hughes, G. W. (1981). Scanning laser ophthalmoscope. *IEEE Transactions on Biomedical Engineering*, (7), 488-492.

Webb, R. H., Hughes, G. W., & Delori, F. C. (1987). Confocal scanning laser ophthalmoscope. *Applied Optics, 26*(8), 1492-1499.

Weiss, S., & Schaeffel, F. (1993). Diurnal growth rhythms in the chicken eye: Relation to myopia development and retinal dopamine levels. *Journal of Comparative Physiology A, 172*(3), 263-270.

Wildsoet, C., & Wallman, J. (1995). Choroidal and scleral mechanisms of compensation for spectacle lenses in chicks. *Vision Research, 35*(9), 1175-1194.

Wildsoet, C. (2003). Neural pathways subserving negative lens-induced emmetropization in chicks--insights from selective lesions of the optic nerve and ciliary nerve. *Current Eye Research, 27*(6), 371-385.

Wildsoet, C. F. (1997a). Active emmetropization--evidence for its existence and ramifications for clinical practice. *Ophthalmic & Physiological Optics : The Journal of the British College of Ophthalmic Opticians (Optometrists), 17*(4), 279-290. S0275-5408(97)00003-3 [pii]

Wildsoet, C. F. (1997b). Active emmetropization--evidence for its existence and ramifications for clinical practice. *Ophthalmic & Physiological Optics : The Journal of the British College of Ophthalmic Opticians (Optometrists), 17*(4), 279-290.

Wildsoet, C. F., Howland, H. C., Falconer, S., & Dick, K. (1993). Chromatic aberration and accommodation: Their role in emmetropization in the chick. *Vision Research, 33*(12), 1593-1603.

Wilson, B. J., Decker, K. E., & Roorda, A. (2002). Monochromatic aberrations provide an odd-error cue to focus direction. *Journal of the Optical Society of America A-Optics Image Science and Vision, 19*(5), 833-839.

Wong, T. Y., Klein, R., Klein, B. E., & Tomany, S. C. (2002). Refractive errors and 10-year incidence of age-related maculopathy. *Investigative Ophthalmology & Visual Science, 43*(9), 2869-2873.

Wright, A. F., Chakarova, C. F., El-Aziz, M. M. A., & Bhattacharya, S. S. (2010). Photoreceptor degeneration: Genetic and mechanistic dissection of a complex trait. *Nature Reviews Genetics, 11*(4), 273-284.

Wyant, J. C., & Creath, K. (1992). Basic wavefront aberration theory for optical metrology. (pp. 1-53). NY: Acedemic Press.

Zhu, X., McBrien, N. A., Smith, E. L.,3rd, Troilo, D., & Wallman, J. (2013). Eyes in various species can shorten to compensate for myopic defocus. *Investigative Ophthalmology & Visual Science, 54*(4), 2634-2644. 10.1167/iovs.12-10514 [doi]